Investigating Statistical Modeling Approaches for Reservoir Characterization in Waterfloods from Rates Fluctuations

by

Kun-Han Lee

A Dissertation Presented to the
FACULTY OF THE VITERBI SCHOOL of ENGINEERING
UNIVERSITY OF SOUTHERN CALIFORNIA
In Partial Fulfillment of the
Requirements for the Degree
Ph. D.
(ELECTRICAL ENGINEERING)

October 2010

Dedication

Po-Hsien Lee

Yun-Ru Chen

Yun-Fang Lu

Acknowledgements

I would like to express my sincere appreciation and gratitude to my supervisor, Dr. Antonio Ortega, for his support throughout my graduate studies at the University of Southern California. I have been fortunate to have an advisor who gave me the freedom to explore on my own, and at the same time the guidance to recover when my steps faltered. I am grateful to his guidance, patience, and encouragement.

I owe my gratitude to Dr. Iraj Ershaghi, for his support of many useful discussions and suggestions. He has made many insightful comments from the petroleum engineering aspects at different stages of my research. Without him my thesis would not have been completed. Thanks are also due to Dr. Mendel for serving as members of my dissertation committee and Dr. Kuo and Dr. Jenkins for serving as committee members of my qualify exam. Their valuable comments and suggestions were really appreciated.

I would like to thank to several PhD students in Petroleum Engineering: Nelia Jafroodi, Amir Mohammad Nejad, Mohammad Javaheri and Reza Rastegar Moghadam. They cooperate with me to finish all the numerical simulations and make many valuable discussions. I am also indebted to the staff of the CiSoft project for their help and continuous support.

Many friends have helped me stay sane through these difficult years. Their support and care helped me overcome setbacks and stay focused on my graduate study. I greatly value their friendship.

Most importantly, none of this would have been possible without the love and patience of my family. They to whom this dissertation is dedicated to, has been a constant source of love, concern, support and strength all these years. I would like to express my heart-felt gratitude to my family.

Table of Contents

Dedication ii

Acknowledgements iii

List Of Tables viii

List Of Figures ix

Abstract xi

Chapter 1: Introduction 1
- 1.1 Background . . . 1
- 1.2 A New Research Trend . . . 3
- 1.3 Research Contributions . . . 5

Chapter 2: New Predictive Models 8
- 2.1 Linear Time-invariant System . . . 9
- 2.2 Revisiting the Capacitance Model . . . 10
- 2.3 Finite Impulse Response Model . . . 13
  - 2.3.1 Discrete Model . . . 14
- 2.4 Distributed Capacitance Model . . . 15
  - 2.4.1 Interpretation of Model . . . 20
- 2.5 Multivariate ARX Model . . . 21
  - 2.5.1 Discrete Model . . . 26
- 2.6 Finding the Model Parameters . . . 26
- 2.7 Summary . . . 29

Chapter 3: Model Validation and Comparison 30
- 3.1 Validation of Models . . . 31
- 3.2 Simulation Setting . . . 33
  - 3.2.1 Permeability Map . . . 35
  - 3.2.2 Injection Rate Setting . . . 37
  - 3.2.3 Other Setting . . . 39

3.3 Validation Results for Interwell Connectivity . . . 39
3.3.1 Quantitative Verification . . . 43
3.4 Physical Constraints on Parameters . . . 44
3.5 Model Comparison . . . 49
3.5.1 Number of Parameters . . . 49
3.5.2 Prediction Performance Comparisons . . . 50
3.6 Comparison Results . . . 51
3.6.1 Noise Sensitivity Analysis . . . 56
3.7 Discussions . . . 58
3.7.1 Drawbacks of Purely Statistical Methods . . . 58
3.7.2 Large Scale Problems . . . 59
3.7.3 Suggestions for Using Predictive Models . . . 61
3.8 Summary . . . 62

Chapter 4: Linear Modeling Framework 63
4.1 Linear Models for Well Interactions . . . 63
4.2 A Framework for Predictive Models . . . 65
4.2.1 Capacitance Model . . . 66
4.2.2 Distributed Capacitance Model . . . 67
4.2.3 Double Pole Model [39] . . . 68
4.2.4 Finite-Impulse-Response Model . . . 69
4.2.5 Multivariate ARX Model . . . 71
4.2.6 Higher Order Models . . . 72
4.3 Conclusion . . . 73

Chapter 5: Prediction Under Controlled Producers 74
5.1 Interpreting M-ARX Model . . . 75
5.2 Prediction for Shut-In Producers . . . 77
5.2.1 Simulation Results . . . 79
5.3 Prediction for Constrained Producers . . . 81
5.3.1 Simulation Results . . . 83

Chapter 6: Injection Rates Design 89
6.1 Literature Review . . . 90
6.1.1 Optimal Input Design . . . 90
6.1.2 Channel Estimation in Communication . . . 92
6.2 A Novel Deterministic Approach for Input Sequence Design . . . 94
6.2.1 Inverse-repeat signals . . . 94
6.2.2 Property of a Set of Inverse-Repeat Signals . . . 95
6.2.3 Design Example . . . 97
6.2.4 Discussion . . . 98
6.3 Stochastic Approach . . . 100
6.3.1 Criterion for Injection Rate Design . . . 101

6.3.1.1 MISO case 103
6.3.1.2 MIMO case 104
6.3.1.3 The Crest Factor 105
6.3.2 A Design Procedure 106
6.3.3 Design Example: Application to CM 108
6.3.4 Simulation Results 111
6.3.5 Comparison to Deterministic Approach 115
6.4 Conclusion 117

Chapter 7: Conclusions and Future Work **118**
7.1 Conclusions 118
7.2 Future Work 120

Reference List **122**

List Of Tables

3.1 Simulation Settings for CMG simulator. 34

3.2 Estimated values of interwell connectivity for Scenario A. 40

3.3 Average absolute differences of interwell connectivities between CM and other models for Scenario A. 40

3.4 Estimated values of interwell connectivity for Scenario B. 42

3.5 Average absolute differences of interwell connectivities between CM and other models for Scenario B. 43

3.6 Estimated interwell connectivities for peripheral injector pattern (Scenario E, F, and G). 45

3.7 Number of parameters used for different models. 50

4.1 Different predictive models and the characteristics of their transfer function. 73

5.1 The number of parameters needed to be retrained when a producer is shut-in. 80

6.1 Non-zero DFT indexes fro inverse-repeat signals. 96

List Of Figures

2.1 The impulse response of Capacitance Model. 11

2.2 Analogous RC circuit for capacitance model. 12

2.3 Representative element for distributed capacitance model. There is a high permeability channel between the injector and producer. . . 17

2.4 Impulse response curves of distributed capacitance model for different τ_1 and τ_2. The injected water of injector is also shown. 19

2.5 Interpretation of distributed capacitance model in terms of CMs. . . 21

2.6 Scenario with multiple injection and production wells. The red shadow areas represent the pore volume related to that producer. 22

2.7 Diagram of the modeling process of M-ARX model. 27

3.1 Permeability map for channel case (Scenario A): channel case. . . . 34

3.2 Permeability map for streak case (Scenario B). 35

3.3 Permeability map for homogeneous case (Scenario C). 35

3.4 Permeability map for multiple fractures case (Scenario D). 36

3.5 Permeability map for Scenarios E, F, and G. 36

3.6 Injection rates for Scenarios A-D. 37

3.7 Injection rates set for Scenario F. 38

3.8 Injection rates assigned for Scenario G. 39

3.9 Estimated interwell connectivities for Scenario A. 41

3.10 Estimated interwell connectivities for Scenario B. 43

3.11 Estimated interwell connectivities for peripheral injector pattern (Scenario E, F, and G). 46

3.12 Performance evaluation of different models on the Scenario C 52

3.13 Performance evaluation of different models on the Scenario D. . . . 53

3.14 Performance evaluation of different models for Scenario A. 54

3.15 Performance evaluation of different models for Scenario G. 55

3.16 Noise sensitivity analysis for different models for Scenario A. 57

5.1 The CRMP and M-ARX model in 2-injectors/2-producers scenario. 75

5.2 Performance of prediction error for production rates based on M-ARX model in Scenario A with $P4$ shut-in. 81

5.3 Prediction of production rates by M-ARX model in Scenario A with $P4$ shut-in.. 82

5.4 Prediction results for Constrained P1. 84

5.5 Prediction results for Constrained $P2$. 85

5.6 Prediction results for Constrained $P3$. 86

5.7 Prediction results for Constrained $P4$ with 600 bbl/day. 87

5.8 Prediction results for Constrained $P4$ with 2500 bbl/day. 88

6.1 Illustration of non-zero frequency indexes for inputs with different periods. 96

6.2 An example for designed set of inverse-repeat signals. 98

6.3 Block diagram for the procedure which generates the set of inputs for injection rate design. 107

6.4 A realization of designed injection rates used for performance evaluation. 113

6.5 Performance plot for injection rates design with different sequences. 114

6.6 Performance plot for injection rates design with both deterministic and stochastic approaches. 116

Abstract

Reservoir characterization is important for reservoir management and performance optimization. For waterflood optimization, traditionally several techniques have been suggested, most of which are either too time-consuming or the data needed are often unavailable. There is a new research trend to overcome these limitations by applying advanced statistical techniques on only injection and production data, which are often readily available for any waterflood operations.

In this work, we follow this trend to formulate the reservoir characterization and forecasting problems in waterflood projects using a system identification framework: the injection rates are seen as inputs; the production rates are seen as the outputs; and the reservoir is considered as a dynamic system. By addressing the properties of general linear dynamic systems, we discuss the limitations of previous models and build three new predictive models to characterize some reservoir behavior, such as producer-to-producer interactions, which was not considered in previous literature. Then we discuss a general parameter estimation approach under the prediction-error framework.

For model evaluation, we propose two techniques: one is based on evaluating their prediction ability on a fresh data set, while the other is based on comparing the interpretations they provide about certain reservoir characteristics with the ground truth. All proposed models are verified by these two approaches. To perform a comparative analysis, we provide a practical metric to compare the prediction

performance of different proposed models under various scenarios. From the results, we make several observations and suggestions for reservoir engineers to use the models.

To clarify the relationship between different models, we develop a general linear modeling framework and demonstrate that all proposed models can be considered as special cases within this framework. Moreover, the transfer function of the general linear model can be interpreted to provide insight on reservoir characteristics. Also, the relationship between different models can easily be built from this work.

We propose a multivariate autoregressive model to characterize situations in which a producer is shutting-in or a new producer is being brought online. As a totally new application, we introduce a novel "constrained producer" approach which that only requires minimal changes in production rates (e.g., limiting them to some level below their normal production capacity) to predict the performance after a producer is shut-in. This allows us to handle various "what if" scenarios in waterflood management.

Finally, to achieve a better model estimation, the patterns of injection rates play an important role. We addressed the problem of designing a set of injection rates to achieve a better estimation of target parameters in the reservoir. Two different approaches, deterministic and stochastic approaches, are discussed. For the deterministic approach, we propose a new procedure using a set of inverse-repeat signals to design a set of signals with zero cross-correlation property. For stochastic approach, we applied a common approach in system identification and evaluate all design procedures on some predictive model.

Chapter 1

Introduction

1.1 Background

Waterflooding is a common operation in many petroleum reservoirs. It refers to a process where some wells, denoted as injectors, inject water into the reservoir in order to increase the reservoir pressure and displace the oil to some surrounding wells, which denoted as producers. The pressure gradient between injectors and producers helps in increasing oil production.

To maximize oil recovery by waterflooding, it is useful to "understand" the underground structure of the reservoirs. Traditionally, there are several approaches to estimate the reservoir characteristics among wells. Among these methods, multiple-well tests (interference and pulse tests [27]), a type of pressure-transient test ([53] [24]), have been developed to establish communication between wells and determine the interwell reservoir properties. Basically these approaches rely on matching pressure response from wells to a theoretical model of reservoir. Using a nonlinear parameter estimation, some crucial reservoir characteristics can be approximated. Refer to Kamal [29] for a review on this topic. For these tests, the costs are significant because the amplitudes of responses are small (sometimes less than 1 psi) and

precise pressure measurements are needed to get meaningful data. On the other hand, downhole pressure recorders data are not available for most of the field operations. This becomes an impediment for routine application of these techniques.

As a alternative, tracer tests have widely been used for mapping flow communication among wells. Tracer studies can also be useful for estimation of reservoir parameters, such as reservoir swept volume, fluid velocities, and flow geometry in a reservoir. Basically this method requires injecting some chemicals (tracers) in some wells and observing the tracer concentration curve on the produced fluid from the surrounding wells. Such information is used to estimate the underground flow in the reservoir. For instance, Abbaszadeh-Dehghani and Brigham [1] [2], and Oliver [13] showed some successful flow-simulation and field examples. However, conducting frequent tracer tests is often uneconomical and time consuming. Moreover, tracer testing cannot provide a dynamic view of the system: an estimate of the flow characteristics is obtained after the testing, but the model parameters cannot be updated unless a new test (e.g., using a different tracer) is conducted.

Besides characterization, engineers sometimes need to have a more complete understanding of the reservoir as well as the ability to forecast the future flows of the fields in order to improve the waterflood management. To achieve this, comprehensive reservoir simulations are widely used to simulate the whole reservoir (or region-of-interests in the reservoir) by integrating all information available for the reservoir. With the reservoir simulation approach, it is possible to predict both the reservoir and individual well performance and decide on a better strategy for management and decision-making. However, in this kind of approach, the integration of numerous data types throughout the life of the reservoir is required, and this is time-consuming and costly. Some techniques for managing reservoir uncertainty have been proposed including improved sampling techniques (such as using Monte

Carlo simulation [43] [40]) or speeding up the model simulation (such as using the coarse grid simulation [26] or a predictive model [20]). But these kinds of reservoir simulations are still not suitable for many field applications because of the high complexity. Furthermore, some of the inputs for building this model may not available or determinable. As a result, it is rather impractical for reservoir engineers to use complex simulation models for daily monitoring of operations.

1.2 A New Research Trend

Injection and production rates are the most abundant data available in any waterflood operation and they often correlate to each other in some complex manner in the reservoir. Recently, a variety of methods have been used to express the rate performance of a production well as a function of injection rates in the surrounding injectors. In all these works, the reservoir is viewed as a system that converts an input signal (injection rate at injector) into an output signal (production rate at producer) and the goal is to analyze input and output signals to estimate some characteristics of the reservoir. If this can be achieved, the estimated parameters can be used to facilitate waterflood management and optimization.

As an example, Heffer *et al.* [22] used Spearman rank correlations to relate injector-producer pairs and associated these relations with geomechanics. Panda and Chopra [50] used artificial neural networks to determine the interactions between injection and production rates. Albertoni and Lake [3] estimated the connectivity between wells based on a linear model using the multiple linear regression (MLR) method. Gentil [15] explained the physical meaning of MLR constants by presenting the connectivity weight as a function of transmissibility. This trend turned to a predictive modeling approach in 2006, in which Yousef *et al.* [64] [65]

improved previous work by building a simple reservoir model, called the capacitance model, to describe the relationship between injection and production wells. They used a parameter to describe the effects of compressibility, in addition to transmissibility, between the injection-production interwell channels. Liang *et al.* [38] used this model, accompanied with a fractional-flow model, to perform the oil rates optimization procedure in waterfloods. Sayarpour *et al.* [55] used the model and presented analytic solutions to three different reservoir-control volume scenarios. This facilitates the capacitance model's application for rapid assessment at different levels of a field study, from a single well, to a group of wells, and to an entire field. Weber *et al.* [62] extended this work to large scale reservoirs and Izgec and Kabir [25] made a comparison between the model and transient-pressure approaches, and proved that it is valid for both before and after the water breakthrough. Although this work has been successful, the possible use of alternative predictive models, together with theoretical discussions from a system identification point of view, have never been investigated and are proposed for the first time in this thesis.

The above approaches all assumed the system (reservoir) is time-invariant during some period of time. In 2007, Liu *et al.* [39] proposed an extended Kalman filter approach to characterize the reservoir by assuming that the parameters in the model will change over time (time-varying system), so that the Kalman filter is used to track and estimate the model parameters. Independent of these works, Thiele and Batycky [59] [60] estimated the connectivity between wells using streamline-based workflow. Their approach requires building a complete stream flow reservoir model for the region of interest, which is hard to achieve for most fields with daily operations.

1.3 Research Contributions

In our work, we follow the predictive modeling approach by addressing the problem of estimating reservoir properties in waterfloods from injection/production rates and note that it can be seen as a system identification problem, where injection rates are inputs and production rates are outputs. System identification refers to the process of building mathematical models of systems based on measured data. Before the parameters are identified, it is necessary to build a relatively simple but reliable (depending on applications of need) model. We denote these models as predictive models (because the main objective of these models is to predict the reservoir behavior) in this thesis. The model can be built by first principles (e.g., conservation of momentum, mass, and energy), or empirically, or as a combination of both approaches.

The state-of-the-art capacitance model (CM) [64] and its applications can be seen as a pioneering predictive modeling approach. But, in spite of its success, CM still has some limitations and many other possible predictive models still have not been investigated. Our first contribution is to build three new predictive models: the first one is the finite-impulse-response model, which leads to impulse responses with more general shapes than those possible within the capacitance model. The second one is the distributed capacitance model, which extends the concepts of CM to more heterogeneous reservoir scenarios. The third one is the multivariate autoregressive model. This model takes into consideration the producer-to-producer relationships, which are not captured in all previous modeling approaches.

As a second contribution, we first propose two approaches for model evaluation: (1) evaluating their prediction ability on a fresh data set; (2) comparing their interpretation in terms of reservoir characteristics to the ground truth knowledge

for that reservoir. We verify all proposed models using both evaluation methods. The so-called "grey-box" approach for model estimation procedure is also introduced and fully investigated in this dissertation. Moreover, we define a practical metric and compare the prediction performance of all models under various scenarios, and make some suggestions to reservoir engineers about how to select among these predictive modeling approaches.

The third contribution is that we provide a unified framework for predictive modeling. We first show that all predictive models proposed up to now all belong to a special case of a general linear dynamic model. Moreover, from this framework, we show that the transfer function of this general linear model can be interpreted in terms of some reservoir characteristics (by given its poles) in the interwell region between each well pair. Finally, the relationship between different models can be easily seen from this framework.

We demonstrate a totally new application of the multivariate autoregressive model: forecasting the performance when some producer is shutting-in or some new producer is brought into operation. Using this model, one only needs to constraint producers to operate at a certain rate in order to estimate the impact of a well shut-in, while all previous modeling approaches actually require to actually shut-in the well for forecasting, thus potentially reducing overall production significantly. This new application makes it much more practical to control producers in order to predict performance under several possible "What if" scenarios, which is our fourth contribution.

Our last contribution is to consider the injection rate designs. It can be easily shown that the shapes of the inputs (injection rates) affect the model estimation results noticeably. To the best of our knowledge, the improvements for reservoir parameter estimation that can be achieved by carefully designing injection rates

have not been discussed in the literature. There are two different approaches: deterministic and stochastic. For deterministic approach, we propose a new procedure based on the property of inverse-repeat signals and that can generate a set of periodic signals with vanishing cross-correlation to each other. For stochastic approach, we apply a procedure in system identification to reservoir applications and demonstrate its performance on some predictive model.

The outline of this dissertation is as follows: In chapter 2, we develop three new predictive models by that address the limitations of the previous proposed models. In chapter 3, we discuss the Verification these new models with different approaches, and making a comparative analysis of these models so that reservoir engineers have guidelines to use them. We also investigate the grey-box approach for modeling and summarizing its influence. In chapter 4, we provide a general and unified framework for all predictive models, and clarifying the relationship between different models. Moreover, we try to interpret the transfer function of linear model as some reservoir characteristics in the field. In chapter 5, we develop a novel application for multivariate autoregressive models. This new application makes it much more practical to control producers in order to predict performance under several possible "What if" scenarios, without actually shutting-in the wells. In chapter 6, we investigate different ways of injection rate design to improve the parameter estimation for the predictive models. We develop a new deterministic procedure to generate a set of injection rates with vanishing cross-correlation to each other, and apply a common stochastic procedure to field applications. Both methods are evaluated by some predictive model.

Chapter 2

New Predictive Models

In mature waterfloods, fluids are produced by two main factors: either they correspond to the primary production rates from the reservoir itself, or they are due to the pressure gradients caused by fluid injections. As discussed in the introduction, new techniques aim to capture the well interactions using statistical techniques based on the fluctuations of injection and production data. The core procedure relies on modeling for the reservoir, especially between injection and production wells. These predictive models can be estimated using a common methodology: (1) building the models based on physical principles and statistical techniques; (2) estimating the parameters in the models mainly by rate information; (3) using the trained models to characterize the reservoir or predict the future performance.

In this chapter, we propose and develop several new predictive models. We first discuss the general linear time-invariant system, and revisit the state-of-the-art modeling approach: capacitance model (CM). By addressing the limitations of CM, we propose several new models. The first one is the finite impulse response (FIR) model, which releases the constraints on the impulse response shape of CM. This leads to improvement of the prediction performance for some scenarios. Second, we

generalize the concepts of CM to deal with more heterogeneous reservoir cases. We call this approach the distributed capacitance model (DCM).

The above models are all based on using injection rates to predict the future production rates. All these models do not consider changes in production in certain wells may affect other wells. To address the producer-to-producer interactions, we propose a new model: multivariate autoregressive with extra inputs (M-ARX).

Finally, we discuss a general approach for finding the model parameters. This approach is based on minimizing the residues between actual and estimated production rates, which involves some non-linear optimization procedures. The so-called "linear-in-the-parameter" property is discussed which leads to a much less complex optimization.

2.1 Linear Time-invariant System

From the system point of view, if we have M inputs and N outputs, and assuming the system is linear and time-invariant (LTI), the outputs $y_j(t)$ with $j = 1, ..., N$ can be expressed as

$$y_j(t) = y_j(t_0) + \sum_{i=1}^{M} u'_{ij}(t) \tag{2.1}$$

where $u'_{ij}(t)$ is a filtered version of the input u_i:

$$u'_{ij}(t) = u_i(t) * h_{ij}(t) = \int_{\xi=0}^{\infty} u_i(t-\xi) h_{ij}(\xi) d\xi \tag{2.2}$$

The $h_{ij}(t)$ is denoted as the impulse response between input i and output j. Basically (2.1) and (2.2) mean that the output can be expressed as a linear combination of some filtered version of the inputs. If we assume that the reservoir in the region-of-interest (ROI) is a LTI system, the injectors are inputs, and the producers are

the outputs, as we will see, the main difference between various linear models is depending on how they describe the impulse response $h_{ij}(t)$, which accounts for any shape of attenuation and delays between the injector i and producer j. If one injects a water pulse into the reservoir, which leads to changes in production over time, the impulse response $h_{ij}(t)$ describes these changes. As the waterflood project begins, it denotes secondary oil recovery period. During this period, the primary production curve stays relatively constant compared to the influence caused from injection rate fluctuations, so the constant value $y_j(t_0)$ can be seen as the primary depletion effects.

2.2 Revisiting the Capacitance Model

In this section, we revisit the capacitance model, as a predictive modeling approach from rate fluctuations [63] [64]. The CM is based on deriving a total mass balance equation with compressibility. Take one injector-producer well pair in a drainage volume as a representative element, the governed material balance differential equation is given by:

$$c_t V_p \frac{d\overline{p}}{dt} = u(t) - y(t), \tag{2.3}$$

where c_t is the total compressibility, V_p is the drainage pore volume, $\overline{P}$ is the average pressure in V_p, $u(t)$ is the injection rate (input) and $y(t)$ is the total gross production rate (output). Also, a linear productivity model can be used to relate pressure to rates:

$$y = J(\overline{P} - P_{wf}) \tag{2.4}$$

where P_{wf} and J are the flowing bottom hole pressure (BHP) and productivity index of the producer, respectively. Note that (2.4) holds only for stabilized flow,

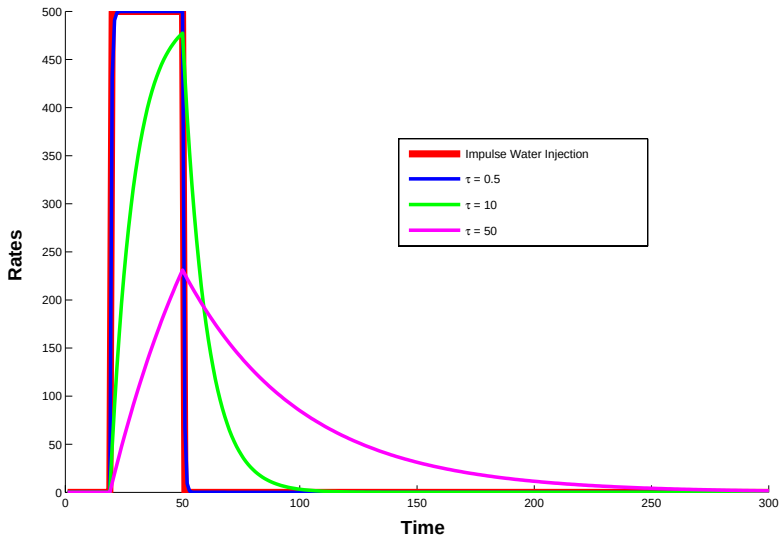

Figure 2.1: The response of capacitance model by step injection. Different colors show the responses of different time constant τ.

so its appropriateness can only be established by numerical simulation [64]. By eliminating the average pressure on (2.3) and (2.4) using these two equations, and solving the differential equation, the resulting production rates can be expressed as:

$$\begin{aligned} y(t) &= y(t_0)e^{\frac{-(t-t_0)}{\tau}} + \frac{e^{-t/\tau}}{\tau}\int_{\xi=t_0}^{\xi=t} e^{\xi/\tau} i(\xi)d\xi \\ &\quad + J\left[P_{wf}(t_0)e^{\frac{-(t-t_0)}{\tau}} - P_{wf}(t) + \frac{e^{-t/\tau}}{\tau}\int_{\xi=t_0}^{\xi=t} e^{\xi/\tau} P_{wf}(\xi)d\xi\right] \end{aligned} \tag{2.5}$$

where the τ is defined as the "time constant" of the drainage volume:

$$\tau = \frac{c_t V_p}{J} \tag{2.6}$$

and t_0 is the initial time.

(2.5) summarizes the capacitance model, and is easy to interpret: it shows that the production rates of the producer can be divided into three components. The

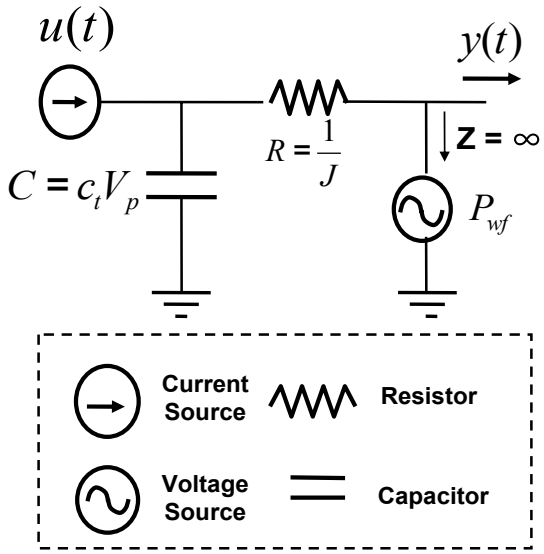

Figure 2.2: Analogous resistor-capacitor circuit for capacitance model.

first term accounts for primary production depletion. The second component is the contribution from the injection rates. The impulse response shape is determined by the variable τ, and Fig. 2.1 shows the response curve of different τs. The last component is the influence of production rates caused by the change on bottom-hole pressure of the producer.

We can make an analogy between the CM and the resistor-capacitor (RC) circuit, shown in Fig. 2.2. This analogy highlights the resistive and capacitance effects of this model: the fluid flowing into the reservoir is like the electric current in the circuits, and the reservoir behaves like a capacitance with $C = c_t V_p$ and a resistance with $R = \frac{1}{J}$, and the time constant τ is equal to $R \times C$. So generally speaking, the CM tries to model the reservoir with its capacitance effects, together with its resistive effects. For this reason, several researchers have called this model "capacitance-resistive model" or CRM for short [54] [62].

This representative element can easily be extended to multiple injectors and producers using superposition principle. For each injector-producer pair, weights

or coefficients, λ_{ij}, are defined to incorporate the fact that one injector is shared by more than one producer, and τ_{ij} describes the impulse response shape between the injector i and producer j. For the formulas and further reference, see [64] for more discussions.

2.3 Finite Impulse Response Model

For CM with multiple wells, the λ_{ij} accounts for the weight of this impulse response, and τ_{ij} accounts for the shape of the response. If we try to model the reservoir by a general LTI system, the drawbacks of CM is it only uses one parameter τ to describe the response shape. From a petroleum engineering point of view, it only uses one parameter to characterize the attenuation and delays between each injector-producer well pair. Even in numerical simulations, we can easily see that one parameter is not enough for describing the shape of impulse response [35]. Thus, we develop a new model by relexing the constraints on the impulse response and only assume that the response is finite (which is reasonable for physical phenomenon). This leads us to the finite-impulse-response (FIR) model.

This model can be built directly from the general LTI system description: suppose we have M injectors and N producers in the ROI, the FIR model can be written the same as (2.7) and (2.8), where now the length of impulse response is limited to L (which means the response is finite). That is, the model can be expressed as

$$y_j(t) = y_j(t_0) + \sum_{i=1}^{M} u'_{ij}(t) \tag{2.7}$$

with

$$u'_{ij}(t) = u_i(t) * h_{ij}(t) = \int_{\xi=0}^{L} u_i(t-\xi) h_{ij}(\xi) d\xi. \tag{2.8}$$

The (2.7) and (2.8) represents the basic FIR model, where the production rate of each well depends on its surrounding injectors and is captured by the finite impulse response. The FIR model can be approximated to other predictive models, provided that the response length of the FIR model L is large enough. But the penalty of doing this is also obvious: it may requires an unnecessarily large number of parameters. This will be discussed in more detail in Chapter 3.

2.3.1 Discrete Model

For any predictive model, history matching on performance data is a necessary step for estimating parameters in the models. Injection and production rates are measured by sampling, so discrete models are preferable in general. For FIR model, we discretize the integrals in (2.8) leading to

$$y_j(n) = y_j(n_0) + \sum_{i=1}^{M} u'_{ij}(n) \tag{2.9}$$

and

$$u'_{ij}(n) = u_i(n) * h_{ij}(n) = \sum_{m=0}^{L-1} u_i(n-m)h_{ij}(m) \tag{2.10}$$

where L is the length of $h_{ij}(n)$, and n is the discrete index, $n \in Z$. As in the continuous case, 2.9 and 2.10 state that the total production rate at time n is a function of the primary production component and the injection history between n and $n - L + 1$.

After constructing the FIR model, the next step is to estimate the unknown parameters in the model. We will discuss a general approach for training the model parameters in Section 2.6.

2.4 Distributed Capacitance Model

In (2.3) and (2.4), the pressure support that helps maintain production rates at producers is denoted as the average pressure in the reservoir. The "average" pressure accounts for the averaging effects which are caused by the whole interwell region of the reservoir, including any heterogeneity and discontinuity in-between. If the reservoir between injector-producer pair includes some heterogeneity, such as the presence of some high permeability channels, fractures or faults, the analytic solution of CM [64] should be modified to take the heterogeneity into consideration. To address this, we consider a new representative element, which is constructed by one injector and one producer with a fracture or high permeability channel in-between. This is illustrated in Fig. 2.3. The high permeability channel divides the interwell region into two parts, and for each part, we can derive the material balance differential equation with a linear injectivity (productivity) equation, similar to CM. Mathematically, the equations in first region can be expressed as:

$$u(t) - u_f(t) = c_{t1} V_{p1} \frac{d\overline{P}_1}{dt} \tag{2.11}$$

where c_{t1} is the compressibility of the first interwell region; V_{p1} is the drainage pore volume for this region; $\overline{P}_1$ is the average pressure in V_{p1}; $u(t)$ is the injection rate and $u_f(t)$ is the total liquid flowing from this region to the high permeability channel. The linear injectivity equation for this region can be expressed as:

$$u_f = J_1 \overline{P}_1 \tag{2.12}$$

where J_1 is the injectivity index of the injector. Similarly, we can derive equations for the second region:

$$u_f(t) - y(t) = c_{t2} V_{p2} \frac{d\overline{P}_2}{dt} \tag{2.13}$$

and

$$y = J_2 \left(\overline{P}_2 - P_{wf} \right) \tag{2.14}$$

where J_2 is the productivity index and P_{wf} is the flowing bottom hole pressure (BHP) of the producer. (2.11), together with (2.13), state that the net rates of mass depletion from the drainage volume are proportional to the change of average pressure in the first and second regions, respectively. Combining these four equations and eliminating the average pressure $\overline{P}_1$ and $\overline{P}_2$, we get:

$$\tau_1 \tau_2 \frac{d^2 y}{dt^2} + (\tau_1 + \tau_2) \frac{dy}{dt} + \tau_1 \tau_2 J_2 \frac{d^2 P_{wf}}{dt^2} + \tau_2 J_2 \frac{dP_{wf}}{dt} = u(t) - y(t) \tag{2.15}$$

where τ_1 and τ_2 are the "time constant" of the drainage volume similar to the definition of CM. They are defined by:

$$\tau_1 = \frac{c_{t1} V_{p1}}{J_1} \text{ and } \tau_2 = \frac{c_{t2} V_{p2}}{J_2} \tag{2.16}$$

Although the $\frac{dP_{wf}}{dt}$ term appeared explicitly in capacitance model, pressure data are often not available on a daily basis in real fields. For most applications, researchers assume that the changes in BHP are slow compared to the fluctuations in injection and production rates. Thus we assume that the terms relating to $\frac{d^2 P_{wf}}{dt^2}$ and $\frac{dP_{wf}}{dt}$ are close to zero and can be removed from the equation. Note that our new proposed model still has the ability to incorporate the BHP data when they are available. It

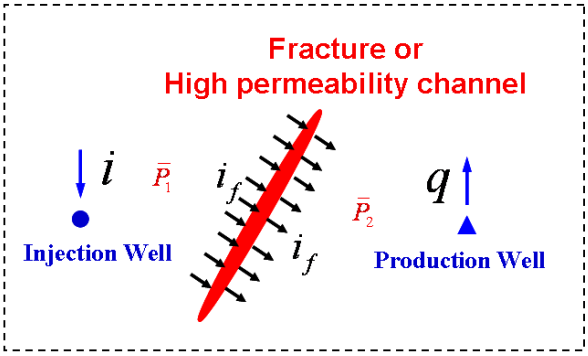

Figure 2.3: Representative element for distributed capacitance model. There is a high permeability channel between the injector and producer.

only needs to re-derive the equations to include these terms, but this is out of the scope of most daily applications so we just skip the derivations here.

After removing the BHP terms, (2.15) is a linear second order differential equation with constant coefficients, and the solution is well-known:

$$y(t) = \begin{cases} \left[c_1 e^{\frac{-t}{\tau_1}} + c_2 e^{\frac{-t}{\tau_2}}\right] + \frac{1}{\tau_1 - \tau_2}\left[\int_0^t e^{\frac{\xi - t}{\tau_1}} u(\xi) d\xi - \int_0^t e^{\frac{\xi - t}{\tau_2}} u(\xi) d\xi\right] & \text{if } \tau_1 \neq \tau_2 \\ \left[c_1 e^{\frac{-t}{\tau_1}} + c_2 t e^{\frac{-t}{\tau_1}}\right] + \frac{1}{\tau_1^2}\int_0^t (t - \xi) e^{\frac{\xi - t}{\tau_1}} u(\xi) d\xi & \text{if } \tau_1 = \tau_2 \end{cases} \tag{2.17}$$

The case $\tau_1 = \tau_2$ rarely happens in real geological situations. Thus here we discuss the latter case without the loss of generality. In this case, the first term accounts for the primary production associated with the total gross production; the second term is the contribution from the injected water and describes the interactions between injection and production rates. Note that (2.17) is the basic form of the model.

The impact from injected water can be shown more clearly in terms of convolution between injection rate and a particular shaped function; that is, we can rewrite (2.17) as:

$$y(t) = \left[c_1 e^{\frac{-t}{\tau_1}} + c_2 e^{\frac{-t}{\tau_2}}\right] + u(t) * \left[\frac{1}{\tau_1 - \tau_2}\left(e^{\frac{-t}{\tau_1}} - e^{\frac{-t}{\tau_2}}\right)\right] \tag{2.18}$$

and from a system point of view, the impulse response $h(t)$ can be expressed as:

$$h(t) = \frac{1}{\tau_1 - \tau_2}\left(e^{\frac{-t}{\tau_1}} - e^{\frac{-t}{\tau_2}}\right) \tag{2.19}$$

The influence of water injection in the injection history is described by the time constants τ_1 and τ_2. The time constants, similar to CM, can be seen a direct measurement of dissipation of the pressure waves between injector-to-fracture and fracture-to-producer. As an illustration, Fig. 2.4 shows $h(t)$ with several different τ_1 and τ_2. If one of the values of τ is small, the model behaves just like the original CM; otherwise, the new model leads to a "smoother" response than CM, as shown in Fig. 2.4.

As in Section 2.3.1, in order to apply this model to real field applications, it should be discretized with some selected discretization interval. The discrete version of the model is given by:

$$y(n) = \left[c_1 e^{\frac{-n}{\tau_1}} + c_2 e^{\frac{-n}{\tau_2}}\right] + \frac{1}{\tau_1 - \tau_2}\left[\sum_{k=0}^{n} e^{\frac{k-n}{\tau_1}} u(k) - \sum_{k=0}^{n} e^{\frac{k-n}{\tau_2}} u(k)\right] \tag{2.20}$$

(2.20) can also be written in terms of convolution between injection rate and impulse response function:

$$y(n) = \left[c_1 e^{\frac{-n}{\tau_1}} + c_2 e^{\frac{-n}{\tau_2}}\right] + u(n) * h(n) \tag{2.21}$$

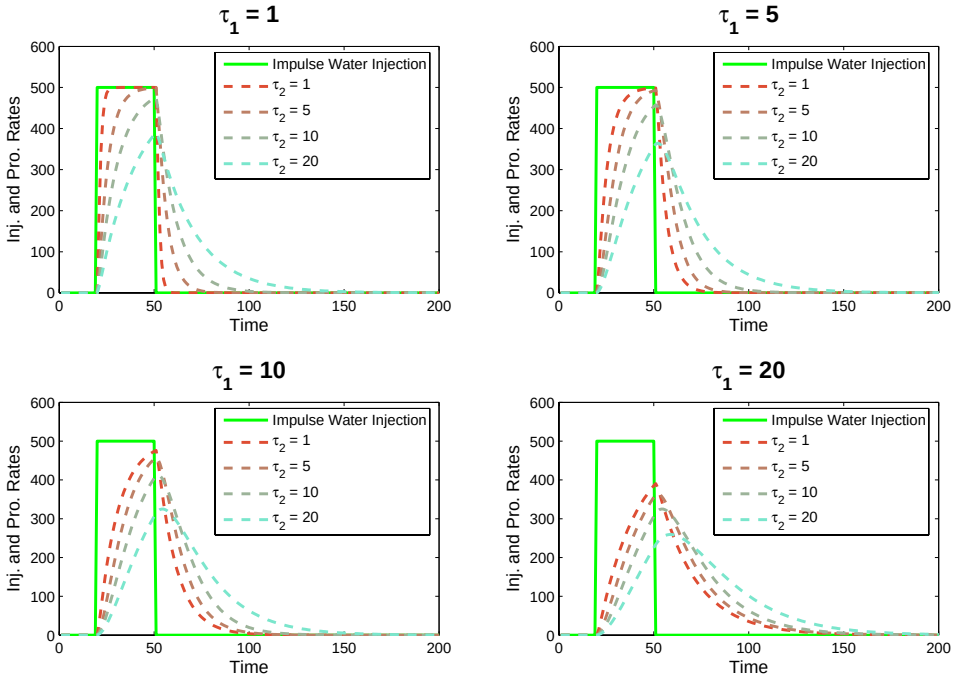

Figure 2.4: Impulse response curves of distributed capacitance model for different τ_1 and τ_2. The injected water of injector is also shown.

where the impulse response function $h(n)$ is defined by

$$h(n) = \frac{1}{\tau_1 - \tau_2}\left(e^{\frac{-n}{\tau_1}} - e^{\frac{-n}{\tau_2}}\right) \tag{2.22}$$

As in the continuous case, (2.21) states the total production rate at time step n can be divided into two components. The first term accounts for the primary depletion of the production rates, and the second term is the contribution of injected water.

In general, there are many injectors and producers in a reservoir. The production rates at one producer are often supported by several surrounding injectors. So we need to generalize our proposed model to the multiple producers and injectors case.

Given M injection wells and N production wells in the ROI, we use coefficients or weights λ_{ij} with $i = 1, 2, ..., M$ and $j = 1, 2, ..., N$ in order to capture the fact

that one producer is supported by more than one injector (similar to CM). Putting these weights into the expression, the generalized model between the producer j and the M surrounding injectors can be expressed as

$$y_j(n) = c_1 e^{\frac{-n}{\tau_p}} + \sum_{i=1}^{M} \lambda_{ij} i_i(n) * h_{ij}(n) \tag{2.23}$$

The first term accounts for the primary production of this producer, and represented by an exponential decay function of "total effect" time constant τ_p. The impulse response function for this well pair, $h_{ij}(n)$, is defined as

$$h_{ij}(n) = \frac{1}{\tau_{ij1} - \tau_{ij2}} \left(e^{\frac{-n}{\tau_{ij1}}} - e^{\frac{-n}{\tau_{ij2}}} \right) \tag{2.24}$$

τ_{ij1} and τ_{ij2} are two parameters which represent the dissipation of pressure wave between injector i and producer j when this well pair is the only active well pair in the reservoir. (2.23), together with (2.24), represent the distributed capacitance model for the multiple wells case.

For the estimation of model parameters, see Section 2.6.

2.4.1 Interpretation of Model

This model can be seen as a cascading of two CMs, that is, where the output of first CM becomes the input of the second CM, and these two CMs are combined together to form a bigger system, as shown in Fig. 2.5. This is because we can see the each interwell region in the considered scenario (see Fig. 2.3) as a relative homogeneous region, and separated by some discontinuous region (e.g., high permeability channel in Fig. 2.3). It is this interpretation that led us to call this model as **Distributed Capacitance Model** (DCM).

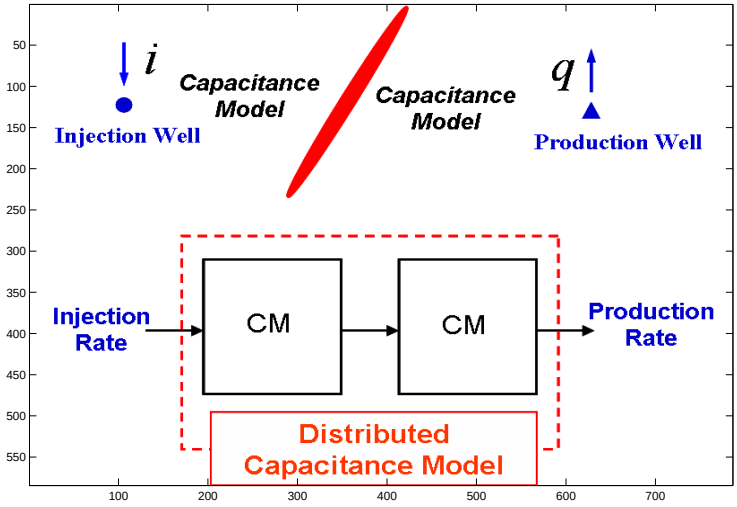

Figure 2.5: Interpretation of distributed capacitance model in terms of CMs.

Thus, DCM can also be interpreted in terms of some particular geological features. For example, if the reservoir has many layers and the injection wells and production wells are in different layers, they must communicate with each other by passing some interface between different layers. These layers may be relatively homogeneous, so the total communication path can be seen as the pressure passing two different regions, which means the path is heterogeneous even though each region is homogeneous. In these kinds of situations, the proposed DCM is more suitable than CM because it accounts for some heterogeneity between the interwell regions. Moreover, DCM will behave similarly to CM when one of the parameters τ is small, so DCM can be seen as a generalized version of CM.

2.5 Multivariate ARX Model

For all proposed models up to now, the production rates are described as a linear combination of some filtered version of injection rates from surrounding injection

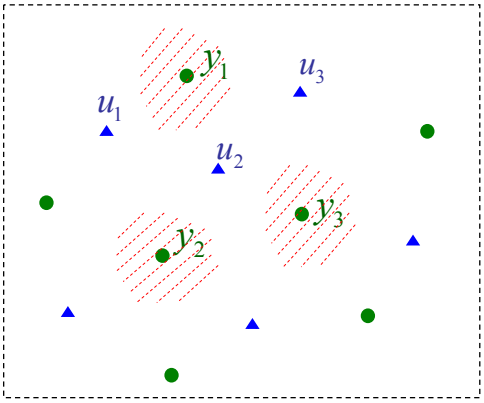

Figure 2.6: Scenario with multiple injection and production wells. The red shadow areas represent the pore volume related to that producer.

wells. Generally speaking, in this kind of approaches, the influences from other producers are approximated by the injection rates of injection wells. This means that the influence a producer on neighboring producers is ignored and the production rates are modeled only as a function of injectors in the reservoir. To achieve a better estimation, we develop a multivariate autoregressive with extra inputs (M-ARX) model in [33] to take the producer-to-producer interactions into account.

Most predictive models first consider a 1-injector/1-producer scenario, and then extend the derived relationship to multiple injectors and producers using the superposition principle. In this kind of approach, every producer is treated independently. To account for this producer-to-producer influence, we will follow a derivation similar to that leading to the CM in [64], but considering the whole reservoir including multiple injectors/producers.

We consider a ROI in the reservoir with M injectors and N producers, as shown in Fig. 2.6. For the region close to a given producer j, the material balance equations are given by a set of differential equations:

$$\begin{cases} c_t V_{p1} \dfrac{d\bar{P}_1}{dt} &= \displaystyle\sum_{i=1}^{M} \alpha_{1i} u_i(t) - \sum_{j=1}^{N} \beta_{1j} y_j(t) \\ c_t V_{p2} \dfrac{d\bar{P}_2}{dt} &= \displaystyle\sum_{i=1}^{M} \alpha_{2i} u_i(t) - \sum_{j=1}^{N} \beta_{2j} y_j(t) \\ &\vdots \\ c_t V_{pN} \dfrac{d\bar{P}_N}{dt} &= \displaystyle\sum_{i=1}^{M} \alpha_{Ni} u_i(t) - \sum_{j=1}^{N} \beta_{Nj} y_j(t) \end{cases} \tag{2.25}$$

where V_{pj} with $j = 1, ..., N$ is the drainage pore volume related to producer j; $\bar{P}_j$ is the average pressure in V_{pj}. α_{ki} and β_{kj} with $k = 1, ..., N$ are the weight factors for injection rates $u_i(t)$ and production rates $y_j(t)$, respectively. This set of equations is similar to the material balance equation of CM as shown in (2.3). Note that for ROIs with closed boundaries, we will also have that $\sum_{k=1}^{M} \alpha_{ki} = 1$ and $\sum_{k=1}^{N} \beta_{kj} = 1$, but for most practical use scenarios for the model, these conditions often no longer hold because of the open boundary around the ROI. We also use a linear productivity model to change the pressure variables in the set of equations into rates. This set of linear productivity model equations can be expressed as

$$\begin{cases} y_1(t) &= J_1(\bar{P}_1 - P_{1,wf}) \\ y_2(t) &= J_2(\bar{P}_2 - P_{2,wf}) \\ &\vdots \\ y_N(t) &= J_N(\bar{P}_N - P_{N,wf}) \end{cases} \tag{2.26}$$

where $P_{j,wf}$ with $j = 1, ..., N$ is the flowing bottom-hole-pressure (BHP) of producer j and J_j is the productivity index of that producer. Substituting for the average pressure in (2.25) using (2.26), we get

$$\begin{cases} \tau_1 \dfrac{dy_1(t)}{dt} + \tau_1 J_1 \dfrac{dP_{1,wf}(t)}{dt} & = & \displaystyle\sum_{i=1}^{M} \alpha_{1i} u_i(t) - \sum_{j=1}^{N} \beta_{1j} y_j(t) \\ & \vdots & \\ \tau_N \dfrac{dy_N(t)}{dt} + \tau_N J_N \dfrac{dP_{N,wf}(t)}{dt} & = & \displaystyle\sum_{i=1}^{M} \alpha_{Ni} u_i(t) - \sum_{j=1}^{N} \beta_{Nj} y_j(t) \end{cases} \tag{2.27}$$

where τ_j with $j = 1, ..., N$ is the "time constant" of the drainage volume of producer j and is defined by

$$\tau_j = \frac{c_t V_{pj}}{J_j} \tag{2.28}$$

In (2.27), the BHP terms $\dfrac{dP_{j,wf}(t)}{dt}$ are often set to zero because we assume that the BHPs are changing slowly, as compared to the changes in injection and production rates, as discussed in Section 2.4. This assumption is important in practical uses of the model because for many fields the BHP information is often not available. Therefore most injector-producer modeling techniques make this assumption. For techniques that can be used in situations where large variations of BHP occur, refer to [30].

Here we assume that changes in BHPs are negligible, and divide each of the equalities in (2.27) by its corresponding τ_j, so that (2.27) becomes

$$\begin{cases} \dfrac{dy_1(t)}{dt} & = & \displaystyle\sum_{i=1}^{M} b_{1i} u_i(t) - \sum_{j=1}^{N} a_{1j} y_j(t) \\ & \vdots & \\ \dfrac{dy_N(t)}{dt} & = & \displaystyle\sum_{i=1}^{M} b_{Ni} u_i(t) - \sum_{j=1}^{N} a_{Nj} y_j(t) \end{cases} \tag{2.29}$$

We define a set of variables $b_{ki} = \alpha_{ki}/\tau_j$ and $a_{kj} = \beta_{kj}/\tau_j$. The equalities in (2.29) are the 1^{st}-order multivariate autoregressive model with some extra inputs (1^{st}-order M-ARX model). The order of the model refers to the maximum order of the differential operator (a first order differential operator is used in (2.29)) This modeling approach is well-known in time series analysis and system identification research [28] [52]. For convenience, the M-ARX model is often expressed in matrix form. Let $\mathbf{y}$ and $\mathbf{u}$ represent the production rate and injection rate vectors, respectively; that is,

$$\mathbf{y}(t) = [y_1(t) \quad y_2(t) \quad ... \quad y_N(t)]^T \tag{2.30}$$

and

$$\mathbf{u}(t) = [u_1(t) \quad u_2(t) \quad ... \quad u_M(t)]^T \tag{2.31}$$

We also define two coefficient matrices $\mathbf{A}$ and $\mathbf{B}$ as

$$\mathbf{A}_c = \begin{bmatrix} a_{11} & \cdots & a_{1N} \\ \vdots & \ddots & \vdots \\ a_{N1} & \cdots & a_{NN} \end{bmatrix} \tag{2.32}$$

$$\mathbf{B}_c = \begin{bmatrix} b_{11} & \cdots & b_{1M} \\ \vdots & \ddots & \vdots \\ b_{N1} & \cdots & b_{NM} \end{bmatrix} \tag{2.33}$$

where $\mathbf{A}_c$ is N by N and $\mathbf{B}_c$ is N by M and the subscript c denotes the continuous model. Thus, (2.29) can be expressed in matrix form as

$$\frac{d\mathbf{y}(t)}{dt} + \mathbf{A}_c\mathbf{y}(t) = \mathbf{B}_c\mathbf{u}(t) \tag{2.34}$$

where $\mathbf{A}_c$ represents the "characteristic" of the autoregressive behavior of the system, while $\mathbf{B}_c$ represents the weighting coefficients from the system inputs $\mathbf{u}$.

2.5.1 Discrete Model

Discretizing (2.29), we can get the following expression

$$\mathbf{y}(k+1) = -\mathbf{A}\mathbf{y}(k) + \mathbf{B}\mathbf{u}(k) \tag{2.35}$$

The matrices $\mathbf{A}$ and $\mathbf{B}$ are both coefficient matrices and correspond to the autoregressive behavior and the input weights of the system, respectively. (2.35) shows that the production rate of any producer at time instant $t = k+1$, can be computed in terms of two factors: one that depends on ALL production rates at time instant $t = k$; the other on the injection rates at $t = k$. This means that the system outputs (production rates) are described by both the new inputs (injection rates) and a feedback loop from the outputs of the previous time instant, as shown in Fig. 2.7.

After the M-ARX model is built, the next step is to estimate the unknown coefficients in the model. For the model training process, please refer to Section 2.6.

2.6 Finding the Model Parameters

To estimate the unknown model parameters, the most common approach is to try to "fit" the observed data using a quadratic function of the fitting-errors [41]. Suppose

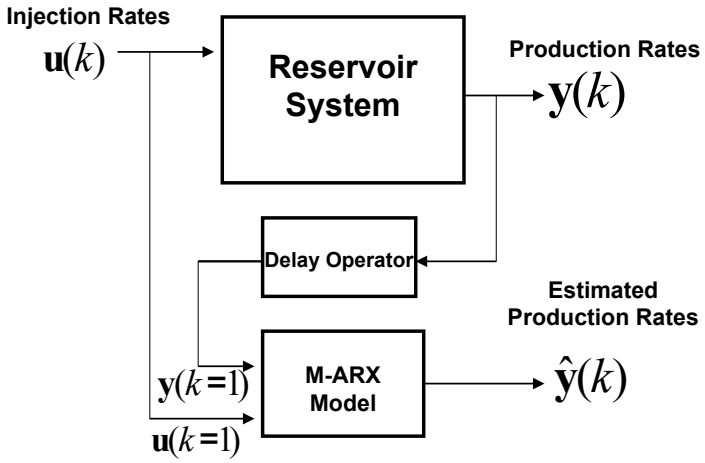

Figure 2.7: Diagram of the modeling process of M-ARX model.

we have a model `M` with some parameter vector $\boldsymbol{\theta}$, then we try to minimize the following criterion:

$$V_K(\boldsymbol{\theta}) = \frac{1}{2K} \sum_{k=1}^{K} \left[\mathbf{y}(k) - \hat{\mathbf{y}}(k|\boldsymbol{\theta})\right]^T \left[\mathbf{y}(k) - \hat{\mathbf{y}}(k|\boldsymbol{\theta})\right] \tag{2.36}$$

where $\hat{\mathbf{y}}(k|\boldsymbol{\theta})$ denotes the vector of predicted production rates at time k under model `M` with parameter value $\boldsymbol{\theta}$. For example, for CM, $\boldsymbol{\theta}$ is

$$\boldsymbol{\theta} = \left[\lambda_{11} \quad ... \quad \lambda_{MN} \quad \tau_{11} \quad ... \quad \tau_{MN}\right]^T \tag{2.37}$$

For each particular value of $\boldsymbol{\theta}_*$, we have a corresponding $V_K(\boldsymbol{\theta}_*)$, so the optimization procedure is basically searching the minimum value over a space with dimension $M \times N \times 2$. This can be achieved by some iterative search methods, such as gradient or steepest-descent method. For further reference, see [41].

The above procedure discusses the general approach for estimating model parameters. In our work, this method still involves many computations and we only follow some simpler procedure from [63]. That is, we first start from $\tau_{ij} = 0.1$ to 30 with increasing 0.1 each time. For each fixed τ_{ij}, the remaining parameters in criterion $V_K(\boldsymbol{\theta})$ are λ_{ij}s, which can be solved by multiple linear regression. After iterating among all possible τ_{ij}, we choose the parameter set which has the minimum value of V_K as the optimization results. For DCM, We also follow the same procedure, with iterating among both $\tau_{ij,1}$ and $\tau_{ij,2}$ now.

The optimization procedure of (2.36) is a nonlinear optimization problem. To solve these kinds of problems is often computationally expensive and no global minimum solutions can be guaranteed. On the other hand, both the FIR and M-ARX models have the property of being "linear-in-the-parameter", which means that the parameters are linear on the criterion function (for a discussion of the linear-in-the-parameters property of models, see [23]). This allows the use of linear regression techniques for parameter estimation. To see this, we take the M-ARX model as an example (the procedure for FIR model is similar). We first define a parameter matrix as follows:

$$\boldsymbol{\theta} = [\mathbf{A} \quad \mathbf{B}]^T \tag{2.38}$$

and the vector of regressors (regression vector) as

$$\varphi(k) = \begin{bmatrix} -\mathbf{y}(k-1) \\ \mathbf{u}(k-1) \end{bmatrix} \tag{2.39}$$

So that the predicted production rate values at time k become

$$\hat{\mathbf{y}}(k|\boldsymbol{\theta}) = \boldsymbol{\theta}^T \varphi(k) \tag{2.40}$$

and the minimization of the criterion

$$V_K(\boldsymbol{\theta}) = \frac{1}{2K}\sum_{k=1}^{K}\left[\mathbf{y}(k) - \boldsymbol{\theta}^T\varphi(k)\right]^T\left[\mathbf{y}(k) - \boldsymbol{\theta}^T\varphi(k)\right] \tag{2.41}$$

can be seen as N different linear regressions, corresponding to each row of $\boldsymbol{\theta}^T$, all with the same regression vector $\varphi(k)$. Thus minimizing (2.41) will be equivalent to solving the N linear regressions.

2.7 Summary

In this chapter, we have developed three different predictive models. The first one was the FIR model, which allows very flexible modeling of the shape of impulse response using a set of unknown parameters. The second model, DCM, was developed as a generalization of CM, which can deal with more heterogeneous scenarios. Then we also proposed the third model, M-ARX model, to address the interactions between producers to producers to facilitate the model building, which is deficient in consideration for previous models. Finally, we discuss a general approach for estimating the model parameters, and the linear-in-the-parameters property was also pointed out.

Chapter 3

Model Validation and Comparison

In this chapter, we first discuss the model validation issue. The central question is: after building the model, how can we determine whether the model is suitable for field applications or not? Do we have any validation step to double-check the model we just built? To answer these questions, we will discuss two different approaches to validate a predictive model in the reservoir: the first is trying to validate models based on their prediction ability; another is trying to validate models by interpreting the model parameters and comparing them to known geological features (or characteristics estimated from other approaches).

The information we have used for building models up to now is often purely statistical, with only limited physical knowledge involved. In order to build a stronger model, we also investigate the use of "grey-box" modeling approach on predictive models. The grey-box approach refers to integrating some physical knowledge into optimization procedures. Finally, we provide a comparative analysis by proposing a prediction-error metric under various scenarios. Some noise sensitivity analysis is also performed to deal with situations encountered in real fields. From the simulation results, together with the theoretical discussions, we make some suggestions for reservoir engineers to use the predictive models on field applications.

3.1 Validation of Models

To test whether a predictive model is suitable or not, there are two common approaches: the first approach is to evaluate its prediction ability. This can be achieved by validation on a given data set. The second approach is to validate by the interpretation of parameters. This can be achieved by comparing the estimated parameters against the theoretical values of the synthetic data or known geological features of the real fields. We will discuss both validation procedures in the section.

To examine whether a built model is suitable for a physical system, the most natural approach is to evaluate model behavior on a fresh data set that has not been used for training [57]. Thus, given a historic data set, we can separate it into two data sets: the estimation (or training) data set and the validation (or testing) data set. We first estimate the model parameters on the estimation data set, then compute and measure the error on the validation data set. In addition, we can use this validation procedure to evaluate different predictive models and favor the model that shows the better prediction performance on a fresh data set. This leads to the quantitative comparisons between models, which will be discussed later in this chapter.

A second way to evaluate a model is to first estimate the model parameters, which are often related to some characteristics of inter-well region, such as permeability or porosity, and then compare the estimated values against the ground truth or some known geological features (of real field data). Although sometimes only qualitative comparisons are available, this kind of evaluation highlights one very important practical usage of model: it can be used to indicate and estimate some important reservoir characteristics of the reservoir. In our problem, the most

important reservoir characteristics are the static gains between each input-output pair in the system. The static gains between well pairs are interpreted as the effective contribution from a particular injector to a specific producer, and are given different names by different authors, e.g., interwell connectivity in the context of CM [64] [54]; injector-producer relationships for Kalman filter approaches [39] [67]; effective flow units for active method and FIR model [34] [35]. The reader should keep in mind that although these are different names, they all refer to the static gain of the system, and we will use these terms interchangeably in our work.

The static gains are easy to calculate for different predictive models. For CM and DCM, the static gain between the i-th injection well (input i) and the j-th production well (output j) is denoted as λ_{ij} and appears in the models explicitly. For FIR model, λ_{ij} can be estimated as:

$$\lambda_{ij} = \sum_{n=0}^{L-1} h_{ij}(n). \tag{3.1}$$

For the 1^{st} order M-ARX model, the static gain λ_{ij} can be estimated easily from z-domain. To see this, we apply the z-transform in (2.29) and get:

$$z\mathbf{Y}(z) = -\mathbf{A}\mathbf{Y}(z) + \mathbf{B}\mathbf{U}(z) \tag{3.2}$$

where $\mathbf{Y}(z)$ and $\mathbf{U}(z)$ are the z-transforms of $\mathbf{y}(k)$ and $\mathbf{u}(k)$, respectively. Then we can write the relationship between $\mathbf{Y}(z)$ and $\mathbf{U}(z)$ as:

$$\begin{aligned} \mathbf{Y}(z) &= (z\mathbf{I} + \mathbf{A})^{-1}\mathbf{B}\mathbf{U}(z) \\ &= \left(\mathbf{I} + \mathbf{A}z^{-1}\right)^{-1}\mathbf{B}z^{-1}\mathbf{U}(z), \end{aligned} \tag{3.3}$$

where $\mathbf{I}$ denotes the N by N identity matrix. (3.3) uses the matrix fraction description (MFD) for the transfer function matrix between $\mathbf{Y}(z)$ and $\mathbf{U}(z)$. For detailed discussions about MFD, see [28]. The frequency domain representation can be obtained by setting $z = e^{j\omega}$ where ω denotes the angular frequency. By definition, the static gain (interwell connectivity) represents the cumulative effect of total injection on total production and thus can be computed as the transfer function at $\omega = 0$, i.e., at the zero frequency. In z-domain, the zero frequency corresponds to $z = 1$ and if we substitute this into (3.3) we obtain

$$\left.\frac{\mathbf{Y}(z)}{\mathbf{U}(z)}\right|_{z=1} = (\mathbf{I} + \mathbf{A})^{-1}\,\mathbf{B}, \tag{3.4}$$

which can be interpreted as follows: once the M-ARX model parameter matrices $\mathbf{A}$ and $\mathbf{B}$ have been computed, the interwell connectivities are represented by the N by M matrix $(\mathbf{I} + \mathbf{A})^{-1}\,\mathbf{B}$, in which the element on j-th row and i-th column denotes the interwell connectivity between injector i and producer j. This shows the M-ARX model can be used to estimate the interwell connectivity, as can be done for other predictive models.

3.2 Simulation Setting

In this section, we will validate and compare different models using using a numerical flow-simulator, named CMG [42], under various scenarios. To make it more clear, we summarize in Table 3.1.

For the pattern of injection and production wells, we use three different patterns: (1) five-spot with five injectors and four producers (Scenarios A and B); (2) line-drive with six injectors and three producers (Scenarios C and D); (3) peripheral

Table 3.1: Simulation Settings for CMG simulator.

Scenario	Inj. & Pro. Pattern	Permeability Map	Inj. Rate
A	five-spot	channel (Fig. 3.1)	From [63] (Fig. 3.6)
B	(5-inj./4-pro.)	streak (Fig. 3.2)	
C	line-drive	homogeneous (Fig. 3.3)	
D	(5-inj./4-pro.)	multiple fractures (Fig. 3.4)	
E	peripheral injector	hydraulic fractures	one injector
F	(8-inj./6-pro.)	(Fig. 3.5)	step (Fig. 3.7)
G			variable (Fig. 3.8)

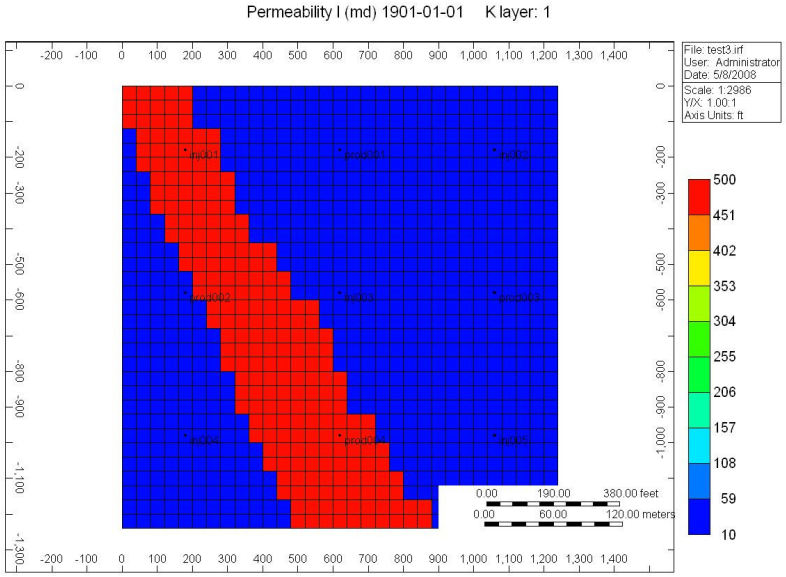

Figure 3.1: Permeability map for channel case (Scenario A). Note that Producer 4 is included in the high permeability area.

injectors with 8 injectors and 6 producers (Scenarios E, F, and G). It constructs with all producers close to the center and surrounded by injectors.

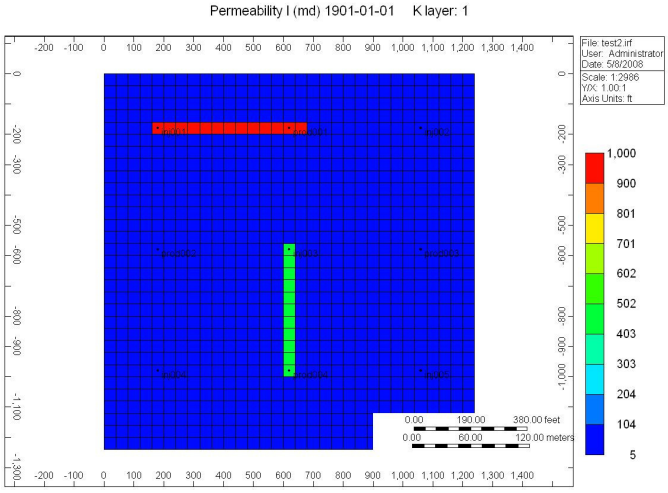

Figure 3.2: Permeability map for streak case (Scenario B). Note that well pairs $I1$-$P1$ and $I3$-$P4$ are connected by high permeability channels.

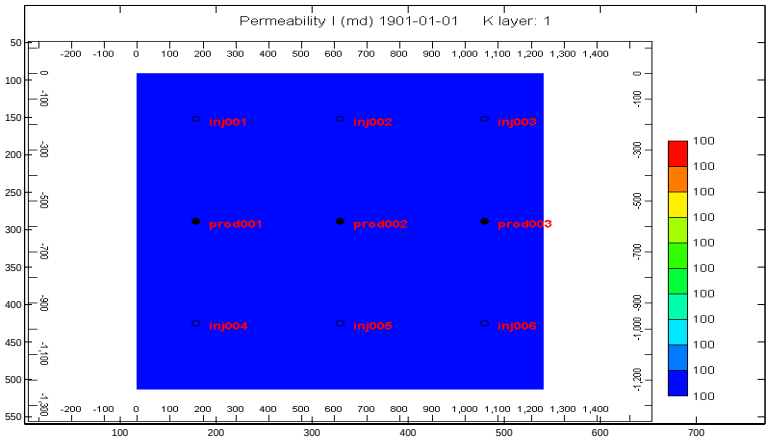

Figure 3.3: Permeability map for homogeneous case (Scenario C).

3.2.1 Permeability Map

For the five-spot pattern, we test two different permeability maps: (1) channel case, where there is a large area passing through Producer 4 with permeability of 500 md and the background permeability is of 10 md; (2) streak case: there are two high

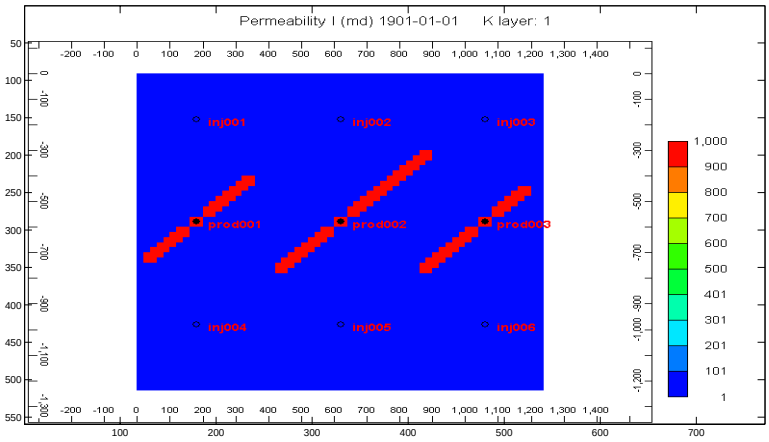

Figure 3.4: Permeability map for multiple fractures case (Scenario D).

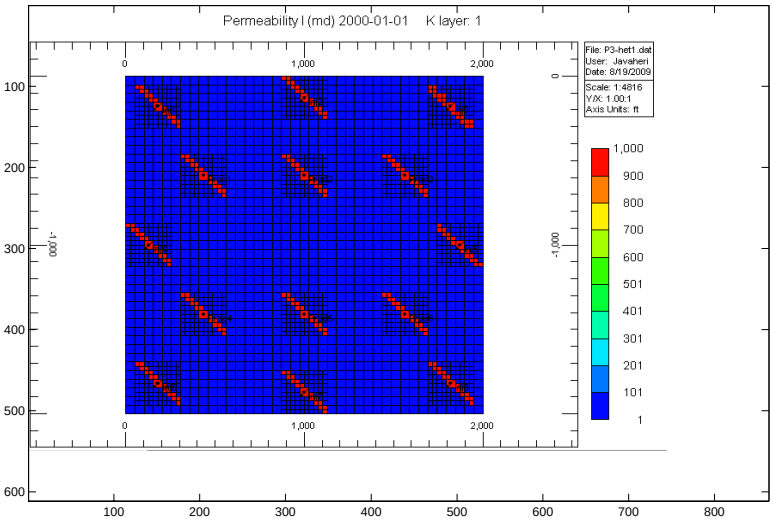

Figure 3.5: Permeability map for Scenarios E, F, and G.

permeability streaks passing through $I1$ to $P1$ and $I3$ to $P4$, and they are with permeability of 1000 md and 500 md, respectively (Fig. 3.2).

For the line-drive pattern, it also has two different permeability settings: (1) homogeneous case: there is an isotropic permeability of 100 md for all directions

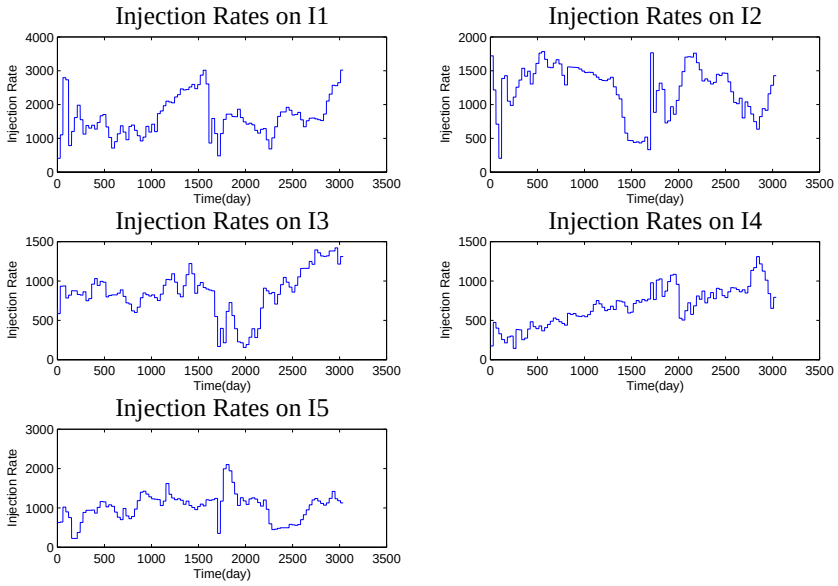

Figure 3.6: Injection rates for Scenarios A-D. For Scenarios C and D, we randomly generate the injection rates for Producer 6.

(Fig. 3.3); (2) multiple fractures case: there are three fractures (high permeability channels) of permeability 1000 md passing through the production wells with different lengths and all lay in about 45 degree direction (Fig. 3.4).

For the peripheral injectors pattern (Scenarios E, F, and G), the reservoir has a background permeability of 1 md, and there are 14 fractures of 1000 md passing through all injection and production wells, with a 135 degree orientation (3.5). The fractures passing through wells are analogous to the hydraulic fractures.

3.2.2 Injection Rate Setting

For five-spot and line-drive patterns (Scenarios A-D), the injection rates we used are the same as those used in [63], which were obtained from a real oilfield. These rates are shown in Fig. 3.6.

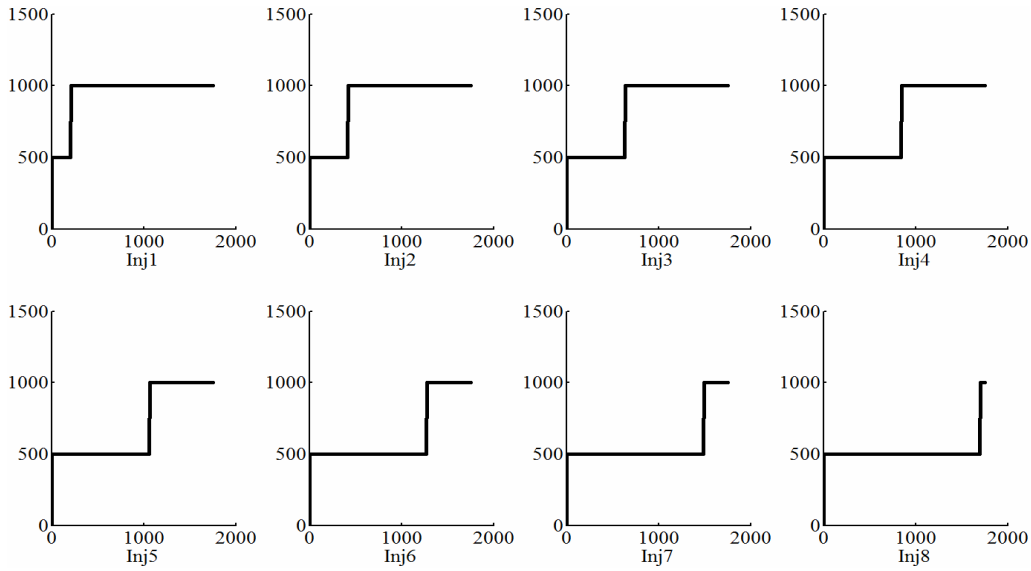

Figure 3.7: Injection rates set for Scenario F. At one time, only one injector changes the injection rate from 500 to 1000 bbl/day.

Injection rates is the only difference between Scenario E, F, and G. For Scenario E, we only inject water into one injector at a time and observe the response from other wells, so we denote this scenario as one injector case. For Scenario F, we have a step function in each injector, as shown in Fig. 3.7. We denote this scenario as step case. For Scenario G, each injection rate is set to constant for each 200 days, and all injection rates are made to vary randomly between a predetermined set of values, as shown in Fig. 3.8. This scenario is denoted as variable case. We will discuss why we use three different kinds of injection rates for the peripheral injector pattern in Section 3.3.

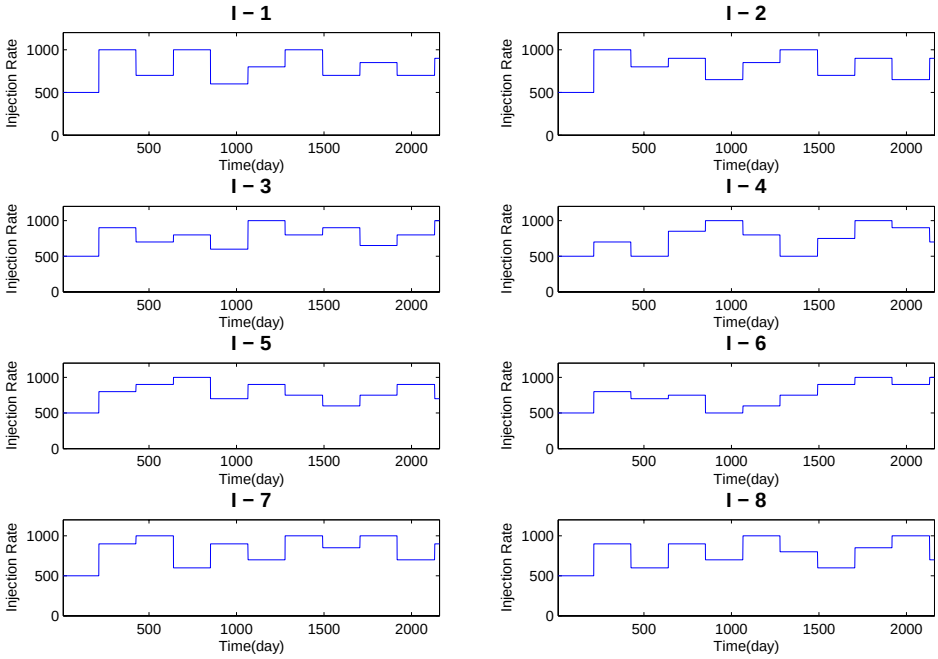

Figure 3.8: Injection rates set for Scenario G.

3.2.3 Other Setting

In all cases we simulate two component water and oil fluid systems, and have only vertical wells, with the sampling interval set to 1 day, that is, assuming that daily data are available. Five-spot and line-drive patterns (Scenarios A-D) simulate a five-layered reservoir, while for the peripheral injectors pattern (Scenarios E, F, and G), we consider one-layered reservoir simulation.

3.3 Validation Results for Interwell Connectivity

In order to validate proposed models, we use the models we built to estimate the static gain (interwell connectivity) of each well pair for Scenarios A and B. The

Table 3.2: Estimated values of interwell connectivity for Scenario A.

	CM				**FIR Model**			
	Pro 1	Pro 2	Pro 3	Pro 4	Pro 1	Pro 2	Pro 3	Pro 4
Inj 1	0.035	0.060	0.020	0.892	0.035	0.060	0.020	0.890
Inj 2	0.182	0.029	0.222	0.567	0.185	0.029	0.226	0.567
Inj 3	0.052	0.045	0.053	0.847	0.048	0.045	0.049	0.847
Inj 4	0.037	0.031	0.018	0.901	0.039	0.031	0.020	0.906
Inj 5	0.042	0.017	0.130	0.809	0.042	0.017	0.129	0.809
	DCM				**M-ARX Model**			
	Pro 1	Pro 2	Pro 3	Pro 4	Pro 1	Pro 2	Pro 3	Pro 4
Inj 1	0.035	0.060	0.020	0.893	0.023	0.063	0.015	0.905
Inj 2	0.182	0.029	0.222	0.566	0.181	0.030	0.222	0.566
Inj 3	0.052	0.045	0.053	0.847	0.083	0.038	0.066	0.812
Inj 4	0.038	0.031	0.018	0.898	0.069	0.025	0.033	0.870
Inj 5	0.042	0.017	0.130	0.811	0.024	0.020	0.121	0.830

Table 3.3: Average absolute differences of interwell connectivities between CM and other models for Scenario A.

Model	Avg. abs. diff. to CM
FIR model	0.0015
DCM	0.0006
M-ARX model	0.0131

results are validated via comparisons with the state-of-the-art approach, CM, and also with the ground truth of the simulators.

For the Scenario A, the total data available are approximately three thousand days. This three thousand days period includes both before and after water breakthrough time. We used 75th to 2074th day, totally 2000 days as the training period, to estimate the static gains (interwell connectivity) of the system. The results are shown in Table 3.2 and Fig. 3.9.

From the results, the estimated interwell connectivities from FIR model, DCM and 1^{st} order M-ARX model are all highly consistent with the values estimated

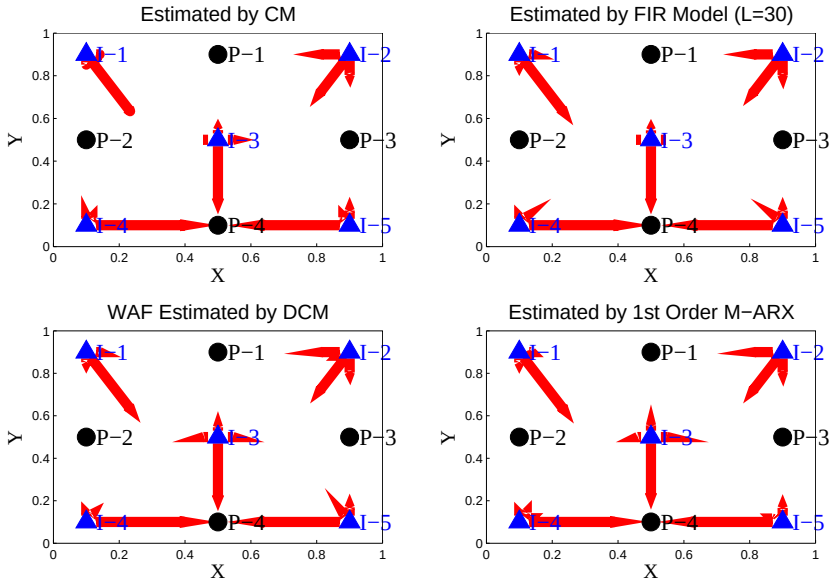

Figure 3.9: Estimated interwell connectivities with different predictive models for Scenario A. Note that the longer arrows, represent the larger values.

from CM. To be more specific, the average absolute differences between CM and other models are shown in Table 3.3. This shows that all predictive models can generate highly consistent results when they are used to estimate the interwell connectivities. If we compare the estimated results against the ground truth of Scenario A (Fig. 3.1), the results are also consistent with qualitative descriptions that can be inferred from the ground truth. For example, because $P4$ is inside the high permeability area, we expect that for all injectors the largest interwell connectivities values will correspond to $P4$, which is the case for the estimated values from all models. This further validates the results we got from all proposed predictive models. Of course, the estimated interwell connectivities could be wrong even if all the results are consistent, so we will provide quantitative verification in the next section.

For the Scenario B, we used the 75th to 2074th days as the training period to estimate the interwell connectivity. The results are shown in Table 3.4 and Fig. 3.10.

Table 3.4: Estimated values of interwell connectivity for Scenario B.

	CM				**FIR Model**			
	Pro 1	Pro 2	Pro 3	Pro 4	Pro 1	Pro 2	Pro 3	Pro 4
Inj 1	0.962	0.012	0.009	0.032	0.961	0.012	0.008	0.029
Inj 2	0.519	0.009	0.179	0.287	0.532	0.009	0.182	0.289
Inj 3	0.101	0.005	0.008	0.899	0.084	0.006	0.003	0.890
Inj 4	0.153	0.167	0.030	0.640	0.161	0.169	0.029	0.640
Inj 5	0.140	0.018	0.170	0.655	0.135	0.018	0.173	0.671
	DCM				**M-ARX Model**			
	Pro 1	Pro 2	Pro 3	Pro 4	Pro 1	Pro 2	Pro 3	Pro 4
Inj 1	0.962	0.012	0.009	0.032	0.966	0.012	0.009	0.030
Inj 2	0.519	0.009	0.179	0.287	0.521	0.009	0.180	0.287
Inj 3	0.101	0.005	0.008	0.898	0.091	0.006	0.006	0.899
Inj 4	0.153	0.166	0.029	0.640	0.149	0.169	0.030	0.646
Inj 5	0.140	0.019	0.171	0.655	0.141	0.017	0.170	0.655

Similar to the Scenario A (channel case), the estimated interwell connectivities from all models are highly consistent with the values estimated from CM. The average absolute differences between CM and other models are shown in Table 3.5. If we compare the results with the ground truth of Scenario B, the estimated values are also consistent with the geological features of the permeability distribution (Fig. 3.2). To see this, we examine the estimated interwell connectivities between $I1$-$P1$ and $I3$-$P4$, which are very large values (close to 1), which indicates high permeability channels exist between these well pairs. In short, both Scenario A and B validate that all proposed predictive models can generate estimated interwell connectivities similar to CM, and that these estimates are consistent with the geological features of the ground truth in the simulations.

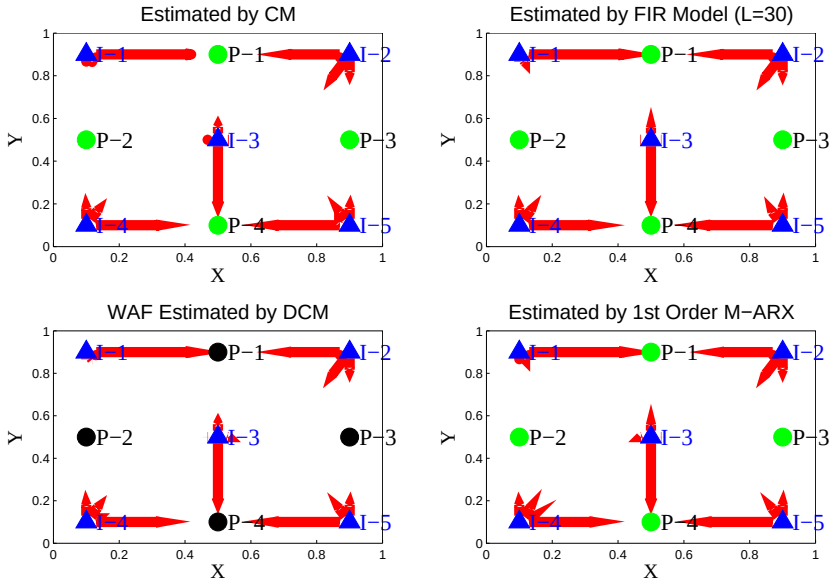

Figure 3.10: Estimated interwell connectivities with different predictive models for Scenario B. Note that the longer arrows, represent the larger values.

Table 3.5: Average absolute differences of interwell connectivities between CM and other models for Scenario B.

Model	Avg. abs. diff. to CM
FIR model	0.0050
DCM	0.0001
M-ARX model	0.0021

3.3.1 Quantitative Verification

To quantitatively verify the estimated interwell connectivities, we consider scenarios E, F, and G, which have different kinds of injection rates. In Scenario E, we shut-in all injectors except for one target injector each time, injecting some constant water into this target injector, then observing the total fluid obtained from each producers. The ratio between the produced fluid and the injected water can be calculated and is a good approximation to the interwell connectivity for the corresponding well pair.

This is because the definition of interwell connectivity is the effective contribution to a producer from a particular injector.

For Scenario F, we keep constant on all injection rates, and only change one injection rate to another constant at each time. The injection rates are shown in Fig. 3.7. As this target injection rate changes to another constant value, we would expect all production rates to increase by different amounts. The ratio between the increased fluid of this producer and the injected amount of water in the injector is also a good approximation to the interwell connectivity for this well pair.

Scenario G is designed for validation of proposed predictive models. The simulation time is 2160 days and we use the data obtained from Scenario G to estimate the interwell connectivities. The estimated values are compared with the value obtained (directly from the simulation data and divisions on the data) from Scenario E and F. Here we only show the estimated interwell connectivities for FIR model, and all other models have similar estimations. The results are shown in Table 3.6 and also plotted in Fig. 3.11. From the results, we found the estimated interwell connectivities are highly consistent with the simulation results, which strongly justifies the use of predictive models for the estimation of interwell connectivity.

3.4 Physical Constraints on Parameters

When the statistical identification techniques are applied assuming a "black box" model structure (i.e., no insights about the physical system are used), sometimes they produce unrealistic results which are not compatible with the underlying physical reality. For example, the use of CM sometimes results in negative interwell connectivity values [64], which contradicts what we expect to be the reservoir behavior. While some models can relate some or all their parameters to the reservoir

Table 3.6: Estimated interwell connectivities from both simulations and FIR model for peripheral injector pattern (Scenario E, F, and G).

	Scenario	Pro 1	Pro 2	Pro 3	Pro 4	Pro 5	Pro 6
	E	0.73	0.14	0	0.025	0	0
Inj 1	F	0.73	0.15	0.05	0.05	0.01	0.00
	G	0.74	0.15	0.05	0.05	0.01	0.00
	E	0.18	0.48	0.27	0.	0	0
Inj 2	F	0.19	0.48	0.28	0.01	0.01	0.00
	G	0.19	0.48	0.28	0.00	0.01	0.00
	E	0	0.13	0.75	0	0	0
Inj 3	F	0.04	0.14	0.75	0.00	0.01	0.05
	G	0.04	0.14	0.75	0.00	0.01	0.05
	E	0.37	0.01	0	0.48	0.04	0
Inj 4	F	0.38	0.05	0.01	0.49	0.06	0.01
	G	0.38	0.04	0.01	0.50	0.06	0.01
	E	0	0.04	0.47	0	0.01	0.38
Inj 5	F	0.01	0.06	0.48	0.01	0.05	0.39
	G	0.01	0.06	0.49	0.01	0.05	0.39
	E	0.01	0	0	0.75	0.13	0
Inj 6	F	0.05	0.01	0.00	0.74	0.14	0.04
	G	0.05	0.01	0.00	0.75	0.15	0.04
	E	0	0	0	0.26	0.48	0.18
Inj 7	F	0.01	0.01	0.01	0.28	0.48	0.20
	G	0.02	0.01	0.01	0.29	0.48	0.20
	E	0	0	0.02	0.01	0.14	0.73
Inj 8	F	0.00	0.01	0.04	0.03	0.13	0.70
	G	0.01	0.01	0.05	0.04	0.16	0.74

characteristics, these parameters can also be constrained by some general physical knowledge. In general, this identification process is often denoted as "grey-box" modeling [61]. In our problem, an important constraint is the static gain between each input-output pair in the system, whose value should be between zero and one. As mentioned before, the static gains between well pairs can be interpreted as the effective contribution from a particular injector to a producer, and should have a non-negative impact that can be no greater than one. Theoretically speaking, the

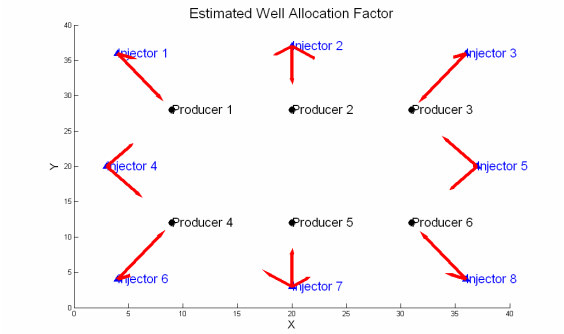

(a) Calculated by Scenario E.

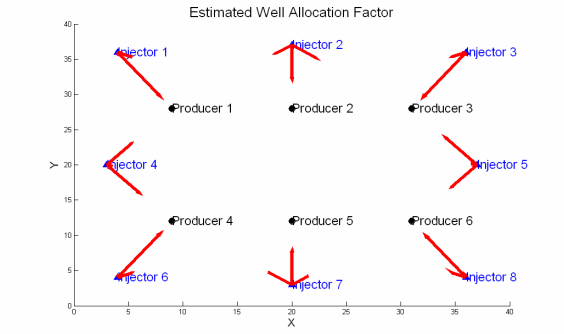

(b) Calculated by Scenario F.

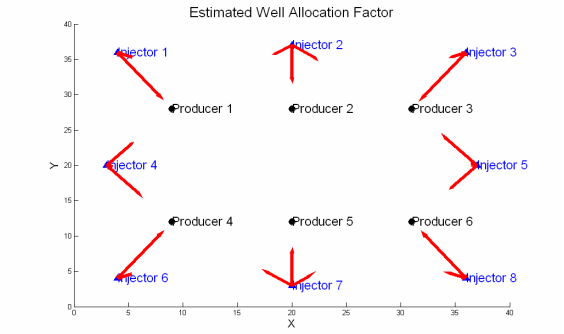

(c) Estimated by FIR model for Scenario G.

Figure 3.11: Estimated interwell connectivities for peripheral injector pattern (Scenarios E, F, and G). Note that the longer arrows, represent the larger values.

constraints on static gains can be applied to all interwell models: the static gains are the zero frequency behavior ($z = 1$ in z-domain) of the system. In other words, the constraints can be written as

$$\mathbf{0} \leq \mathbf{H}(z)|_{z=1} \leq \mathbf{1} \text{ (element-wise)} \tag{3.5}$$

where $\mathbf{H}(z)$ is the z-transform of the matrix of impulse response $\mathbf{h}(n)$. In some models, such as CM, DCM and FIR, the constraints on the system are equivalent to constraints on linear combination of parameters. For example, in FIR model, the constraints become:

$$\mathbf{0} \leq \begin{bmatrix} \sum_{k=0}^{L} h_{11}(k) & \cdots & \sum_{k=0}^{L} h_{M1}(k) \\ \vdots & \ddots & \vdots \\ \sum_{k=0}^{L} h_{1N}(k) & \cdots & \sum_{k=0}^{L} h_{MN}(k) \end{bmatrix} \leq \mathbf{1} \text{ (element-wise)} \tag{3.6}$$

Furthermore, since fluid production cannot be negative, the impulse response cannot be negative at any time, and their sum should also smaller or equal to 1. So that in addition to (3.6), we also have constraints for each FIR coefficient:

$$0 \leq h_{ij}(k) \leq 1 \quad \text{for all } i, j, k. \tag{3.7}$$

For CM and DCM, the static gains correspond to the parameters (λ_{ij}), so the constraints apply to them directly; that is,

$$0 \leq \lambda_{ij} \leq 1 \quad \text{for all } i, j,. \tag{3.8}$$

For these models, the linear constraints on parameters can be integrated into the optimization procedures to have a more reasonable and reliable estimation of model

parameters. Generally speaking, the linear inequality constraints will form a convex set, and if the estimation criterion (2.36) is convex on the parameter vector $\boldsymbol{\theta}$, we can solve the optimization by some general methods from convex optimization [7]. But the optimization work is much too involved. In our work, we extend a simple methods provided by [63]. Taking CM for example, we first assume the τ is given, then the criterion function (2.36) becomes linear on the remaining parameters λ_{ij}. So given the linear constraints on λ_{ij}, we can perform quadratic programming to minimize (2.36). Then we iterate on different possible τ to find the smallest parameter set which has the minimum value of (2.36). For DCM, we can use a similar procedure to estimate the model parameters. For FIR model, because of its "linear-in-the-parameter" property, it is particularly easy to use the linear constraints. Linear objective function with linear constraints can be solved by quadratic programming method [7].

The "grey-box" modeling approaches are particularly preferable when the provided system information is very limited, so that not many training data are available. In these more challenging situations, the black-box approaches often result in models that violate the constraints imposed by some common physical knowledge.

On the contrary, the static gains of the M-ARX model cannot be expressed as a linear combination of its parameters, which makes these kinds of physical constraints much harder to integrate into the M-ARX modeling procedure. For these models, we can only examine the appropriateness of the models by checking the system behaviors in order to determine whether it satisfies the physical constraints.

3.5 Model Comparison

In this section, we perform a comparative analysis of all proposed predictive models (including the state-of-the-art CM work). For all models, the "Grey-box" .approaches are also included if possible. The simulation results, together with some theoretical analysis, leads to some general suggestions for using the predictive models for field applications in the next section.

3.5.1 Number of Parameters

The number of model parameters plays a crucial role for the quality of the model. Basically we would like to include more unknown parameters into the model in order to describe all possible responses for the reservoir, but increasing the number of unknowns also increases the uncertainty for parameter estimation. In particular, the quality of the model may be more easily affected by noise in the observed data. In general, the best model structure for identifying a system is a trade-off between [41]:

- Flexibility: The model structure should provide good capabilities of describing different possible systems. This can be achieved by adding more parameters or putting the parameters in "strategic positions".

- Parsimony: Do not use unnecessarily parameters; the model parameterization should be kept as parsimonious as possible.

Table 3.7 shows the number of parameters used for different interwell models with an example of 5 injectors and 4 producers. From the table, we can see that the FIR model has the largest degree of flexibility with a large number of unknown parameters, while other models have a comparable number of parameters. This

Model	# of Parameters	5-inj/4-pro
CM	$M \times N \times 2$	40
DCM	$M \times N \times 3$	60
z-domain	$M \times N \times 2$	40
FIR	$M \times N \times L$	600 ($L = 30$)
1^{st} order M-ARX	$M \times N + N^2$	36

Table 3.7: Number of parameters used for different models.

means that the FIR model should have worse noise performance than other models, as will be shown by a noise sensitivity analysis in the Section 3.6.1.

3.5.2 Prediction Performance Comparisons

For both theoretical and practical reasons, different predictive models should be evaluated and compared by their prediction ability on observed data that has not been used for training. This is a general methodology known as model validation on fresh data set [41, 57] or out-of-sample forecasts in time series analysis [9, 10].

The quadratic criterion is commonly used for mathematical reasons. Assume we have trained an interwell model with some estimated parameters, denoted as $\mathtt{M}$. Let the predicted production rates on the data set not used for training at time k be denoted as $\hat{\mathbf{y}}(k|\mathtt{M})$, then the prediction error can be expressed as

$$J_{squ}(\mathtt{M}) = \frac{1}{T}\sum_{k=1}^{T} \|\mathbf{y}(k) - \hat{\mathbf{y}}(k|\mathtt{M})\|^2 \tag{3.9}$$

where T is the number of data points in the validation data set. Although this is mathematically convenient, for practical field applications it is often more appropriate to define an error metric that captures the relative error. Defining the absolute difference between the predicted and actual rates:

$$J_{abs}(\mathtt{M}) = \frac{1}{TN} \sum_{k=1}^{T} \sum_{j=1}^{N} |y_j(k) - \hat{y}_j(k|\mathtt{M})| \,, \tag{3.10}$$

a normalized performance measurement R_{abs} can be defined as

$$R_{abs} = \frac{J_{abs}(\mathtt{M})}{\frac{1}{TN} \sum_{k=1}^{T} \sum_{j=1}^{N} |y_j(k)|}. \tag{3.11}$$

This measurement can be interpreted as the "average ratio of errors in prediction" and makes it easy for reservoir engineers to judge if the trained model is "good enough" to use for prediction. We will use (3.11) as the criterion function for our comparisons.

3.6 Comparison Results

We evaluated and compared different models using the simulation data under different scenarios, as indicated in Section 3.2. The grey-box extensions of CM, DCM and FIR model, which impose physical constraints on static gains, are included in our comparisons. In the simulation, we denote the original CM and DCM as the "Unconstrained CM" and "Unconstrained DCM", respectively. The grey-box CM and DCM, we denote as "Constrained CM" and "Constrained DCM", respectively. For the FIR model, we only simulate the grey-box case, which incorporates the

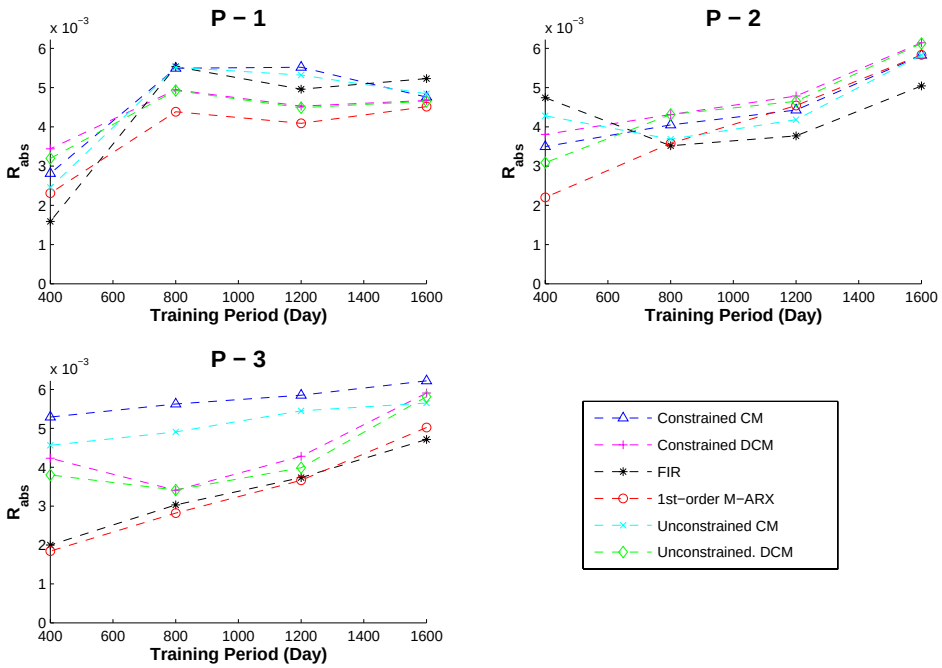

Figure 3.12: Performance evaluation of different models on the Scenario C. All models have reasonably good predictions in this case. Note that $P-1$, $P-2$ and $P-3$ represent the producers 1, 2 and 3, respectively.

physical constraints (3.6) and (3.7) into the model. This is because in some cases, the FIR model without constraints has much worst results than other approaches.

We first show the estimation results using the data from Scenario C (homogeneous case). The simulation time is 2835 days. Various training periods are chosen, and the days after the 1800th are selected as the validation period. The prediction results are evaluated via R_{abs} for all producers, as shown in Fig. 3.12. The results show that all models have reasonably good predictions in this case, with the maximum $R_{abs} \approx 0.006$, i.e., average prediction errors of about 0.6%.

Then we turn to estimation results of the Scenario D (multiple fractures case). The simulation time are the same as we have done in Scenario C, and the results are shown in Fig. 3.13. In this scenario, the 1^{st}-order M-ARX model performs

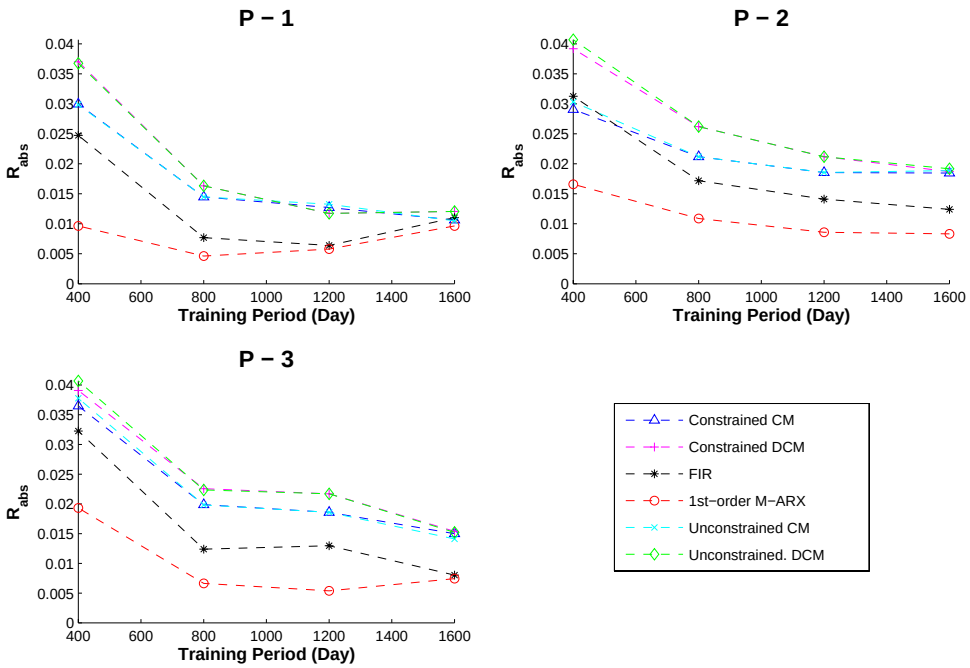

Figure 3.13: Performance evaluation of different models on the Scenario D. From the results, the M-ARX model performs the best for all training periods of all producers, and (constrained) FIR model perform almost in the second place. Note that $P-1$, $P-2$ and $P-3$ represent the producers 1, 2 and 3, respectively.

the best for all training periods of all producers, and (constrained) FIR model perform almost in the second place. The constrained CM and DCM perform slightly better than unconstrained ones, but not too much gain is achieved when taking into consideration physical constraints. If we take producer 2 for example, the M-ARX model achieve $R_{abs} \approx 0.01$ to 0.02, which is less than half the R_{abs} achieved by CM or DCM.

The next simulation is using the setting of Scenario A. Its simulation time is 3040 days, and various training periods of 500, 1000, 1500 days are chosen and the period after 2000 days is used as the validation period. The R_{abs} of prediction results for all producers are shown in Fig. 3.14. From the results, all models have good predictions and the maximum R_{abs} value is about 0.03, which means the

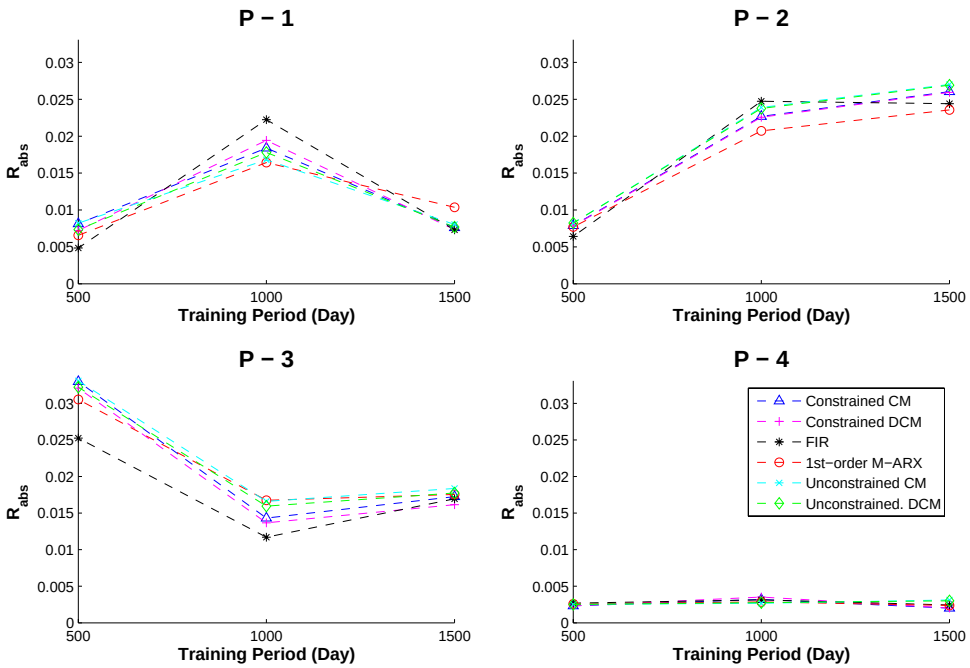

Figure 3.14: Performance evaluation of different models for Scenario A. There is no model that can always outperform the others. Note that $P-1$, $P-2$, $P-3$ and $P-4$ represent the producers 1, 2, 3 and 4, respectively.

maximum average prediction-errors are about 3%. If we compare the performance of different models, there is no model that can always outperform the others, and all are good enough to satisfy most applications.

The last simulation is for the Scenario G (variable injection case). The simulation time is about 2160 days. The training periods are chosen as 600, 1000, 1400 and the period after 1600 days is used as the validation period. For the results, the unconstrained CM and DCM are much worse than other models, sometime leading to totally useless predictions. For example, the R_{abs} for producer 2 using the unconstrained CM is about 33% average prediction errors. This is also the case for modeling via unconstrained DCM. If we consider the static gains (interwell connectivities), we will find that there are many unreasonable values, such as values much

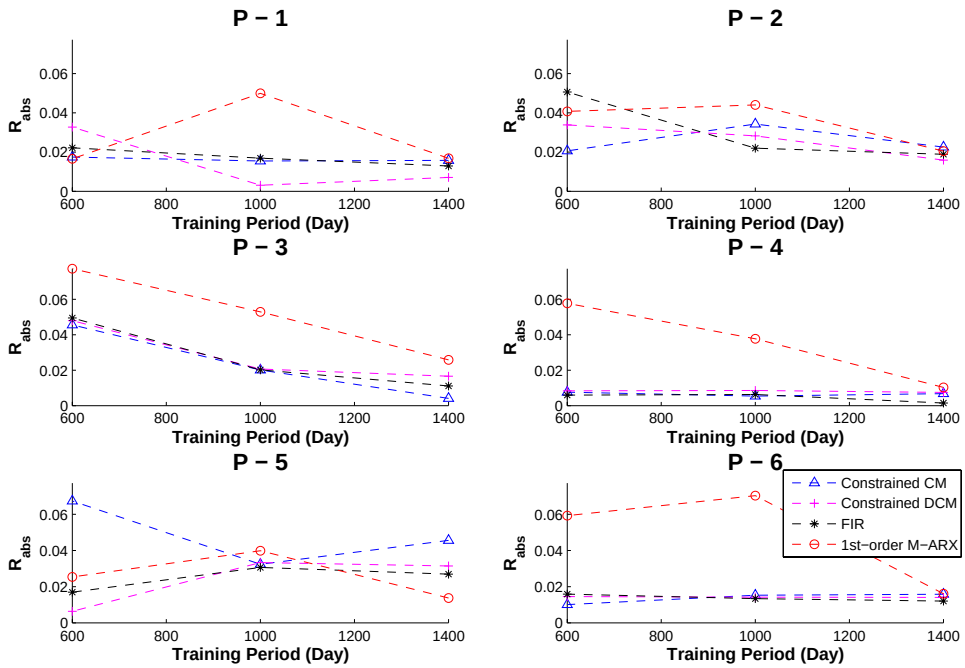

Figure 3.15: Performance evaluation of different models for Scenario G. From the results, the 1^{st} M-ARX model performs worse for most of the situations. Note that $P-1$, $P-2$, $P-3$, $P-4$, $P-5$ and $P-6$ represent the producers 1, 2, 3, 4, 5 and 6, respectively.

higher than 1 or negative values. For the performance, we only show constrained CM and DCM, together with (constrained) FIR model and 1^{st} order M-ARX model, which is shown in Fig. 3.15. As the results shows, the 1^{st} M-ARX model performs worse for most of the situations. This is because the 1^{st} M-ARX model is the only one that does not integrate the physical constraints into the model, while other "constrained" models are built taking this information into consideration. We will discuss why this affects the prediction results for this case in Section 3.7.

3.6.1 Noise Sensitivity Analysis

In real applications, the measured rates often are subject to measurement errors, especially on the producers. To address this kind of problem, we perform a noise sensitivity analysis by adding different levels of white noise (uncorrelated, zero mean and normally distributed) into the production rates and evaluating the performance of different models from this artificial noisy data. Part of this analysis has been done in previous literature, see [64] [33] for details. In this work, we extend this prior work to provide a general evaluation of noise sensitivity for all models. While the white noise does not correspond to what the observed in the real field data, using this analysis can still provides us about the robustness of various models. Because different models have different parameters, we cannot compare the models only by measuring the difference of estimated parameters between noiseless and noisy data. To solve this, we choose the static gains (interwell connectivities or injector-producer relationships) as the comparison basis; that is, we calculate the absolute differences of the static gains estimated by various models between noiseless and noisy data and plot them together.

For the analysis, we choose the data from Scenario A. We add white noise of different energy levels to the production rates. The noise level is measured by the signal-to-noise ratio (SNR) in dB, which is defined as

$$SNR(dB) = 10 \cdot log \frac{P_{signal}}{P_{noise}} \tag{3.12}$$

where P_{signal} and P_{noise} are the signal and noise powers, respectively. Because of the randomness of the noise, we perform 50 realizations (with respect to the white noise) and obtain the average measurement errors. We also include the FIR model

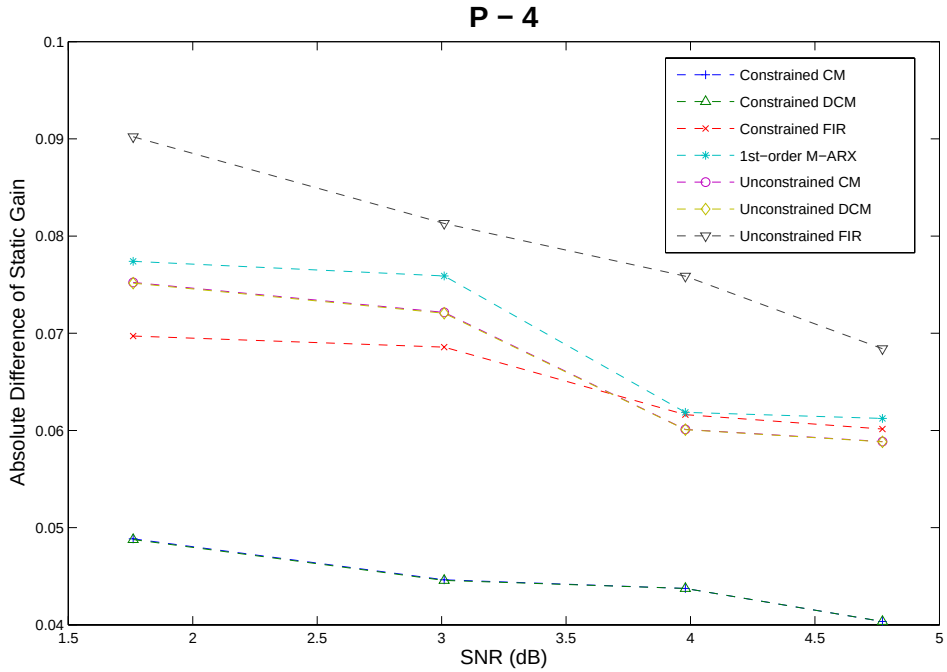

Figure 3.16: Noise sensitivity analysis for different models for Scenario A. The comparisons are made by calculating the average absolute differences of the static gains estimated under noiseless and noisy production rates data.

without using any physical constraints, which is denoted as "unconstrained FIR" model. The results are shown in Fig. 3.16.

From the results, the constrained approaches of a model all outperform the unconstrained version of same model. If we compare unconstrained FIR, CM, DCM and 1^{st} order M-ARX model, or the constrained CM, DCM and FIR model, in both cases the FIR model has the worst performance. This is because the FIR model uses many more parameters than the other models, which increases the estimation uncertainty under noisy environment. The constrained FIR model has similar performance to that of the 1^{st} order M-ARX model, which again shows the power of grey-box modeling approaches. Of course, both constrained CM and DCM have the best performance.

3.7 Discussions

3.7.1 Drawbacks of Purely Statistical Methods

All the interwell models presented in this thesis can be considered as statistical modeling approaches: we try to understand the whole system from only the statistical analysis of the data sent to the system and the data generated by the system. For these kinds of approaches, if the measured input and output data are not "informative" enough to provide sufficient information in order to build reliable models, the models may not able to track the "true" behavior of the system. In this work, the injection rates of Scenario G are different from those of Scenario A-D because they are much more collinear (see [63], [34] and Section 6 for more discussions of collinearity). If we check the static gains estimated by M-ARX model in this case, we will find that there are some negative values between some well pairs. But the static gains estimated by 1^{st} M-ARX model in other cases are all between 0 and 1. In the Scenario G, the designed injection rates are all constant for most of the time, and only change at some time instants. The statistical modeling approach can only gain information when the rates are fluctuating, which means injection data with constant rates is not helpful for building the models. That is the reason why while the 1^{st} M-ARX model has good performance in other cases, but it is not so suitable for Scenario G.

In real field applications, it is not uncommon to face a situation where the given injection and production rates are not informative enough, e.g., the injection rates are often kept relatively constant during normal operations or the training data available are very limited. For all cases, we suggest that it is always better to use the "grey-box" modeling approach by combining physical constraints. For some models it may be difficult to combine the physical constraints into the optimization

procedure, e.g., as in the M-ARX model, it is always a good practice to double-check whether the estimated parameters lead to reasonable reservoir characteristics or not; if the answer is no, we should discard this model and look for other models.

3.7.2 Large Scale Problems

One of the main advantages of using predictive modeling approaches is their ability to describe large scale systems, with computation time significantly lower than that of traditional reservoir simulations. However, applying these predictive models to large reservoirs still presents several challenges. In [62], a good example of applying CM to large scale reservoirs is presented. Most of the procedures discussed in [62] also apply to other predictive interwell models. In this section, we particularly focus on issues associated with dealing with large scale systems.

For any models, the number of unknown parameters increases with the number of injection and production wells in the ROI, which means we will face a large number of system unknowns when applying these techniques to large scale reservoirs. Statistically speaking, given enough data for parameter estimation, including more injectors into the optimization procedure of modeling will often generate a better fit to the historic matching, but sometimes results in an unrealistic and unreliable model. This is because the built models are statistical (even with some physical constraints) without involving any geological considerations. For example, if by coincidence a particular pair of injection and production wells has some common distinct changes during a period of time, they will have relatively large connectivity (static gain) even if they are far away from each other in the reservoir. Common knowledge of the reservoir often assumes that two wells should have very limited interactions if they are far away from each other, except if there exist some special

fractures connecting them. To reduce these kinds of errors, we need to decide a suitable region of interest (ROI) for each producer (or injector). Only injectors and producers in this ROI are considered for building models, and the connectivity of outside wells is assumed to be zero. So now the problem becomes how to decide a suitable ROI. There are several common approaches for this:

- Set a threshold distance for the ROI. So given the target producer (or injector), the ROI is a circle with the radius chose as the threshold. [62]

- Use a similar strategy as the first one but with the shape of the ROI chosen as an ellipse instead of a circle. This situation accounts for some prior field knowledge available which indicates that there are some parallel fractures in the field. The ROI along with the directions of fractures should be the semi-major axis.

- Use a prediction error approach. begin with the target producer, and increase the radius (or semi-major/semi-minor axis) of ROI, which in order to include more and more and increasing number of wells, and use these models for production rate prediction and to calculate the prediction error. When the prediction errors are below some threshold, we use this circle (or ellipse) as ROI [67]

The threshold can be decided based on field experience. It often needs some experience from the reservoir engineers to decide a suitable threshold, and it depends on the field conditions. In [62], 4000 ft was chosen for their target reservoir. The prediction error approach is used because it can provide reasonable prediction for the target producer. This is the approach used by [67]. In short, the prediction error approach may get better prediction results and no field experience is needed.

But as a penalty, much more computation is involved and may still result in large connectivity for well pairs that are far away from each other.

3.7.3 Suggestions for Using Predictive Models

From the above comparative analysis of different models, we can make some suggestions for the use of linear predictive models:

1. Always use historic data for validation of prediction ability before applying any predictive models. This will give us some ideas about how good the models are.

2. Always use the "grey-box" extensions of the models when the physical constraints can be imported into the optimization procedures. For models without grey-box extension, the results should be verified by checking some physical characteristics, e.g., the static gain. If these characteristics are not compatible with the physical reality, we need to discard the model and look for a new one.

3. In terms of computational complexity, we can use the 1^{st} M-ARX model for fast evaluation. Because of the "linear-in-the-parameter" property, the parameters in M-ARX model can be easily estimated by linear regression technique. Then we check the physical characteristics and the prediction errors via cross-validation. If the results are compatible with the physical reality but the prediction errors remain high, it is likely that the linear assumption is not suitable for the field. We should change to other modeling approaches or try the LTV approaches.

4. If the measurement errors of the rate information are high or the injection rates are highly collinear, the "constrained" CM/DCM approaches are preferable as they require fewer parameters and are more robust.

3.8 Summary

In this chapter, we discussed the verification and comparisons of predictive models. For verification, there are two schemes used in this work. The first one is verification via prediction ability on fresh data set. The second one is via the interpretation of interwell connectivity against ground truth (synthetic data) or some geological features (field data). We also discussed the so-called "grey-box" approach of predictive models, the advantages of using it are investigated. Finally, we defined a prediction-error based metric and compare all proposed predictive models. Some suggestions for reservoir engineers are made from the results of comparative analysis.

Chapter 4

Linear Modeling Framework

Having evaluated and compared different models, some theoretical questions about statistical modeling remain open: what is the relation between the different models? Is there a unified framework that can include all models? Are there alternative models with similar or better performance?

In this chapter, we develop a linear modeling framework that allows us to integrate all predictive models proposed to date. Different predictive models are expressed as special cases of this framework. Also, the relationships between different models become much clearer when we use this framework.

4.1 Linear Models for Well Interactions

Suppose we have M injection wells with the sequence of injection rates at the i-th injector denoted as $u_i(k)$, and N production wells with the sequence of production rates at the j-th producer denoted as $y_j(k)$, where k denotes the time index for the measurement data of rates. We also assume the system behavior can be approximated as being linear. If the system response does not change for a period of

time, i.e., it can be seen as time-invariant, the linear model can be expressed using a rational transfer function via z-transform:

$$\begin{bmatrix} Y_1(z) \\ \vdots \\ Y_N(z) \end{bmatrix} = \begin{bmatrix} \frac{C_{11}(z)}{D_{11}(z)} & \cdots & \frac{C_{M1}(z)}{D_{M1}(z)} \\ \vdots & \ddots & \vdots \\ \frac{C_{1N}(z)}{D_{1N}(z)} & \cdots & \frac{C_{MN}(z)}{D_{MN}(z)} \end{bmatrix} \begin{bmatrix} U_1(z) \\ \vdots \\ U_M(z) \end{bmatrix}, \tag{4.1}$$

which can be written in matrix form as:

$$\mathbf{Y}(z) = \mathbf{G}(z)\mathbf{U}(z) \tag{4.2}$$

where $U_i(z)$ and $Y_j(z)$, $i = 1, ..., M$ and $j = 1, ..., N$, are the z-transforms of $u_i(k)$ and $y_j(k)$, respectively. $C_{ij}(z)$ and $D_{ij}(z)$ are polynomial functions of z. Another commonly used description is the matrix fraction description (MFD) for multivariate systems [28], which is analogous to the rational transfer function of univariate (single-input and single-output) systems. In the MFD, (4.2) can be expressed as:

$$\mathbf{Y}(z) = \left[\mathbf{D_L}(z)^{-1}\mathbf{N_L}(z)\right]\mathbf{U}(z) \tag{4.3}$$

$$= \mathbf{U}(z)\left[\mathbf{N_R}(z)\mathbf{D_R}(z)^{-1}\right] \tag{4.4}$$

where all $\mathbf{D_L}(z)$, $\mathbf{N_L}(z)$, $\mathbf{N_R}(z)$ and $\mathbf{D_R}(z)$ are all matrices where each element is a polynomial function of z. (4.3) is called left MFD, and (4.4) is called right MFD. $\mathbf{D_L}$, $\mathbf{D_R}$ are analogous to the denominator in the univariate case, and similarly $\mathbf{N_L}$, $\mathbf{N_R}$ are analogous to the numerator. We will use MFD for model description when it is more convenient.

Although various predictive modeling approaches have been proposed since 2006 [64] [39] [35] [33], we propose for the first time that all these predictive modeling for describing the interactions between wells can be seen as special cases of the linear time-invariant (LTI) models of (4.2) or (4.3). Although in this thesis only LTI systems are discussed, all the models can be extended to linear time-varying (LTV) systems, where now the parameter estimation methods become recursive in nature [41] and continuously update the current estimate. The transfer function representation of LTV systems are much more involved and out of the scope for this paper. For a reference about more details on the transfer function representation of LTV systems, see [4].

Also we need to note that although the behavior of many physical systems, including reservoirs, is nonlinear, it is still useful to approximate the system first using linear models. As we will show in the simulation results, the numerical flow simulator we use [42] makes no linearity assumptions, but its results can be reasonably matched and predicted using some LTI modeling approaches. Moreover, the LTV system is related to linearization of a nonlinear system around a certain trajectory [41], although we do not exploit the possibility of tracking nonlinear behavior in this work. In this work, we mainly focus on the linear modeling for LTI systems.

4.2 A Framework for Predictive Models

In this section, we focus on putting the models introduced in Chapter 3 into the transfer function matrix representation to show that they are actually a special case of linear modeling approach. Using this linear modeling framework, we can

also extend the existing models to higher order and interpret the model parameters easily.

4.2.1 Capacitance Model

As introduced in Section 2.2, in discrete form, the CM can be expressed as [64]

$$y(k) = \quad y(0)e^{\frac{-k}{\tau}} + \frac{1}{\tau}\sum_{\xi=0}^{k} e^{(\xi-k)/\tau}u(\xi) \tag{4.5}$$

where τ accounts for the attenuation and delays between wells. Applying the z-transform and assuming that the initial state is negligible at the time when a waterflood project begins, i.e., that production is essentially almost zero at that time, we can compute the transfer function in z-domain as:

$$Y(z) = \frac{1}{1 - e^{\frac{-1}{\tau}}z^{-1}}U(z), \tag{4.6}$$

which shows that in CM, there is a pole located at $z = e^{-1/\tau}$.

The CM can be easily extended to the multiple wells case using the superposition principle [64]. In this case, the z-domain expression for the transfer function becomes:

$$\begin{bmatrix} Y_1(z) \\ \vdots \\ Y_N(z) \end{bmatrix} = \begin{bmatrix} \frac{\lambda_{11}}{1-e^{\frac{-1}{\tau_{11}}}z^{-1}} & \cdots & \frac{\lambda_{M1}}{1-e^{\frac{-1}{\tau_{M1}}}z^{-1}} \\ \vdots & \ddots & \vdots \\ \frac{\lambda_{1N}}{1-e^{\frac{-1}{\tau_{1N}}}z^{-1}} & \cdots & \frac{\lambda_{MN}}{1-e^{\frac{-1}{\tau_{MN}}}z^{-1}} \end{bmatrix} \begin{bmatrix} U_1(z) \\ \vdots \\ U_M(z) \end{bmatrix} \tag{4.7}$$

where λ_{ij} with $i = 1, ..., M$ and $j = 1, ..., N$ are the weight factors (interwell connectivity). The time constants τ_{ij}, extended from single injector/producer case, play a role as a pole (at $z = e^{\frac{-1}{\tau_{ij}}}$) between the i-th input and j-th output. This shows

that CM is a special case of the general LTI model (4.1), which possesses one pole for each injector-producer well pair.

Besides, because the interpretation of CM in terms of reservoir characteristics has been fully discussed in [63] [64] (also see Section 2.2 for a brief discussion), this gives us a way to connect the transfer function representation to the characteristics in the reservoir. A pole in transfer function representation can be interpreted as the resistive and capacitance effects of the interwell region, since this is an interpretation that has been proposed for the CM. Moreover, the location of the pole is $e^{\frac{-1}{R_{ij}C_{ij}}}$, where R_{ij} and C_{ij} represent the equivalent resistive and capacitance effects between injector i and producer j, respectively.

4.2.2 Distributed Capacitance Model

In the distributed capacitance model (DCM) introduced in Section 2.4, for the single injector and single producer case, the production rates can be expressed as

$$q(k) = \left[c_1 e^{\frac{-k}{\tau_1}} + c_2 e^{\frac{-k}{\tau_2}}\right] + \frac{1}{\tau_1 - \tau_2}\left[\sum_{\xi=0}^{k} e^{\frac{\xi-k}{\tau_1}} u(\xi) - \sum_{\xi=0}^{k} e^{\frac{\xi-k}{\tau_2}} u(\xi)\right] \tag{4.8}$$

where τ_1 and τ_2 account for the attenuation and delays of the regions between wells, and are analogous to the time constant τ in CM. We can easily derive the corresponding transfer function in the z-domain:

$$Y(z) = \frac{1}{(1 - e^{\frac{-1}{\tau_1}} z^{-1})(1 - e^{\frac{-1}{\tau_2}} z^{-1})} U(z) \tag{4.9}$$

This shows that DCM leads to a transfer function with two poles at $z = e^{\frac{-1}{\tau_{ij,1}}}$ and $z = e^{\frac{-1}{\tau_{ij,2}}}$ in order to describe the injector-to-producer relationships. Comparing (4.9) to (4.6), it is clear that DCM is equivalent to cascading two CMs, with time

constants τ_1 and τ_2, respectively [32]. Similar to CM, the DCM can be extended to the multiple wells case using the superposition principle, so that the transfer function becomes

$$\begin{bmatrix} Y_1(z) \\ \vdots \\ Y_N(z) \end{bmatrix} = \begin{bmatrix} \frac{\lambda_{11}}{(1-e^{\frac{-1}{\tau_{11,1}}}z^{-1})(1-e^{\frac{-1}{\tau_{11,2}}}z^{-1})} & \cdots & \frac{\lambda_{M1}}{(1-e^{\frac{-1}{\tau_{M1,1}}}z^{-1})(1-e^{\frac{-1}{\tau_{M1,2}}}z^{-1})} \\ \vdots & \ddots & \vdots \\ \frac{\lambda_{1N}}{(1-e^{\frac{-1}{\tau_{1N,1}}}z^{-1})(1-e^{\frac{-1}{\tau_{1N,2}}}z^{-1})} & \cdots & \frac{\lambda_{MN}}{(1-e^{\frac{-1}{\tau_{MN,1}}}z^{-1})(1-e^{\frac{-1}{\tau_{MN,2}}}z^{-1})} \end{bmatrix} \begin{bmatrix} U_1(z) \\ \vdots \\ U_M(z) \end{bmatrix} \tag{4.10}$$

where λ_{ij} with $i = 1, ..., M$ and $j = 1, ..., N$ have the same meaning as in CM and can also be interpreted as the interwell connectivities in the reservoir. The time constants $\tau_{ij,1}$ and $\tau_{ij,2}$ are extended from single well pair case and model the two poles at $z = e^{\frac{-1}{\tau_{ij,1}}}$ and $z = e^{\frac{-1}{\tau_{ij,2}}}$ between the i-th input and j-th output. In general, the DCM behaves as a second-order (two poles) LTI system for each input-output pair, where the numerators are described by a constant (zero-order) now.

4.2.3 Double Pole Model [39]

The double pole model (initially introduced in [39] with the name of "z-domain model") is a two parameter auto-regressive model for the single well pair case. In this case, the transfer function of the model can be expressed in z-domain as

$$H(z) = \frac{\gamma z^{-1}}{(1 - \alpha z^{-1})^2} \tag{4.11}$$

where γ and α are the unknown parameters. Obviously, this model describes the system behavior with a double pole at α and a weight coefficients γ. Similar to CM

and DCM, this model can be extended to the multiple wells case by the superposition principle and expressed as

$$\begin{bmatrix} Y_1(z) \\ \vdots \\ Y_N(z) \end{bmatrix} = \begin{bmatrix} \frac{\gamma_{11}}{(1-\alpha_{11}z^{-1})^2} & \cdots & \frac{\gamma_{M1}}{(1-\alpha_{M1}z^{-1})^2} \\ \vdots & \ddots & \vdots \\ \frac{\gamma_{1N}}{(1-\alpha_{1N}z^{-1})^2} & \cdots & \frac{\gamma_{MN}}{(1-\alpha_{MN}z^{-1})^2} \end{bmatrix} \begin{bmatrix} U_1(z) \\ \vdots \\ U_M(z) \end{bmatrix} \tag{4.12}$$

If we compare (4.12) with (4.10), we can see that double pole model is a special case of DCM, where now the two poles in DCM overlap and become a double pole ($e^{-1/\tau_{ij,1}} = e^{-1/\tau_{ij,2}} = \alpha_{ij}$). The weight factors γ_{ij} in double pole model play similar roles as λ_{ij} in CM and DCM, all indicating the static gains of the system (different names are used by different authors: interwell connectivity in CM [64] and DCM; injector-producer relationship in double pole model [39] [67]). This also means that the z-domain model can be interpreted and related to some reservoir characteristics in a similar way as the DCM.

4.2.4 Finite-Impulse-Response Model

As the finite-impulse-response (FIR) model introduced in Section 2.3, the production rates of j-th producer can be expressed as

$$y_j(k) = \sum_{i=1}^{M} u_i(k) * h_{ij}(k) \tag{4.13}$$

where $h_{ij}(k)$ with $k = 0, 1, ..., L-1$ denotes the impulse response of producer j from the i-th injector, which describe the response curve between this input-output pair. The shape of the impulse response can be easily interpreted in terms of some characteristics of the reservoir, see [35] and Section 2.3 for more details.

For the multiple wells, the transfer function of FIR model is expressed as

$$\begin{bmatrix} Y_1(z) \\ \vdots \\ Y_N(z) \end{bmatrix} = \begin{bmatrix} \sum_{k=0}^{L-1} h_{11}(k)z^{-k} & \cdots & \sum_{k=0}^{L-1} h_{M1}(k)z^{-k} \\ \vdots & \ddots & \vdots \\ \sum_{k=0}^{L-1} h_{1N}(k)z^{-k} & \cdots & \sum_{k=0}^{L-1} h_{MN}(k)z^{-k} \end{bmatrix} \begin{bmatrix} U_1(z) \\ \vdots \\ U_M(z) \end{bmatrix}, \quad (4.14)$$

which is a special case of (4.1). This is easily seen by setting $C_{ij}(z)$ equals to $h_{ij}(0) + ... + h_{ij}(L-1)z^{-L+1}$ and $D_{ij}(z) = 1$ for all $i = 1, ..., M$ and $j = 1, ..., N$. So the FIR model belongs to general LTI system with no poles in each well pair.

Moreover, the FIR model can approximate any LTI system provided that the impulse length L is long enough. To see this, we know that each pole can be expressed as an infinite series. For example, in the discrete model, suppose we have a pole at $z = \alpha$ with $|\alpha| < 1$, this pole can be expressed as

$$\frac{1}{1 - \alpha z^{-1}} = 1 + \alpha z^{-1} + \alpha^2 z^{-2} + \alpha^3 z^{-3} + ... \quad (4.15)$$

So each fractional polynomial of z for the i-th input and j-th output can be expressed as

$$\begin{aligned} \frac{C_{ij}(z)}{D_{ij}(z)} &= \frac{C_{ij}(z)}{(1 - \alpha_1 z^{-1})...(1 - \alpha_p z^{-1})} \\ &= C_{ij}(z)(1 + \alpha_1 z^{-1} + \alpha_1^2 z^{-2} + ...)(...)(1 + \alpha_p z^{-1} + \alpha_p^2 z^{-2} + ...) \quad (4.16) \\ &= h_{ij}(0) + h_{ij}(1)z^{-1} + h_{ij}(2)z^{-2} + h_{ij}(3)z^{-3} + ... \end{aligned}$$

here we assume $D_{ij}(z)$ was expressed by p poles $\alpha_1, ..., \alpha_p$ and the last equality holds because $C_{ij}(z)$ is also a polynomial of z. For a stable system, the coefficients h_k converge to zero asymptotically, with the rate depending on the dominant pole (the absolute value of the pole which is closest to the unit circle). Suppose we truncate

the infinite series at $k = L - 1$, this new set of coefficients $\{h_i j(k) | k = 0, ..., L - 1\}$ are the unknown parameters in (4.13), which will be determined from the training data. So this justifies that the FIR model can approximate any possible response within some estimation errors provided the FIR length L is long enough. But the penalty is also obvious: many more unknown parameters are needed than for other models.

4.2.5 Multivariate ARX Model

As for the Multivariate Auto-Regressive with eXogenous (M-ARX) model introduced in Section 2.5 (here we all refer to first-order M-ARX model) for describing injection and production relationships, it can be expressed as

$$\begin{bmatrix} y_1(k) \\ \vdots \\ y_N(k) \end{bmatrix} = \mathbf{A} \begin{bmatrix} y_1(k-1) \\ \vdots \\ y_N(k-1) \end{bmatrix} + \mathbf{B} \begin{bmatrix} u_1(k-1) \\ \vdots \\ u_M(k-1) \end{bmatrix} \tag{4.17}$$

where $\mathbf{A}$ and $\mathbf{B}$ are N by N and N by M coefficient matrices, respectively, which are independent of time index k for a LTI system. (4.17) shows that the production rates at time k can be expressed as a linear combination of both injection and production rates at time $k - 1$. In z-domain, (4.17) becomes

$$\mathbf{Y}(z) = Az^{-1}\mathbf{Y}(z) + \mathbf{B}z^{-1}\mathbf{U}(z) \tag{4.18}$$

Then the transfer function matrix representation becomes

$$\mathbf{Y}(z) = \left(\mathbf{I} - \mathbf{A}z^{-1}\right)^{-1} \mathbf{B}z^{-1}\mathbf{U}(z) \tag{4.19}$$

This expression is obviously the left MFD (4.3) with $\mathbf{D_L}(z) = \mathbf{I} - \mathbf{A}z^{-1}$ and $\mathbf{N_L}(z) = \mathbf{B}z^{-1}$. In other words, the 1^{st} order M-ARX model is a special case of (4.3), with now all elements in denominator matrix $\mathbf{D_L}(z)$ with maximum order of z^{-1}.

As we will show in the Section 5.1, when the coefficient matrix $\mathbf{A}$ is diagonal, the 1^{st}-order M-ARX model will reduce to the capacitance-resistive model with one time constant for each producer (CRMP), which is a special case of CM [54]. In general, the off-diagonal terms of matrix $\mathbf{A}$ are not zeros, which means the 1^{st}-order M-ARX model uses the production rates from other producers, together with the injection rates, in order to estimate the future value of the production rates.

4.2.6 Higher Order Models

By putting all interwell models into the transfer function matrix representation, we can easily extend the interwell models to higher orders. When we try to characterize the reservoir behavior with higher order LTI models (4.2) or (4.3), we basically introduce more poles to describe the system. From the CM [64] and (4.6), the location of each pole can be interpreted as some capacitance and resistive effects in the reservoir. So when higher order models are involved, this can be seen as modeling the reservoir by cascading a series of small fluid-capacitors and fluid-resistors, which implies high heterogeneity along the path of a particular well pair. Although high order models have the potential to describe a broader range of possible systems, there is also a penalty for using them: the number of unknown parameters in these models increases. For more discussions on issues related to number of parameters issue, please refer to Section 3.5.1.

Table 4.1: Different predictive models and the characteristics of their transfer function.

Model	Transfer func.	Pole # and location
CM	$\frac{\lambda_{ij}}{1-e^{\frac{-1}{\tau_{ij}}}z^{-1}}$ (each pair)	One at $z = e^{\frac{-1}{\tau_{ij}}}$
DCM	$\frac{\lambda_{11}}{(1-e^{\frac{-1}{\tau_{ij,1}}}z^{-1})(1-e^{\frac{-1}{\tau_{ij,2}}}z^{-1})}$ (each pair)	Two at $z = e^{\frac{-1}{\tau_{ij,1}}}$ and $z = e^{\frac{-1}{\tau_{ij,2}}}$
Double Pole Model	$\frac{\gamma_{11}}{(1-\alpha_{11}z^{-1})^2}$ (each pair)	Two at $z = \alpha_{ij}$ (double-pole)
FIR Model	$\sum_{k=0}^{L-1} h_{ij}(k)z^{-k}$ (each pair)	No Pole
M-ARX Model	$(\mathbf{I} - \mathbf{A}z^{-1})^{-1}\mathbf{B}z^{-1}$	Depends on $\mathbf{A}$

4.3 Conclusion

In this chapter, we use the general transfer function for LTI system to show that each model belongs to a special case of this model, which means all proposed models are linear models. Moreover, the relationship between different models is investigated, so the interpretation of CM for reservoirs can be easily extended to all models. In summary, Table 4.1 summarizes all proposed models discussed in this chapter.

Chapter 5

Prediction Under Controlled Producers

In waterflood projects, the number of producers sometimes changes, e.g., a producer is shut-in or a new producer is added. To analyze these data sets using conventional predictive models, which assume a fixed number of producers, we would need to divide the whole data period into several smaller intervals, so that the number of producers remains constant in each interval. This is because when the number of producers changes, it leads to a totally different input-output relationship, so that the model parameters need to be re-estimated. Thus, every time a producer is shutting in, we need a new data set to retrain the model parameters.

In this chapter, we investigate the use of M-ARX models for this kind of situation. The M-ARX model can reduce the number of parameters that needs to be retrained as compared to other predictive models. More importantly, the M-ARX model can predict the performance in the shut-in case, only requiring that the producer be set to a constant rate for a while. This makes it much more practical to control producers in order to predict performance under several possible "What if" scenarios.

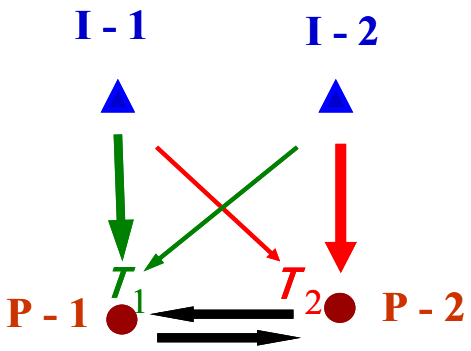

Figure 5.1: The CRMP and M-ARX model in 2-injectors/2-producers scenario. The black arrows denote the contributions from other producers, which are considered in 1^{st} order M-ARX model but not in CRMP.

5.1 Interpreting M-ARX Model

In order to describe the producer-to-producer relationships included in 1^{st} order M-ARX model, we need to understand the relationship between M-ARX model and CM. We first consider a simplified version of CM, named capacitance-resistive model with one time constant for each producer (CRMP), which was proposed in [54]. This model uses one time constant τ for each producer by indicating that for each producer, the pore volume shared with any injectors should be similar, since it corresponds to the region surrounding the well, and therefore they should have similar time constants. The CRMP was proposed with the goal of reducing the number of unknown parameters and simplifying the optimization procedure, while still achieving reasonable prediction results (see [54] for more discussions).

Here we will show that the 1^{st} order M-ARX model can be interpreted as a CRMP that takes into consideration producer-to-producer interactions. To simplify the derivation, suppose we have two injectors and two producers in the ROI, as

shown in Fig. 5.1. Under the CRMP model, the production rates of each producer can be expressed as:

$$y_j(k) = y_j(0)e^{-k/\tau_j} + \sum_{i=1}^{2} \lambda_i u_i(k) \cdot \left[\frac{1}{\tau_j} e^{-k/\tau_j}\right] \tag{5.1}$$

Applying the z-transform in (5.1), we get:

$$\begin{aligned}
\begin{bmatrix} Y_1(z) \\ Y_2(z) \end{bmatrix} &= \begin{bmatrix} \frac{\lambda_{11} z^{-1}}{1-e^{\frac{-1}{\tau_1}} z^{-1}} & \frac{\lambda_{21} z^{-1}}{1-e^{\frac{-1}{\tau_1}} z^{-1}} \\ \frac{\lambda_{12} z^{-1}}{1-e^{\frac{-1}{\tau_2}} z^{-1}} & \frac{\lambda_{22} z^{-1}}{1-e^{\frac{-1}{\tau_2}} z^{-1}} \end{bmatrix} \begin{bmatrix} U_1(z) \\ U_2(z) \end{bmatrix} \\
&= \begin{bmatrix} 1-e^{-\frac{1}{\tau_1}} z^{-1} & 0 \\ 0 & 1-e^{-\frac{1}{\tau_2}} z^{-1} \end{bmatrix}^{-1} \begin{bmatrix} \lambda_{11} z^{-1} & \lambda_{21} z^{-1} \\ \lambda_{12} z^{-1} & \lambda_{22} z^{-1} \end{bmatrix} \begin{bmatrix} U_1(z) \\ U_2(z) \end{bmatrix}
\end{aligned} \tag{5.2}$$

Recalling the M-ARX model expression (3.3) and comparing it with (5.2), this means that when the coefficient matrices $\mathbf{A}$ and $\mathbf{B}$ are as follows:

$$\mathbf{A} = \begin{bmatrix} e^{-\frac{1}{\tau_1}} & 0 \\ 0 & e^{-\frac{1}{\tau_1}} \end{bmatrix}, \tag{5.3}$$

$$\mathbf{B} = \begin{bmatrix} \lambda_{11} & \lambda_{21} \\ \lambda_{12} & \lambda_{22} \end{bmatrix}. \tag{5.4}$$

the 1^{st} order M-ARX model will reduce to the CRMP model, and the coefficients in matrices $\mathbf{A}$ and $\mathbf{B}$ can be interpreted the same way as in the CRMP model. $\mathbf{A}$ being a diagonal matrix can be interpreted by stating that no improvements in modeling accuracy can be achieved by using production rates from other producers in order to estimate production for a given producer, which may happen when the producers are far away from each other (thus with little influence on each other).

Although only shown in the 2-injectors and 2-producers case, the result can be easily extended to cases involving more injectors and producers.

In general, the off-diagonal terms in $\mathbf{A}$ are not zero, and they can be interpreted as representing the contribution from the production rates of other producers. This implies that in the 1^{st} order M-ARX model, the producer-to-producer interactions can be analogous to the injector-to-producer interactions in the CRMP model. To see this, assume the matrix $\mathbf{A}$ in (5.3) has non-zero off-diagonal terms a_{11} and a_{21}, then (5.2) in the time-domain can be expressed as

$$\begin{bmatrix} y_1(k+1) \\ y_2(k+1) \end{bmatrix} = \begin{bmatrix} e^{-\frac{1}{\tau_1}}z^{-1} & a_{12} \\ a_{21} & e^{-\frac{1}{\tau_2}}z^{-1} \end{bmatrix} \begin{bmatrix} y_1(k) \\ y_2(k) \end{bmatrix} + \begin{bmatrix} \lambda_{11} & \lambda_{21} \\ \lambda_{12} & \lambda_{22} \end{bmatrix} \begin{bmatrix} u_1(k) \\ u_2(k) \end{bmatrix}, \tag{5.5}$$

$y_1(k)$, $y_2(k)$ have a similar role as the inputs of $u_1(k)$ and $u_2(k)$. In short, the 1^{st} order M-ARX model can be seen as a generalization of the CRMP model, where now the producer-to-producer interactions are considered in a similar way to the injector-to-producer relationships.

5.2 Prediction for Shut-In Producers

When the production of a target producer is forced to zero (shut-in) during some time period, the question we want to solve is: can we predict the performance of all other producers in the reservoir? Forecasting is important here because on the one hand sometimes producers on daily operations for such as due to maintenance or other reasons. On the other hand, shutting-in producer is sometimes a good solution for waterflood management and optimization, and we need some forecasting ability in order to determine whether a specific producer should be shut-in. When

some producer is shutting-in, the whole system is considered changed and most of the predictive modeling approaches, such as CM or FIR model, can only deal with this kind of situation by considering that the whole fluid distribution has changed, which requires re-training all parameters in the reservoir model. In [30], a compensated capacitance model (CCM) was proposed to reduce the number of parameters that need to be re-trained by introducing a "pseudo-injector" at the well that is being shut-in. In this work, the relations between the pseudo-injector and the producers are also interpreted as producer-to-producer interactions between the shut-in producer and the other producers. Now we will show how to use the 1^{st} order M-ARX model to further reduce the data required for retraining, and also extend the concept of pseudo-injector to deal with a more general scenario.

As shown before, the producer-to-producer interactions in the 1^{st} order M-ARX model can be interpreted as being similar to injector-to-producer interactions in CRMP, so when a producer, e.g., the α-th producer, is artificially shutting in after some time instant, the new production rates $y_j(t)$ on all other producers can be expressed as:

$$\tilde{y_j}(t+1) = y_j(t+1) - y_\alpha(t) * \left[\frac{\lambda_{j\alpha}}{\tau_j} e^{-t/\tau_j} \right] \tag{5.6}$$

where $j = 1, ..., N$ and $j \neq \alpha$; $y_j(t+1)$ and $y_\alpha(t)$ are the original production rates (the predicted production rates without any constrained producer at producer j and producer α, respectively.) (5.6) shows that there is a transient period when constraints on a producer are first imposed, and each producer will have an increasing rate. (Because the interaction $\lambda_{j\alpha}$ between producers j and α is always

negative, the production rate $\tilde{y_j}(t+1)$ will increase.) To highlight the transient effects, $\tilde{y_j}(t+1)$ can be rewritten as

$$\tilde{y_j}(t+1) = y_j(t+1) + y_\alpha(t) \cdot k_j \left[1 - e^{-(t-t_{sh})/\tau_j}\right] \tag{5.7}$$

where t_{sh} denotes the time at which the shut-in begins, and the coefficients $k_j = -\lambda_{j\alpha}$ can be interpreted as the influence of producer α on producer j. As time t increases, $e^{-(t-t_{sh})/\tau_j}$ becomes close to zero, so the $\tilde{y_j}$ can be approximated by

$$\tilde{y_j}(t+1) = y_j(t+1) + y_\alpha(t) \cdot k_j \tag{5.8}$$

We can use (5.7) when the data are in transient period (from the simulation data, usually $t - t_{sh} < \frac{20}{T}$ where T is measured in days) or (5.8) with the data after the transient period. Note that (5.7) and (5.8) can also be derived based on pseudo-injector concepts [30], but a 1^{st} order M-ARX model is being used instead of CM. For (5.7), only two parameters need to be retrained for each producer (k_j and $\tau_{j\alpha}$), and if (5.8) is used, only k_j needs to be estimated. Compared to CCM, which needs to estimate $(M+1) \times N$ unknown parameters (a smaller number of parameters than required by other models), the 1^{st} order M-ARX only needs to re-estimate $(N-1) \times 2$ parameters. Table 5.2 summarizes the number of parameters that need to be retrained for different predictive models.

5.2.1 Simulation Results

In the simulations, we show the application of M-ARX model to the producer shut-in case, where it can be used for performance prediction with a very short re-training period after the shut-in has begun.

Table 5.1: The number of parameters needed to be retrained when a producer is shut-in.

	# of Parameters	5-injectors/4-producers Case
CM	$M \times (N-1) \times 2$	30
FIR Model	$M \times (N-1) \times L$	450 ($L = 30$)
DCM	$M \times (N-1) \times 3$	45
Compensated CM	$(M+1) \times (N-1)$	18
M-ARX Model	$(N-1) \times 2$	6

For the synthetic data, we use the Scenario A introduced in Section 3.2, which is shown in Fig. 3.1. In this case, $P4$ is shut-in from the 730-th day to the 1824-th day. Because $P4$ has the maximum production rates among all producers before shut-in, as the simulation data show, the production rates at all other producers increase significantly during the $P4$ shutting-in period. We use the prediction procedure built on M-ARX model (5.7) to predict the gross production rates during the shut-in period with different training periods after the shut-in begins. The prediction results are also evaluated via the R^2 measurement, which is defined as

$$R^2 = \frac{J_2(\mathtt{M})}{\frac{1}{T}\sum_{k=1}^{T} \|\mathbf{y}(k)\|^2} \tag{5.9}$$

where

$$J_2(\mathtt{M}) = \frac{1}{T}\sum_{k=1}^{T} \|\mathbf{y}(k) - \hat{\mathbf{y}}(k|\mathtt{M})\|^2 \tag{5.10}$$

The results for $P1$ - $P3$ are shown in Fig. 5.2. Also, Fig. 5.3 illustrates the prediction results when re-training period is equal to 20 days. As the results show, we can generate good prediction results when re-training periods are chosen larger than 15 days. This validates this procedure and demonstrates one of the applications on M-ARX model.

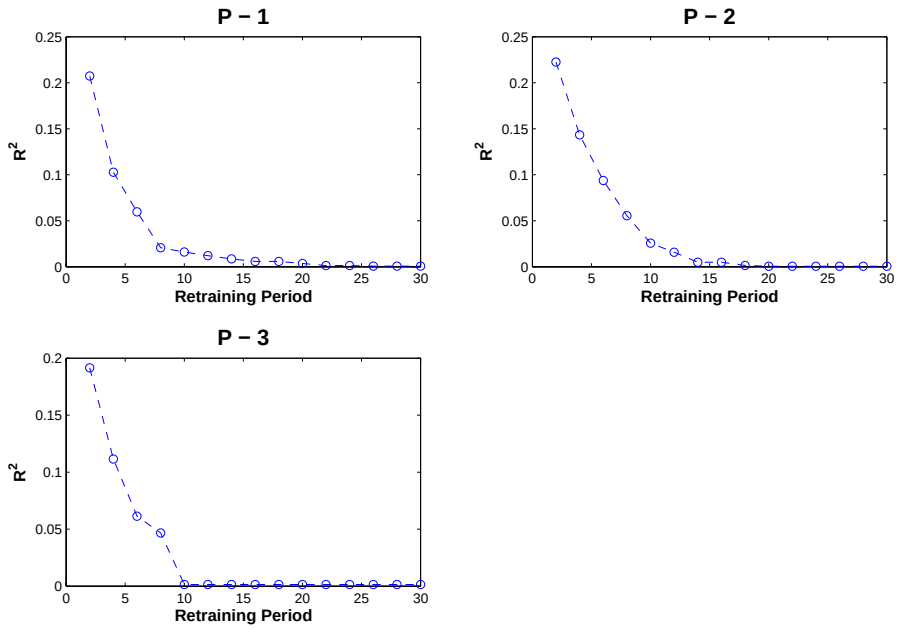

Figure 5.2: Performance of prediction error for production rates based on M-ARX model in Scenario A with $P4$ shut-in from the 705-th day to the 1800-th day. The performance is measured via R^2 and different retraining periods are evaluated.

5.3 Prediction for Constrained Producers

The main drawback of the prediction with a shut-in producer is obvious: we need to close this producer at least for a while in order to predict the long term performance. This heavily limits this application for economic reasons, because any producer shut-in can potentially lead to a decrease of oil production. To successfully handle several "what if" scenarios, we would like to predict the performance after a producer shut-in but requiring minimal changes in production rates so the economic impact of adjusting production for modeling is small. This can be achieved by the use of M-ARX model with producer set to constant rate. For example, we first limit the producer to operate at a certain rate C (we denote the target producer with

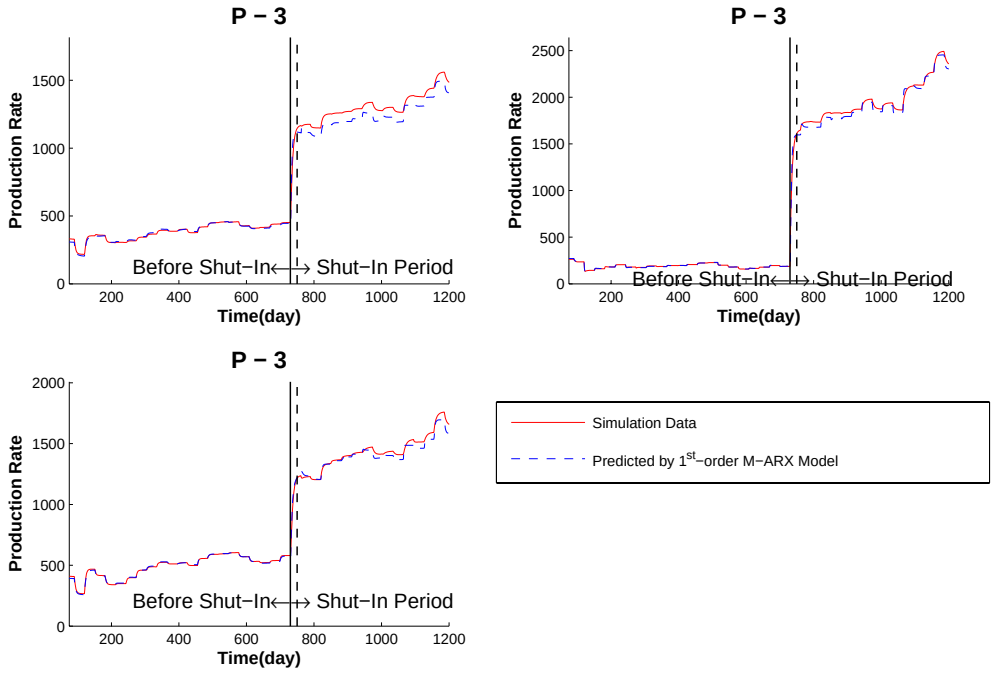

Figure 5.3: Prediction of production rates by M-ARX model in Scenario A with $P4$ shut-in. Note that for retraining data between two black lines (solid and dash) are used.

artificial control, shut-in or set to some rate, as constrained producer in the following discussions). Based on the M-ARX model, in this case (5.7) can be rewritten as

$$\tilde{y_j}(t+1) = y_j(t+1) + (y_\alpha(t) - C) \cdot k_j \left[1 - e^{-(t-t_{sh})/\tau_j}\right] \tag{5.11}$$

This expression can be seen as a general case of (5.7), in which the constant rate C was set to zero. By estimating the parameters using (5.11), we can then predict performance under the scenario where the constrained producer can be set to any rates, including the shut in condition. This of course gives us much more flexibility to forecast performance given that some producers are under artificial control.

Besides, in this situation the estimated parameters k_j can be interpreted as the weight factors of the influence from producer α to producer j, which highlights the

interactions between these two producers. So we can define k_j as the **producer-producer relationship** (PPR), which denotes *the weight factors that characterizes the effective contribution of production decrease of a target production well to the total gross production of surrounding production wells.*

Note that the main novelty of this application is that one does not actually need to shut-in a well (and thus potentially reduce overall production significantly) in order to estimate the impact of a well shut-in, while all previous modeling approaches (including CCM) need to actually do the shut-in for forecasting. We summarize this new constrained producer method as follows:

1. Training phase: the field has been under normal operation (without any constrained producer) for some time period. Then we constrain the target producer for a while (e.g., 30 days in the simulation data). Only these data are needed for the training of M-ARX model.

2. Predicting phase: we use the trained M-ARX model to predict the performance when the target producer is under ANY constrained rates, including the shut-in.

5.3.1 Simulation Results

In the simulations, we show the prediction results for the constrained producer. As the previous section, Scenario A (introduced in Section 3.2) is used, and all settings are the same. The only difference is now we set the target constrained producer to some constant rate after day 730. Using production rate data up to day 760 (which means 30 days are used for re-training the parameters), we can estimate the parameters in (5.11) and use them to predict the performance when the constrained producer is shutting in. Figures 5.4, 5.5 and 5.6 show the prediction results when

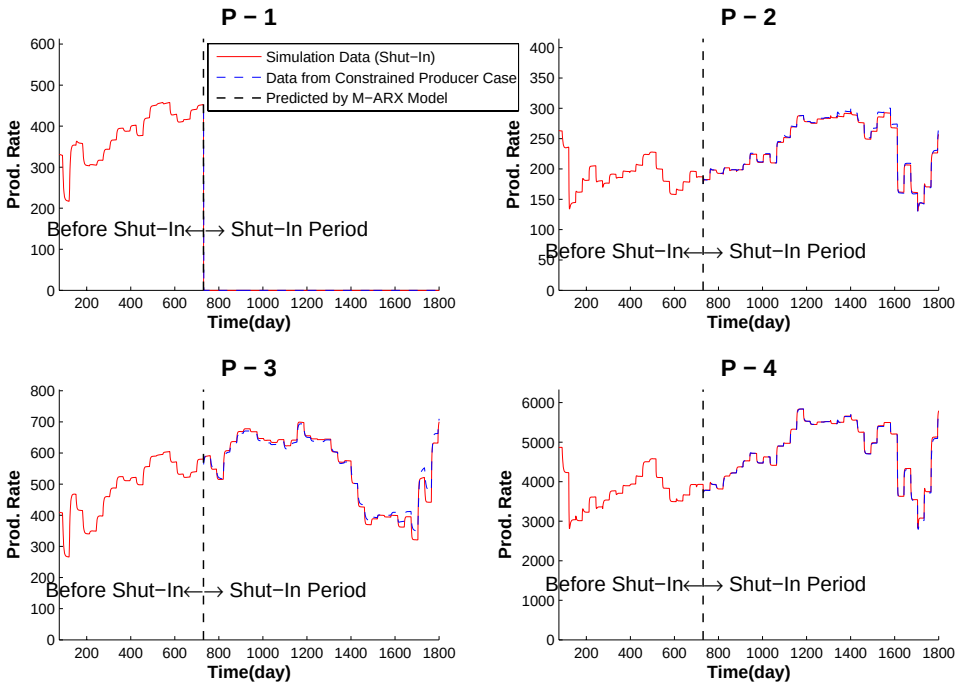

Figure 5.4: Prediction of production rates for $P1$ shut-in by M-ARX model in Scenario A when $P1$ is set to 200 bbl/day.

$P1$, $P2$ and $P3$ are set to constant rate 200, 100, and 200 bbl/day, respectively. For $P4$, we simulate two different constant rates, 600 and 2500 bbl/day, and the results are shown in Figures 5.7 and 5.8. All results show that the constrained producer application is very promising.

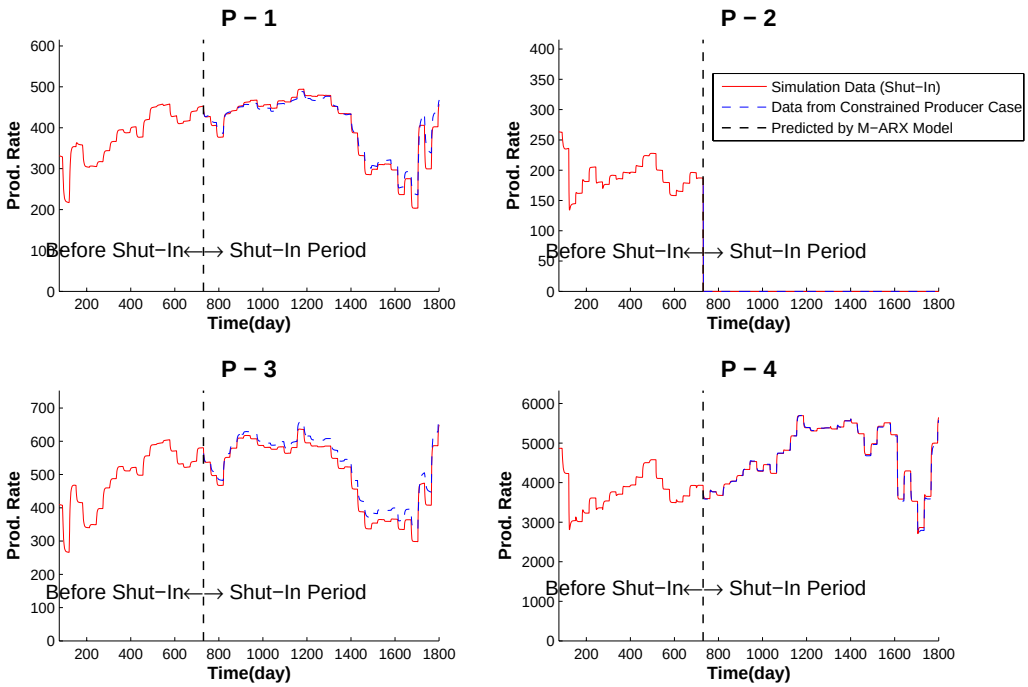

Figure 5.5: Prediction of production rates for $P2$ shut-in by M-ARX model in Scenario A when $P2$ is set to 100 bbl/day.

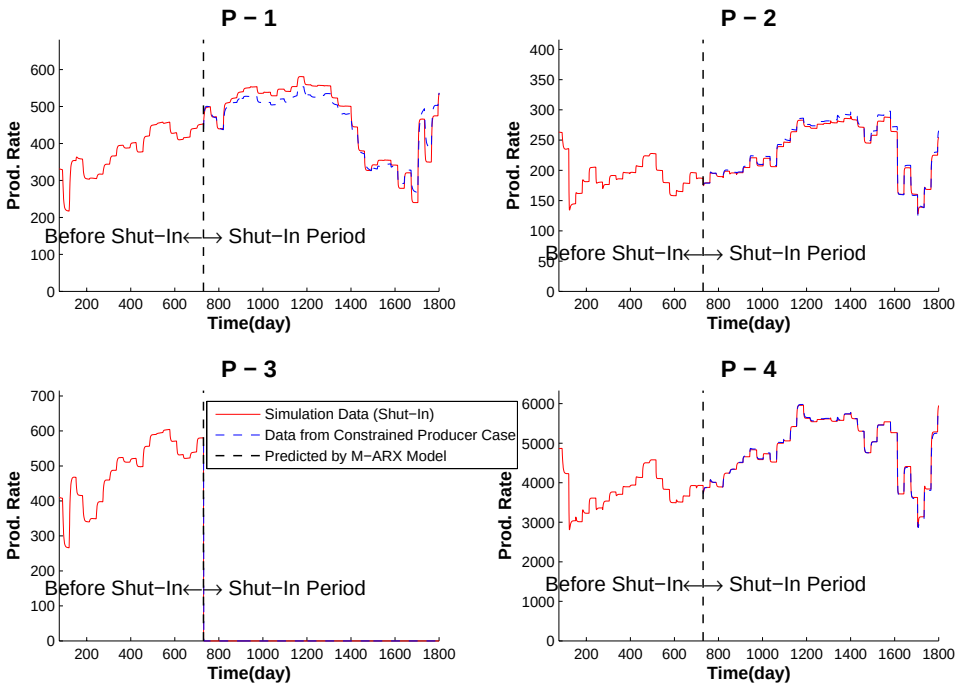

Figure 5.6: Prediction of production rates for $P3$ shut-in by M-ARX model in Scenario A when $P3$ is set to 200 bbl/day.

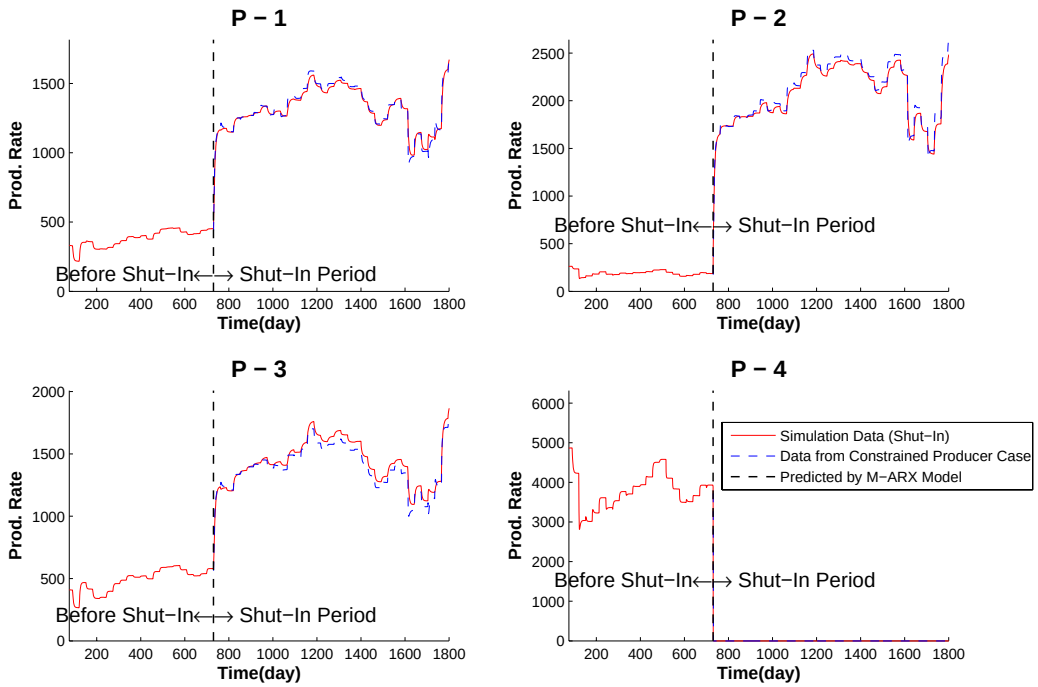

Figure 5.7: Prediction of production rates for $P4$ shut-in by M-ARX model in Scenario A when $P4$ is set to 600 bbl/day.

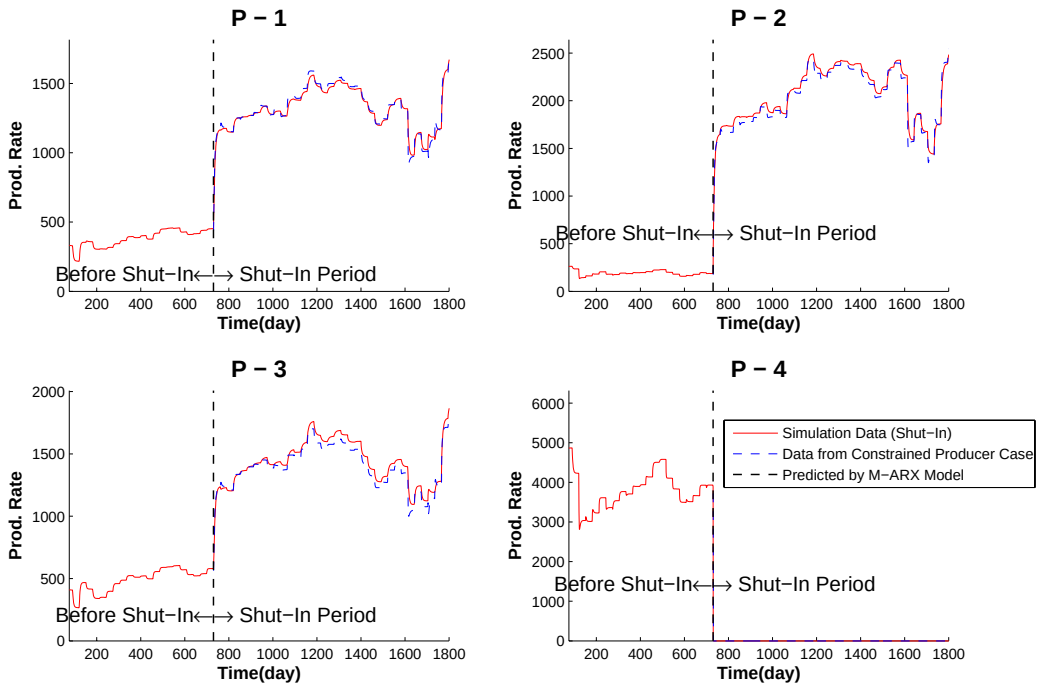

Figure 5.8: Prediction of production rates for $P4$ shut-in by M-ARX model in Scenario A when $P4$ is set to 2500 bbl/day.

Chapter 6

Injection Rates Design

For parameter estimation in dynamic systems, it is desirable to control the conditions under which the data are collected. The objective of this chapter is to investigate the problem of designing inputs so that the collected outputs are as informative as possible with respect to the models to be built using the data. The ultimate goal is to design a set of injection rates based on some criterion in order to facilitate the estimation of model parameters and reservoir characteristics.

In this chapter, we first provide a brief literature review focusing on both system identification and channel estimation in communication systems. Deterministic and stochastic approaches are discussed and a brief comparison is made. For deterministic approach, the novelty of this work is that we propose a novel procedure for designing a set of signals with zero circular cross-correlation for arbitrary shifts. This procedure is based on a property of set of inverse-repeat signals. For the stochastic approach, we first survey input design in system identification and extend the work in the literature to the multiple well case. Another novelty is that we apply a well-known procedure to field applications and evaluate the performance based on some predictive models.

6.1 Literature Review

In this section, we review prior work on input design within two different fields: system identification and channel estimation in communication systems. In both fields the goal is to design the inputs used for probing the system in order to estimate some system characteristics. While the goals are similar, the approaches are totally different. We will focus on the frameworks proposed in each of these fields, namely as deterministic and stochastic approaches, respectively. Finally, some comparisons between these two approaches are provided.

6.1.1 Optimal Input Design

Optimal input design for linear dynamic systems was first considered around 1960 ([36] is one of the earliest contributions) and it became an active area of research in the 1970's. Different qualify measures for the identified model were used. For more comprehensive discussions, see Mehra [46] [47], Zarrop [66], Goodwin and Payne [18] and Goodwin [17]. Until the 1990's, almost all research focused on the minimization of some measure of the variance error of the estimated quantity. The goal was to minimize some objective functions, usually various measures of the covariance matrix $\mathbf{P}_\theta$, where $\boldsymbol{\theta}$ is defined as the parameter vector of the model that is being estimated. An open-loop structure was used in this case. Even though some of the optimal input design work of the 1970's considered closed-loop experiments [48] [49], the objective functions considered at that time were limited to functions of the covariance of the open-loop model parameters.

In the system identification literature, the prediction error method (PEM) [41] is widely used with a full order model structure. The estimated parameter vector,

denoted as $\hat{\boldsymbol{\theta}}_N$, was proven to converge to a Gaussian distribution under some mild assumptions:

$$\left(\hat{\boldsymbol{\theta}}_N - \boldsymbol{\theta}_0\right) \overset{N\to\infty}{\to} N(0, \mathbf{P}_\theta) \tag{6.1}$$

where $\boldsymbol{\theta}_0$ denotes the "true" value of the system parameters and $\mathbf{P}_\theta$ denotes the asymptotic covariance matrix of parameter estimation, which can be estimated from the data. The matrix has been used to judge the "goodness" of different designs because it provides a measure of the average difference between the estimated and the true value of the parameters. The classical approach has been to minimize some scalar function of the asymptotic covariance matrix $\mathbf{P}_\theta$ with constraints on input and/or output power. Examples of criteria that are commonly used are [51]:

$$\text{A-optimality}: \quad \min Tr\left\{\mathbf{P}_\theta\right\} \tag{6.2}$$

$$\text{D-optimality}: \quad \min \det\left\{\mathbf{P}_\theta\right\} \tag{6.3}$$

$$\text{E-optimality}: \quad \min \lambda_{\max}\left\{\mathbf{P}_\theta\right\} \tag{6.4}$$

$$\text{L-optimality}: \quad \min Tr\left\{\mathbf{W}\mathbf{P}_\theta\right\} \tag{6.5}$$

where Tr is the trace function of the matrix, *det* is the determinant of the matrix, λ_{max} represents the maximum eigenvalue of the matrix and $\mathbf{W}$ is a nonnegative weighting matrix.

Both time and frequency domain approaches are considered in the previous literature. For designing the signals in the time domain, the problem typically reduces to a nonlinear optimal control problem with N free variables, in which N is the data length [11]. The resulting complexity was one of the reasons that motivated researchers to solve the input design problem in the frequency domain instead. Making some assumptions, it is possible to derive nice expressions for

the asymptotic covariance matrix. Moreover, it is easier to interpret the results in general for design in the frequency domain.

In short, the optimal input design for system identification is typically based on a stochastic approach where every actual input for the system can be seen as a realization of a process. The criterion used for input design was the spectrum of the input signals, with performance guaranteed achievable when N is large (by asymptotic parameter variance $\mathbf{P}_\theta$). We will discuss how to apply this approach with field applications where the goal is injection rate design later in this chapter.

6.1.2 Channel Estimation in Communication

In communication systems, the multiple-input multiple-output (MIMO) technique has been shown to greatly increase the capacity of wireless systems, and it can fit the growing demand for high data rates in the wireless environment. However, to use the advantages of MIMO systems, accurate channel state information (CSI) is required. If space-time coding is used, an accurate CSI is crucial for the performance of decoders. Therefore, channel estimation plays a key role in MIMO communication systems [19] [8].

Using training sequences is one of the most widely applied approaches for MIMO channel estimation. In this approach, the channel is estimated using the received signal resulting from a predetermined sequence, denoted as training sequence, being sent from the transmitter. There has been a growing interest in the training-based MIMO channel estimation. For example, Hassibi and Hochwald [21] linked the training sequence problem with channel capacity; Marzetta [44] considered the BLAST training using maximum likelihood (ML) method; Li [37] developed a least-square (LS) training-based channel estimation technique for orthogonal

frequency-division multiplexing (OFDM) systems with multiple transmit antennas; Scaglione and Vosoughi [56] improve the LS approach via minimum mean-square-error (MMSE) symbol estimate. As a comprehensive study, Larsson and Stoica [31] gave a general discussion on optimal MIMO training schemes based on LS criterion. Biguesh and Gershman [6] discussed the tradeoffs between LS, scaled LS, and MMSE methods.

The training sequence design was treated as a deterministic approach, that is, the aim is to select the value of training sequences exactly before transmission. Some authors, e.g., [12] and [14], constraint the training sequences to be derived from a finite alphabet (such as BPSK constellation). This work concludes that, except for some special cases, the deterministic optimal training sequence for any length could only be found via exhaustive search, but only possible for short sequences with small alphabet size because of complexity. One of the main conclusions derived from the training-based channel estimation was the optimal sequences should have an impulse-like auto-correlation and zero cross-correlation properties. Actually, the sequence design for good correlation properties was very crucial for some communication fields, such as code division multiple access (CDMA) system, where Gold pair and Kasami sequences are commonly used because of their good correlation properties. For details, see [16]. Because these designs were focused on minimizing the maximum absolute auto-correlation and cross-correlation values, they are not optimal for parameter estimation in dynamical systems.

6.2 A Novel Deterministic Approach for Input Sequence Design

In this section, we approach the input design problem using a deterministic approach. We developed a procedure to generate a set of signals, which have vanishing cross-correlation with each other with arbitrary shifts. To design these inputs, inverse-repeat signals are first introduced and one property of these signals is discovered. Then a new procedure is proposed to generate a set of signals with all zero cross-correlation with each other with arbitrary time shifts.

Note that the procedure described in this section is also valid for continuous signals but here we only discuss the discrete case because for our problem, datasets (inputs and outputs) are all discrete in some time scale (day, week, or month).

6.2.1 Inverse-repeat signals

Inverse-repeat signals are signals $x(n)$ with period N and defined as

$$x(n + \frac{N}{2}) = -x(n) \qquad \text{for } n \in \left[0, \frac{N}{2}\right] \tag{6.6}$$

Inverse-repeat signals are such that their even harmonic frequency components are all equal to zero. That is, they only have non-zero values in the odd-order harmonic frequencies $\pm f_0, \pm 3f_0, \pm 5f_0, ...$ with $f_0 = \frac{2\pi}{N}$. To see this, we just need to calculate

the corresponding N-point discrete Fourier transform (DFT). The DFT of signal x, denote as X, can be calculated as

$$
\begin{aligned}
X(k) &= \sum_{n=0}^{N-1} x(n) e^{\frac{j2\pi nk}{N}} && (6.7)\\
&= \sum_{n=0}^{\frac{N}{2}-1} x(n) e^{\frac{j2\pi nk}{N}} + \sum_{n=0}^{\frac{N}{2}-1} x(n+\frac{N}{2}) e^{\frac{j2\pi k}{N}(n+\frac{N}{2})} && (6.8)\\
&= \sum_{n=0}^{\frac{N}{2}-1} x(n) e^{\frac{j2\pi nk}{N}} - \sum_{n=0}^{\frac{N}{2}-1} x(n)(-1)^n e^{\frac{j2\pi nk}{N}} && (6.9)\\
&= \begin{cases} 2\sum_{n=0}^{\frac{N}{2}-1} x(n) e^{\frac{j2\pi nk}{N}} & \text{for } k \text{ odd} \\ 0 & \text{for } k \text{ even} \end{cases} && (6.10)
\end{aligned}
$$

6.2.2 Property of a Set of Inverse-Repeat Signals

Now, we investigate the non-overlapping frequency components property of a set of inverse-repeat signals. To the best of our knowledge, this property has never been used for input sequence design in the literature.

Considering a signal with period N, when we apply $2N$-point DFT, the frequency domain representation can be obtained by inserting a zero in between each original N-point DFT. This can be written as follows:

$$
\begin{cases} X_{2N}(2k) = X_N(k) & \text{for } k = 0, ..., N-1 \\ X_{2N}(2k+1) = 0 & \text{otherwise} \end{cases} \qquad (6.11)
$$

where X_N and X_{2N} denote the N-point and $2N$-point DFT, respectively. So for an inverse-repeat signal with period N, when we apply the $2N$-point DFT, it will have non-zero values only in frequency components $(\pm f_0, \pm 3f_0, \pm 5f_0, ...) \times 2 = \pm 2f_0, \pm 6f_0, \pm 10f_0, ...$ Following this rule, for an inverse-repeat signal with period

Table 6.1: Non-zero DFT indexes fro inverse-repeat signals.

$2^{\alpha}N$-point DFT for Inverse-Repeat Signal	
Period	Non-zero DFT index
$2^{\alpha}N$	$\pm 1, \pm 3, \pm 5, \pm 7, ...$
$2^{\alpha-1}N$	$\pm 2, \pm 6, \pm 10, \pm 14, ...$
$2^{\alpha-2}N$	$\pm 4, \pm 12, \pm 20, \pm 28, ...$
$\vdots$	$\vdots$
N	$2^{\alpha} \times \{\pm 1, \pm 3, \pm 5, \pm 7, ...\}$

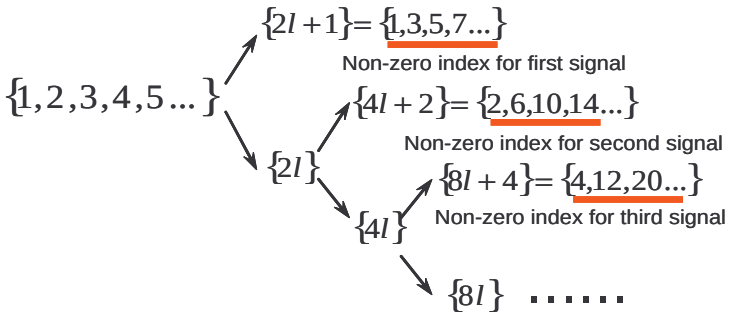

Figure 6.1: Illustration of non-zero frequency indexes for inputs with different periods.

N, if we apply $2^{\alpha}N$-point DFT, it will have non-zero values only at frequencies $\pm 2^{\alpha} f_0, \pm 2^{\alpha} 3 f_0, \pm 2^{\alpha} 5 f_0, ...$ Now suppose we have an inverse-repeat signal set: x_1, x_2, ..., $x_{\alpha+1}$ with different periods $N_1 = N$, $N_2 = 2N$, $N_3 = 4N$, ..., $N_{\alpha+1} = 2^{\alpha}N$, where the number of the set is $\alpha + 1$. When we apply DFT over $2^{\alpha}N$ to all of the signals, they will possess non-zero value for some frequency components as shown in Table 6.1:

Fig. 6.1 shows the non-zero DFT indexes, which obviously form a disjoint set. So we find that signals with different periods occupy non-overlapping frequency components in the frequency domain. This means that if we select signals from the set as inputs to a LTI system, any of two signals will have circular cross-correlation

equal to zero with period $2^{\alpha}N$ with any shifts. This design procedure will be illustrated with an example in the following section.

6.2.3 Design Example

Using the procedure, we can construct a set of discrete $\alpha+1$ inverse repeat signals, whose periods are N, $2N$, $4N$, $8N$,..., $2^{\alpha}N$. To apply this set of signals in practice, a natural way is to choose the periods as small as possible. The smallest period is $N = 2$ (for discrete inverse-repeat signals, the smallest period is 2) and for this signal within one period, it has the a positive value and a negative value, with the same amplitude (normally chosen as $\frac{1}{\sqrt{2}}$ to make the energy normalized to 1). For the signal with period $2N = 4$, it is natural to choose two positive values followed by two negative values with the same amplitude. We can use the same procedure and extend it to the signal with period $2^{\alpha}N = 2^{\alpha+1}$, which has 2^{α} positive values followed by 2^{α} negative values, all with the same amplitude. Fig. 6.2 shows an example for one period of this set of signals with in the $\alpha = 3$ case. As mentioned before, if we choose any two signals from this set, they will have zero circular cross-correlation with period $2^{\alpha+1}$ for arbitrary shifts. This is a very nice property because that means if we set these signals into a multiple-inputs LTI system, each signal will not cause interference to other signals (because of vanishing cross-correlation with period $2^{\alpha+1}$). As a result, this set of signals can be used for some applications if the goal is to separate the influence from different inputs. We will apply this inverse-repeat signal design to some reservoir models and compare the results with those achieved with some well-known deterministic sequences in Section 6.3.5.

In summary, this new procedure is formulated as follows:

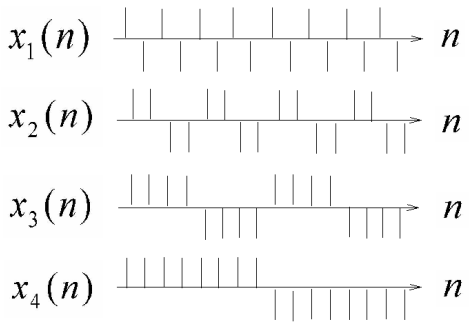

Figure 6.2: This figure shows an example for designed set of inverse-repeat signals. $\alpha = 3$ (period is equal to $2^{\alpha+1} = 16$) and one period is displayed.

1. Deciding the whole period of the input signal set, which is $2^{\alpha}N$ where N is an integer with $N \geq 2$ and $\alpha + 1$ is the number of signals in this set.

2. Choose an arbitrary signal with length $N/2$ that meets the constraints on input signals (e.g., finite-alphabet), and transform it into an inverse-repeat signal by adding the inverse version of itself. Then repeat the signal until its length becomes $2^{\alpha}N$

3. Repeat step 2 with signal lengths N, $2N$, ..., to $2^{\alpha-1}N$. This will generate $\alpha + 1$ inverse-repeat signals with vanishing cross-correlation with each other at arbitrary shifts.

6.2.4 Discussion

This proposed procedure can be used to design a set of signals with perfect cross-correlation property. As a well-known result, chosen as inputs to a dynamic system should be designed by the following rules:

1. Low out-of-phase auto-correlation value (ideal value is zero)

2. Low cross-correlation value (ideal value is zero)

As shown in the CDMA literature, in order to achieve the first goal, the maximum-length-sequence (MLS) or m-sequence was introduced and developed. In order to solve the second goal, Welch's bound [45] was derived to describe the upper bound on performance. Different design techniques, such as Gold pair sequences, Kasami sequence, were proposed to approach this bound [45]. Our proposed procedure try to addresses the problem by optimizing the second design rule, that is, it aims to make the cross-correlation values all equal to zero. In this sense, we reach the ideal value for the second design rule.

The problem with our proposed method is that is has relatively high out-of-phase auto-correlation values. This can be shown in either time or frequency domain. In time domain, the signals in this set have different periods, from N to $2^{\alpha}N$. When we calculate the circular auto-correlation over $2^{\alpha}N$ points, the signal of period N will perform the worst among this set of signals. Its out-of-phase auto-correlation value will reach the maximum value for every shift by N. Of course this does not satisfy the first goal. In frequency domain, the frequency components with non-zero values for signal with period N are only on $2^{\alpha} \times \{\pm 1, \pm 3, \pm 5, \pm 7, ...\}$. As we know, a "good" probing signal should occupy (have non-zero value) as many frequency components as possible in the frequency domain, so the signal with period N is far away from being "good".

The input sequence design problem based on a deterministic approach often has some constraints on the input signals, such that the signals can only be taken in some ranges (usually positive values with some upper and lower bounds). For some industrial applications, the input signals may be even more constrained, e.g., they can only be taken from some discrete values. For all of these cases, it is impossible to design a set of input signals that reaches both the ideal value of both design rules. What makes the design even worse is that the only way to find the optimal

input signals is via exhaustive search, except for some special cases. Sequences with "good" properties according to both rules, such as Gold pair or Kasami sequence, are only optimal for some specific applications, and not always optimal in a more general situation such as parameter estimation of a dynamic system. Our work can be seen as an example of designing a set of "good" input signals with perfect performance in the second design rule, but with suboptimal performance with respect to the first rule. Also, there may be some applications where the cross-correlation property is much more important than the auto-correlation property, and our design can be used to get a good performance in that kinds of applications.

Back to the goal of this chapter, to solve the optimal injection rates problem, we will turn to the stochastic approach in the next section.

6.3 Stochastic Approach

Because of the drawbacks of the deterministic approach, we now consider the stochastic approach. As discussed, this framework is used for most optimal input design work in the system identification literature.

From the system identification literature [41], there are two design criteria for input design. The first consideration is the input signal spectrum. [41] proposed a criterion for the single-input single-output (SISO) case, and we extend it to multiple-inputs single-output (MISO) and multiple-inputs multiple-outputs (MIMO) case. Another design criterion, crest factor, quantifies the amount of input energy into the system. Based on these two criteria, there is a design procedure to come to achieve a compromise between them. The main novelty of this Section is we apply this procedure to field applications with evaluation. An example for estimating parameters in capacitance model is shown and some general discussions are made.

6.3.1 Criterion for Injection Rate Design

For a LTI system, in the system identification literature a complete model is used to describe the LTI system, which we are going to use for the rest of the discussion. Consider a discrete-time LTI system, denoted as $G(z)$ in the z-domain, with inputs $u(t)$, outputs $y(t)$, and additive disturbance with spectrum $\sigma^2 \left|H(e^{j\omega})\right|^2$, the model in the z-domain is expressed as

$$y(t) = G(z)u(t) + H(z)e(t). \tag{6.12}$$

A particular model thus corresponds to specification of the functions G, H and the probability density function (PDF) of $e(t)$. In practice, it is very common to assume that $e(t)$ is Gaussian, in which case the PDF is entirely specified by its first and second moments. The specification of (6.12) in terms of a finite number of numerical coefficients is the most important for the purposes of system identification. That is, the coefficients in question in model (6.12) will the same as parameters to be determined. So we can denote the target parameters by the vector $\boldsymbol{\theta}$ and have a model description

$$y(t) = G(z, \boldsymbol{\theta})u(t) + H(z, \boldsymbol{\theta})e(t), \tag{6.13}$$

The $\boldsymbol{\theta}$ ranges over a subset of $\mathbf{R}^d$, where d is the dimension of $\boldsymbol{\theta}$:

$$\boldsymbol{\theta} \in D_M \subset \mathbf{R}^d \tag{6.14}$$

This is the parameterized LTI model for any modeling approaches.

In [41], for prediction-error methods (PEMs), the covariance matrix of the parameter estimation $\mathbf{P}_\theta$ can be expressed as

$$\mathbf{P}_\theta \propto \sigma^2 \left[E \left(\frac{d\hat{y}(t|\boldsymbol{\theta})}{d\boldsymbol{\theta}} \right) \left(\frac{d\hat{y}(t|\boldsymbol{\theta})}{d\boldsymbol{\theta}} \right)^T \right]^{-1}, \tag{6.15}$$

where $\hat{y}(t|\boldsymbol{\theta})$ is the predicted value of the outputs based on the parameters. The expression (6.15) gives a suggestive hint for the choice of input signals: choose the outputs $y(t)$ and corresponding inputs $u(t)$ so that the predicted output becomes sensitive with respect to target parameters of our interests.

In frequency domain, the asymptotic covariance matrix $\mathbf{P}_\theta$ is given by the inverse of average *information matrix per sample*, $\bar{M}$, as

$$\begin{aligned} \bar{\mathbf{M}} \;\propto\; & \sigma^2 \int_{-\pi}^{\pi} G'_\theta(e^{j\omega}, \boldsymbol{\theta}_0) \left[G'_\theta(e^{-j\omega}, \boldsymbol{\theta}_0) \right]^T \frac{\Phi_u(\omega)}{\Phi_v(\omega)} d\omega \\ & + \sigma^2 \int_{-\pi}^{\pi} H'_\theta(e^{j\omega}, \boldsymbol{\theta}_0) \left[H'_\theta(e^{-j\omega}, \boldsymbol{\theta}_0) \right]^T \frac{\sigma^2}{\Phi_v(\omega)} d\omega \end{aligned} \tag{6.16}$$

provided inputs u and e_0 are independent. Here G'_θ and H'_θ are the $d \times 1$ gradients of G and H. Introducing

$$\tilde{M}(\omega) = \frac{\sigma^2 G'_\theta(e^{j\omega}, \boldsymbol{\theta}_0) \left[G'_\theta(e^{-j\omega}, \boldsymbol{\theta}_0) \right]^T}{\Phi_v(\omega)} \tag{6.17}$$

$$M_e = \sigma^4 \int_{-\pi}^{\pi} \frac{H'_\theta(e^{j\omega}, \boldsymbol{\theta}_0) \left[H'_\theta(e^{-j\omega}, \boldsymbol{\theta}_0) \right]^T}{\Phi_v(\omega)} d\omega \tag{6.18}$$

We have

$$\bar{M}(\Phi_u) = \int_{-\pi}^{\pi} \tilde{M}(\omega) \Phi_u(\omega) d\omega + M_e \tag{6.19}$$

This expression helps us understand the influence of input spectrum to the information matrix: to achieve a large information matrix (small covariance matrix),

the input power should be spent at frequencies where the weight $\tilde{M}(\omega)$ is large, that is, where the Bode plot is sensitive to parameter variations. This expression, together with the intuitions described, help us in designing the desired input signal spectrum. Now we extend the criterion in (6.16) to MISO and MIMO cases.

6.3.1.1 MISO case

The goal now is to extend the design criterion (6.15) and (6.16) to MISO case. Suppose now we have M inputs, for the LTI system model, the output signal can be expressed as

$$y(t) = \sum_{i=1}^{M} G_i(z, \boldsymbol{\theta}) u_i(t) + H(z, \boldsymbol{\theta}) e(t) \tag{6.20}$$

Because the output number is the same as in the SISO case (only one output), we can use the same formula in time domain as in the SISO case:

$$\mathbf{P}_\theta \propto \sigma^2 \left[E \left(\frac{d\hat{y}(t|\boldsymbol{\theta})}{d\boldsymbol{\theta}} \right) \left(\frac{d\hat{y}(t|\boldsymbol{\theta})}{d\boldsymbol{\theta}} \right)^T \right]^{-1} \tag{6.21}$$

In the frequency domain, the expression (6.16) needs to be slightly changed:

$$\begin{aligned} \bar{\mathbf{M}} \quad \propto \quad & \sigma^2 \int_{-\pi}^{\pi} \frac{\mathbf{G}'_\theta(e^{j\omega}, \boldsymbol{\theta}_0) \mathbf{\Phi}_\mathbf{u}(\omega) \left[\mathbf{G}'_\theta(e^{-j\omega}, \boldsymbol{\theta}_0) \right]^H}{\Phi_v(\omega)} d\omega \\ & + \sigma^2 \int_{-\pi}^{\pi} H'_\theta(e^{j\omega}, \boldsymbol{\theta}_0) \left[H'_\theta(e^{-j\omega}, \boldsymbol{\theta}_0) \right]^H \frac{\sigma^2}{\Phi_v(\omega)} d\omega \end{aligned} \tag{6.22}$$

where now $\mathbf{G}'_\theta$ became a $d \times M$ matrix and $\mathbf{\Phi}_\mathbf{u}$ became a $M \times M$ matrix, which are expressed as

$$\mathbf{G}'_\theta(e^{j\omega}) = \begin{bmatrix} \frac{dG_1(e^{j\omega},\theta)}{d\theta_1} & \cdots & \frac{dG_M(e^{j\omega},\theta)}{d\theta_1} \\ \vdots & \ddots & \vdots \\ \frac{dG_1(e^{j\omega},\theta)}{d\theta_d} & \cdots & \frac{dG_M(e^{j\omega},\theta)}{d\theta_d} \end{bmatrix} \tag{6.23}$$

and

$$\mathbf{\Phi_u}(\omega) = \begin{bmatrix} \Phi_{11}(\omega) & ... & \Phi_{1M}(\omega) \\ \vdots & \ddots & \vdots \\ \Phi_{M1}(\omega) & ... & \Phi_{MM}(\omega) \end{bmatrix}, \tag{6.24}$$

where Φ_{ij} represents the cross-spectral density (CSD) function between input i and j. Therefore the matrix $\mathbf{\Phi_u}$ is the CSD matrix over inputs $1, 2, ..., M$.

The expression in the frequency domain gives us a key intuition: if we want some measurement (such as $Tr\left\{\bar{M}\right\}$) of the information matrix to be large, we should make the matrix $\mathbf{\Phi_u}$ as diagonal as possible, that is, all cross-spectral density function Φ_{ij} should be as small as possible (ideally zero) for $i \neq j$, which means all inputs should be uncorrelated to each other. This perfectly matches the second design rule described in the deterministic approach section.

6.3.1.2 MIMO case

In MIMO case, the number of outputs no longer one, so we need to derive the expression for both time and frequency domain. For LTI model, suppose we have N outputs, the output j can be expressed as

$$y_j(t) = \sum_{i=1}^{M} G_{ij}(z, \boldsymbol{\theta}) u_{ij}(t) + H_j(z, \boldsymbol{\theta}) e_j(t) \tag{6.25}$$

for $j = 1, 2, ..., N$. In this expression, we make an assumption that each output is statistically independent of other outputs. For real physical systems, the outputs often interfere with each other, and this is also true for the system we are trying to characterize. The producers in the reservoir will affect each other because the production rates of each producer will affect the bottom-hole flowing pressure on

its well. In our work, however, we still make the independence assumption, which will be verified via simulation data.

In this model and under the PEMs approach, the criterion (6.15) in the time domain becomes

$$\mathbf{P}_\theta \propto \sigma^2 \left\{ E\left[\sum_{j=1}^{N} \left(\frac{d\hat{y}_j(t|\boldsymbol{\theta})}{d\boldsymbol{\theta}} \right) \left(\frac{d\hat{y}_j(t|\boldsymbol{\theta})}{d\boldsymbol{\theta}} \right)^T \right] \right\}^{-1}. \tag{6.26}$$

This is based on the independence of outputs. In the frequency domain, the criterion (6.16) becomes

$$\begin{aligned} \bar{\mathbf{M}} \;\; \propto \;\; & \sum_{j=1}^{N} \sigma^2 \int_{-\pi}^{\pi} \frac{\mathbf{G}'_{\mathbf{j}}(e^{j\omega}, \boldsymbol{\theta}_0) \mathbf{\Phi}_{\mathbf{u}}(\omega) \left[\mathbf{G}'_{\mathbf{j}}(e^{-j\omega}, \boldsymbol{\theta}_0) \right]^H}{\Phi_v(\omega)} d\omega \\ & + \sigma^2 \sum_{j=1}^{N} \int_{-\pi}^{\pi} H'_j(e^{j\omega}, \boldsymbol{\theta}_0) \left[H'_j(e^{-j\omega}, \boldsymbol{\theta}_0) \right]^H \frac{\sigma^2}{\Phi_v(\omega)} d\omega \end{aligned} \tag{6.27}$$

where now $\mathbf{G}'_{\mathbf{j}}(e^{j\omega}, \boldsymbol{\theta}_0)$ is the same as $\mathbf{G}'_\theta(e^{j\omega}, \boldsymbol{\theta}_0)$ but we add the subscript j to denote for output j, and so is the gradient of disturbance vector $H'_j(e^{-j\omega}, \boldsymbol{\theta}_0)$.

The equation (6.35) has a very intuitive interpretation: the energy of desired input signals should be concentrated on the frequencies that are very sensitive to the target parameters (large $\mathbf{G}'_{\mathbf{j}}$) and small noise energy (small Φ_v) so that the target parameters $\boldsymbol{\theta}$ could have a better estimation. We will use this formula, together with other considerations, and take the capacitance model as an example to design a set of signals that fit our need.

6.3.1.3 The Crest Factor

Another consideration for input design is the input power. This is because the covariance matrix is typically multiplied by a term that is inversely proportional

to the input power. For practical situations, the inputs are often limited by some upper and lower values, that is, the input signals u satisfy $\underline{u} \leq u \leq \overline{u}$ where $\underline{u}$ and $\overline{u}$ are defined upper and lower bounds on the signal instantaneous values. Thus a desired property of the waveform can be defined in terms of the *crest factor* C_r. For a zero-mean signal, it is

$$C_r^2 = \frac{\max_t u^2(t)}{\lim_{N\to\infty} \frac{1}{N} \sum_{t=1}^{N} u^2(t)} \tag{6.28}$$

A good signal waveform is one that has a small factor, with a theoretic lower bound of $C_r \geq 1$, which is achieved for binary, symmetric signals.

6.3.2 A Design Procedure

The basic design rule for the input signal design is obvious now: we should design a signal to achieve the desired input spectrum and as small a crest factor as possible at the same time. But these properties are somewhat in conflict. A common and easy choice [41] to achieve the desired spectrum is to pass a white Gaussian noise through a linear filter. By choosing the filter, we can virtually design any signal with the desired spectrum. But the problem is that: this filtered Gaussian white noise may have a large crest factor, so input energy sent to the system remains small. To overcome this, another common approach [41] is to simply take the sign of the filtered signal to make it into a binary signal. This can be adjusted to any desired binary levels. In this design, the crest factor takes the ideal value of 1, but by taking the sign operation, the spectrum of the signal may change. In this situation, we can however check the spectrum of the signal before using it as input signal, to make sure it is acceptable for our need. The main novelty here is that we

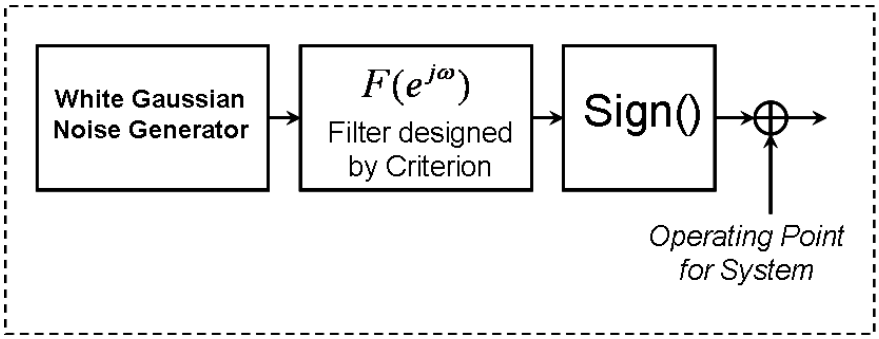

Figure 6.3: Block diagram of a system to generate the set of inputs obtained from the rate design procedure. Note this design comes from the stochastic approach and the signal will be different for each realization.

apply this procedure into field applications and take the state-of-the-art modeling approach CM as a design example to evaluate this method.

This procedure can be summarized as follows:

1. Calculate the input spectrum criterion (6.27) from the data available

2. Design a filter using the criterion and pass a Gaussian white noise through the filter

3. Pass the filtered signal to a sign operator

This diagram of this procedure is shown in Fig. 6.3.

6.3.3 Design Example: Application to CM

We now apply the design procedure to the reservoir problem. The ranges of the injection rates vary for different injectors, and we roughly use the average value of historic data in some time period. The injection rates should also be upper bounded, this is because if the injected water volume is too high, the pressure will be very high and it may break some rock layers and create some fractures. This should be avoided in any case. The injection rates can be as low as zero (shut-in). Thus the injection rate $u_i(k)$ for the injector i has the following constraint:

$$0 \leq u_i(k) \leq u_{max} \qquad \text{for } k = 1, 2, ..., K, \tag{6.29}$$

where K is the time period for our design and this constraint is applied to all injectors $i = 1, 2, ..., M$. Besides, the injection rates should not be selected far away from the normal operating points in order to preserve the linearity assumption.

In order to design a set of injection rates according to the CM, we need to calculate the criterion (6.27) in advance. In CM, the system transfer function g_{ij} between injector i and producer j is expressed as

$$g_{ij}(t) = \frac{1}{\tau_{ij}} e^{\frac{-t}{\tau_{ij}}} \tag{6.30}$$

In the frequency domain, this becomes

$$G_{ij}(e^{j\omega}) = \frac{1}{\sqrt{2\pi}(1 + j\tau_{ij}\omega)} \tag{6.31}$$

Suppose now we are interested in the interwell connectivities λ_{ij} for all injector-producer well pairs. Thus, the target parameter vector $\boldsymbol{\theta}$ is:

$$\boldsymbol{\theta} = \begin{bmatrix} \mathbf{\Lambda_1} \\ \mathbf{\Lambda_2} \\ \vdots \\ \mathbf{\Lambda_N} \end{bmatrix} \tag{6.32}$$

where $\mathbf{\Lambda_i}$ represents the interwell connectivity related to producer i:

$$\mathbf{\Lambda_i} = \begin{bmatrix} \lambda_{1i} \\ \lambda_{2i} \\ \vdots \\ \lambda_{Mi} \end{bmatrix} \tag{6.33}$$

Now we can calculate the criterion (6.27) for the design of input spectrum. The $\mathbf{G}'_{\mathbf{j}}(e^{j\omega}, \boldsymbol{\theta}_0)$ in (6.27) becomes

$$\mathbf{G}'_{\mathbf{j}}(e^{j\omega}, \boldsymbol{\theta}_0) = \begin{bmatrix} & 0 & & \\ & \vdots & & \\ & 0 & & \\ \frac{1}{1+j\tau_{1j}\omega} & 0 & ... & 0 \\ 0 & \frac{1}{1+j\tau_{2j}\omega} & ... & \vdots \\ \vdots & & \ddots & 0 \\ 0 & ... & 0 & \frac{1}{1+j\tau_{Mj}\omega} \\ & 0 & & \\ & \vdots & & \\ & 0 & & \end{bmatrix} \tag{6.34}$$

If we design a set of sequences with zero CSD function, which is easily achieved by generating each signal independently, the criterion (6.27) becomes

$$\bar{\mathbf{M}} \propto \int_{-\pi}^{\pi} \frac{diag\left(\frac{1}{1+\tau_{11}^2\omega^2}\Phi_1(e^{j\omega}), ..., \frac{1}{1+\tau_{MN}^2\omega^2}\Phi_M(e^{j\omega})\right)}{\Phi_v(\omega)} d\omega + \text{ Noise Term} \tag{6.35}$$

Here we do not write the noise term because we focus on the injection rate design, which affects only at the first term of this formula. According to (6.35), we need to design the input spectrum of injector i based on the weights $\frac{1}{1+\tau_{i1}^2\omega^2}$,...,$\frac{1}{1+\tau_{iN}^2\omega^2}$, which means we need to have a rough estimation of the parameters τ_{i1},...,τ_{iN} in advance. This makes sense because unless we know some rough characteristics on the system, we can not design a set of optimized inputs for parameters estimation because the optimal inputs depend on the system behavior. In field application,

we can always have some rough estimation of the system from historical data, so it is not unrealistic to design a set of injection rates optimized for better parameter estimation in a reservoir.

From this interpretation, it seems that we should put the energy into as low frequency as possible. In practice, this is not true because the performance of stochastic approach is only guaranteed by its asymptotic property. To put it into practice, the stochastic approach is only justified by a large data set K, and this is usually not the case for our applications. If the daily data are available for both injection rates and production rates, a typical practical duration for these experiments is on the order of a few months. In this situation, if we put the energy of injection rates on very low frequency components, the parameter estimation performance will degrade because the injection rates will appear to be almost constant during the time-frame chosen to observe the system.

6.3.4 Simulation Results

In our simulation, we assume the underground model is capacitance model, and we consider the five-spot scenario with 5 injectors and four producers. The target parameters are only the interwell connectivity weights λ_{ij} between all injector-producer well pairs, as we have described above. We use (1) a binary white sequence; (2) sequences generated from our procedure with different cutoff frequency. The first-order low-pass filter (LPF) is used in order to design the inputs energy at low frequency components. The first-order LPF in the frequency domain is expressed as

$$H_{LPF}(\omega) = \frac{K}{1 + j\omega T} \tag{6.36}$$

where K is the passband gain and T is the time constant that controls the cut-off frequency for this filter. A larger T means a lower cut-off frequency and the signal passing it will have more energy on the low frequency.

Fig. 6.4 shows one realization of the injection rates for two different sequences: one is a binary white sequence and another is the filtered binary sequence with the time constant T set to 20. The operating points of the injection rates are set to 500 bbl/day and the variations are set to plus or minus 100 bbl/day. The experiment period is set from 60 days to 300 days with a gap of 30 days; that is, from about 2 months to 10 months.

The performance is evaluated with different experiment periods. The noise are all set to Gaussian white noise with standard deviation 30, to simulate the noisy environment for the data gathering and other error factors. The results are shown in Fig. 6.5. Two different sets of system parameters, one with the τ_{ij} range from 1 to 3 and another range from 10 to 15, are presented to simulate two totally different systems. For systems with small τ_{ij}, the variations on injection rates cause a nearly instantaneous and equal change at the producer; on the other hand, the large τ_{ij} result in large attenuation and more time delay. So this simulation presents two extreme cases which are also typical in the CM.

The results show that for these two cases, the filtered binary sequence obtained using the discussed procedure always outperforms the binary white sequence. For the first case (τ_{ij} range from 1 to 3), the performance is similar, and this is because when the time constant τ is small, the reservoir behaves like an all-pass filter, so there is not much improvement for putting inputs energy into the low frequency components. For the second case (τ_{ij} range from 15 to 20), the filtered binary sequence with $T \geq 5$ outperforms white binary sequence noticeably. This is because now the reservoir behaves like a low-pass filter, if we put the input energy into

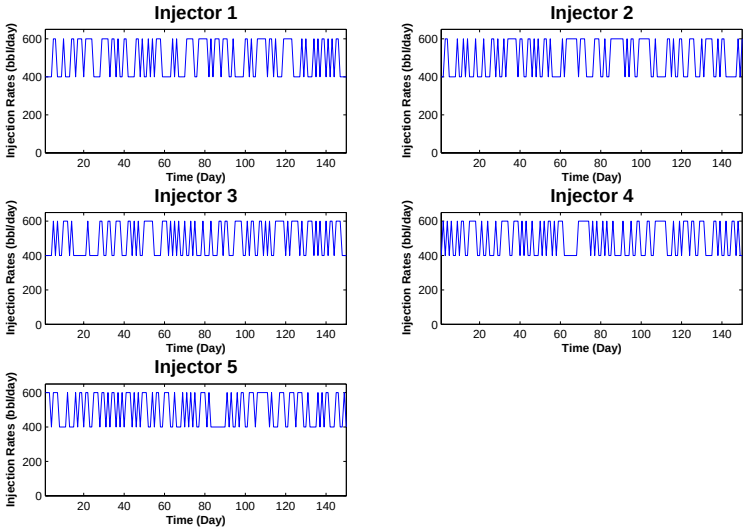

(a) Binary white sequence

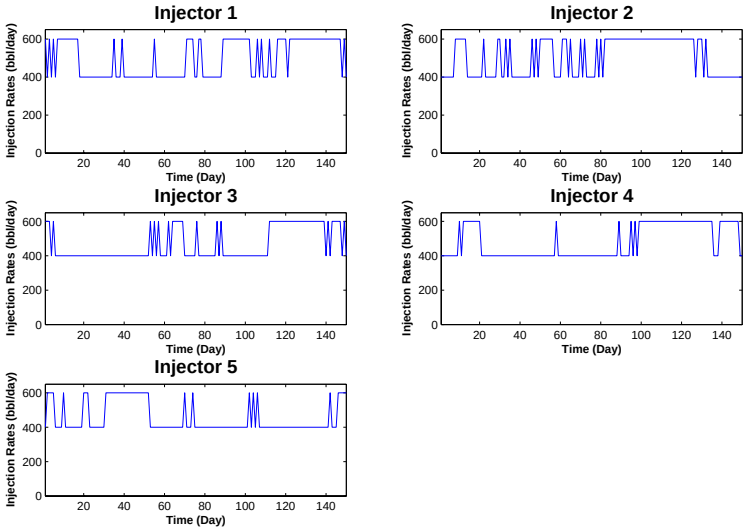

(b) Filtered binary sequence by our procedure

Figure 6.4: A realization of designed injection rates used for performance evaluation. Here we only show two cases: binary white sequence and sequence obtained by proposed procedure with the filter parameter $T = 20$. The noise level is set to SNR = 10.46 dB.

low-frequency components, a significant gain can be achieved. Another interesting phenomenon is for the filtered binary sequence with $T = 20$, which performs much

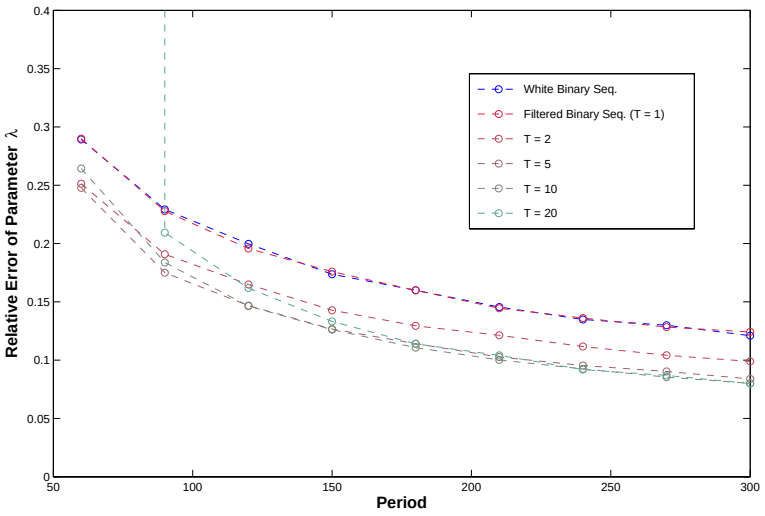

(a) Reservoir parameter τ_{ij}s range from 1 to 3

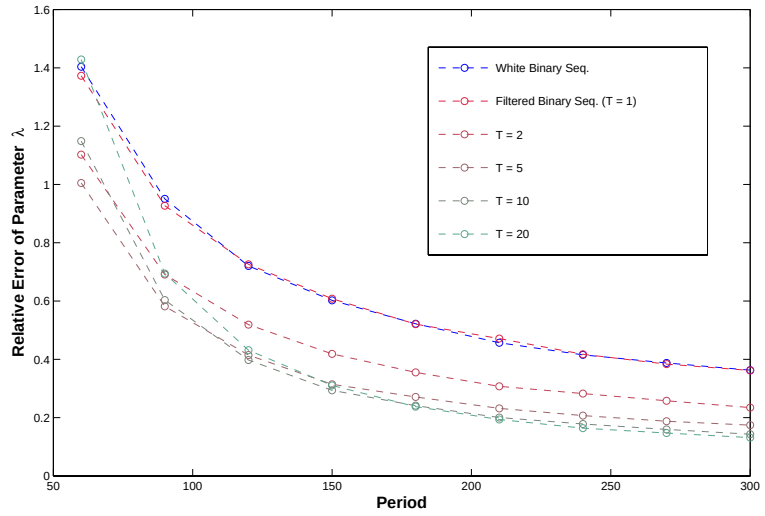

(b) Reservoir parameter τ_{ij}s range from 10 to 15

Figure 6.5: Performance plot for injection rates design with different sequences. The candidate sequences are binary white sequence and filtered binary sequence by our procedure with different cut-off frequencies (controlled by T). The noise level are all set to SNR = 10.46 dB. The results are averaged on 500 realizations.

worse when the experiment period length is small. As we have described, this is

because the performance is only guaranteed asymptotically whereas the experiment period is too short in this case.

Here we only show the application of injection rate design scheme to CM. Following the same procedure, we can apply this scheme on all predictive models, according to the models we decide to use. There are also some potential applications for the injection rate design, such as waterflooding surveillance and monitoring [58] [5]. We will discuss these possible applications in the last chapter.

6.3.5 Comparison to Deterministic Approach

To complete this chapter, we compare all discussed procedures, including both deterministic and stochastic approaches. For the deterministic approach, we choose the proposed inverse-repeat signal design, together with well-known Gold pair and Kasami sequence [16]. For stochastic approach, we show the white binary sequence and the filtered binary sequence with $T = 5$. All simulation settings are the same as in the previous section. The results are shown in Fig. 6.6.

If we only compare deterministic approaches (Inverse-repeat design, Gold pair and Kasimi sequence), the proposed inverse-repeat design almost always outperforms the rest otherdeterministic sequences, especially when the data length is short or the reservoir setting τ_{ij}s are small. For both approaches, the filtered binary sequence has the best performance for all cases except when data length is very short. This means that with careful design, the stochastic approaches can achieve better "average" performance than the deterministic approaches.

We need to note here that for stochastic approaches, the results are the "average" performance on 500 realizations, but for deterministic approaches, the sequences are fixed so the performance is identical for each run. In real field applications, the

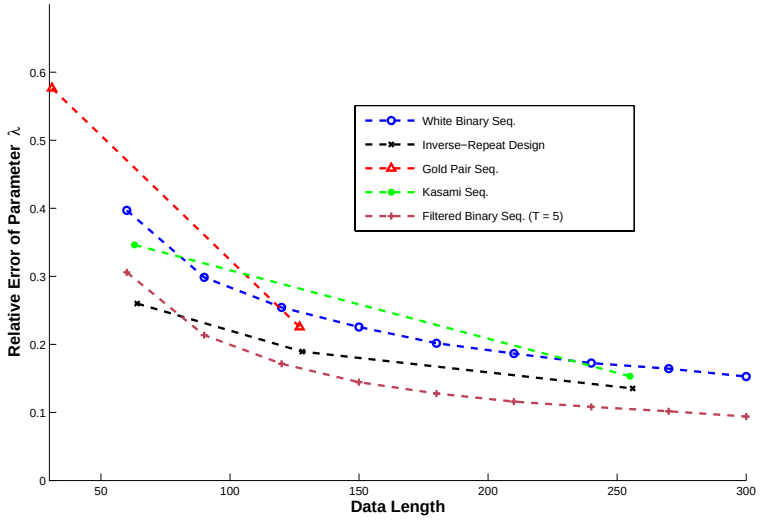

(a) Reservoir parameter τ_{ij}s range from 1 to 3

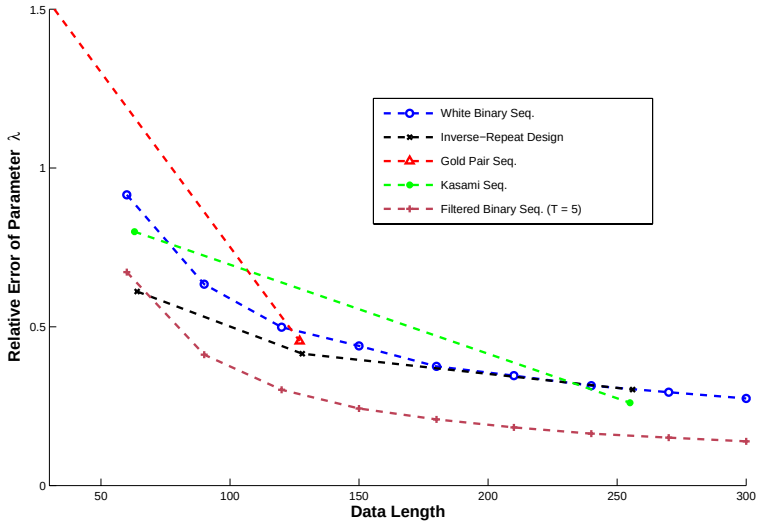

(b) Reservoir parameter τ_{ij}s range from 10 to 15

Figure 6.6: Performance plot for injection rates design with both deterministic and stochastic approaches. The noise level are all set to SNR = 10.46 dB. For stochastic approaches, the results are averaged on 500 realizations.

reservoir engineers need to be careful about this: the performance is only guaranteed on the average sense, not for each realization, so when one realization of the filtered

binary sequence is selected, one needs to examine if any value of its out-of-phase auto-correlation or cross-correlation is large. If it is the case, one should discard this realization and look for another realization to use.

6.4 Conclusion

In this chapter, we investigate the problem of injection rate design for parameter estimation. After the literature review, we first propose a new deterministic approach. We introduce a property for a set of inverse-repeat signals, and use this property to design a set of injection rates having zero cross-correlation with arbitrary shifts. For the stochastic approach, we discuss two criterions: spectrum criterion and input power criterion. We extend the spectrum criterion on SISO case [41] to MIMO case, and apply a design procedure, binary filtered sequence, to field applications. Finally, both deterministic and stochastic approaches are evaluated and compared on capacitance model to show the superiority of the filtered binary sequence design.

Chapter 7

Conclusions and Future Work

7.1 Conclusions

In Chapter 2, we proposed three new predictive models. We first show a general LTI system, and address the limitation of CM on its impulse response shape. The FIR model was developed to release the shape of response curve between injectors and producers. The second model, DCM, was derived by extending the concepts of CM to dealing with more heterogeneous scenarios. When building the model, in order to take the producer-to-producer interaction into consideration, we proposed the M-ARX model to characterize this effect between producers. Finally, we suggested using the prediction-error method to estimate the model parameters. This often involves some non-linear optimization procedure, but the FIR and M-ARX model possess the linear-in-the-parameter property so the optimization can reduce to some kind of linear regression procedure, which makes the estimation much less-computationally intensive.

In Chapter 3, we first discussed two approaches for model validation: (1) validation based on its prediction ability on fresh data set; (2) validation based on

interpretation of model parameters according to some reservoir characteristics. Following this, we verified all proposed models and compared them with the numerical simulation data. We investigated the grey-box approach for model building procedures, and the results were also evaluated completely. Finally, we defined a practical metric based on prediction-errors and provided a comparative analysis of all predictive models using this metric.

In Chapter 4, a unified linear modeling framework was proposed to integrate all predictive models. It was shown that they all can be seen as some special cases of a general linear model, and the transfer function of this linear model can also be interpreted as some reservoir characteristics. Also, the relationships between different models were easily shown under this framework.

In Chapter 5, we demonstrated a totally novel application for M-ARX model. Comparing to other models, hen we use the model to predict the behaviors for a producer shut-in, the number of parameters needed to be retrained by M-ARX model is much fewer. More importantly, we showed that the shut-in performance prediction can be achieved by using the "constrained producer", which means setting this producer to some constant rates (instead of shutting it in) during a period of time. As compared to actual shut-in of a producer, this procedure keeps most of the produced rates, which makes it much more practical when we want to evaluate various "what if" scenarios, in particular those involving a potential shut-in of some wells.

In Chapter 6, we first did a literature survey of the input design problem on two different fields: system identification and channel estimation in communication systems. Two frameworks, deterministic and stochastic approaches, are discussed. For the deterministic approach, we proposed a new procedure for generating a set of input signals with vanishing cross-correlation property. For stochastic approach,

we extended the results in system identification field to MIMO case, and applied a common procedure to field applications to generate a set of "good" injection rates. All proposed procedures were evaluated on the capacitance model.

7.2 Future Work

For future research, the emphasis will lie on combining some automatic control knowledge to extend the current work to waterflood management and optimization. The following recommendations are suggested for future work:

- Most of the predictive models were only verified with synthetic simulation data, but not on real field data. The field data, especially the production rates, are very noisy and with many measurement errors. The linearity assumption of the system and the assumption of constant bottom-hole pressure also need to be calibrated via the field data. Besides, more field trials should be performed to decide the parameters, such as the amplitude of variations, the cut-off frequency and suitable time resolution of the injection patterns, for the injection rate design experiments.

- The discussion of the predictive models focused on gross fluid production rate (oil + water) and assumed that gas is negligible, but actually only the oil production rates that has the important economic values. There are a number of reference discussing the water-to-oil ratio (WOR), i.e., [38] and [54] proposed an oil fractional-flow model to separate the oil rates from the total liquid rates for CM. We should point out here that the model is general to all predictive models, so it can be applied to other models directly without any changes. More simulations and evaluations are needed for this.

- Up to now, the injection rate design problem only focused on the parameter estimation part, without considering waterflood management and optimization. Actually, one of the ultimate goals for understanding the reservoir is to help us in decision-making. Once we have a better understanding of the reservoir, the next step is to make some "smart" decision or changes to increase the oil recovery. This work provides the basis for some approaches to real-time waterflood management and optimization, and it needs to be extended to cover these topics.

- The injection rate design concepts could be further extended to some applications of waterflood surveillance. When the injection rates are designed to have some variations, such as piece-wise constant curves, the correlations between injection/production rates will reveal some information about the reservoir. The injection rates often can be scheduled and controlled automatically and precisely, which means using a designed injection rate on daily field production without disturbing the operation is feasible. Some kinds of real-time monitoring on the waterflood conditions can be achieved by the use of injection rate design.

- The concepts of constrained producers for performance prediction is a totally new idea for the predictive modeling approach, and we demonstrate how to use it to predict the future reservoir behavior when a particular producer is shutting in, but without needing to actually shut in this producer. Up to now, the validation was mainly based on the synthetic simulation data, and only single producer shut-in case was discussed. Conceptually this can be extended to multiple-producers shut-in case. This topic looks very promising and needs more investigation and verification for further studies.

Reference List

[1] M. Abbaszadeh-Dehghani and W.E. Brigham. Analysis of well-to-well tracer flow to determine reservoir heterogeneity. In *Annual California Regional Meeting*, San Francisco, California, USA, March 1982.

[2] M. Abbaszadeh-Dehghani and W.E. Brigham. Analysis of well-to-well tracer flow to determine reservoir layering. *Journal of Petroleum Technology*, pages 2257–2270, 1984.

[3] A. Albertino and Larry W. Lake. Inferring connectivity only from well-rate fluctuations in waterfloods. *SPE Reservoir Evaluation and Engineering Journal*, 6:6–16, 2003.

[4] JA Ball, I. Gohberg, and MA Kaashoek. A frequency response function for linear, time-varying systems. *Mathematics of Control, Signals, and Systems (MCSS)*, 8(4):334–351, 1995.

[5] R.P. Batycky, M.R. Thiele, R.O. Baker, and S.H. Chugh. Revisiting reservoir flood-surveillance methods using streamlines. *SPE Reservoir Evaluation and Engineering Journal*, 11:387–394, 2008.

[6] M. Biguesh and A.B. Gershman. Training-based MIMO channel estimation: A study of estimator tradeoffs and optimal training signals. *IEEE Transactions on Signal Processing*, 54:884–893, 2006.

[7] S.P. Boyd and L. Vandenberghe. *Convex optimization*. Cambridge Univ Pr, 2004.

[8] C. Budianu and L. Tong. On maximal accuracy estimation with output power constraints. *IEEE Transactions on Signal Processing*, 50:2515–2528, 2002.

[9] C. Chatfield. *Time-Series Forecasting*. Chapman & Hall/CRC, 2001.

[10] C. Chatfield. *The analysis of time series: an introduction*. CRC Pr I Llc, 2004.

[11] B.L. Cooley and J.H. Lee. Control-relevant experiment design for multivariable systems described by expansions in orthonormal bases. *Automatica*, 37:273–281, 2001.

[12] S.N. Crozier and D.D. Falconer. Least sum of squared errors (LSSE) channel estimation. In *Proceedings of Inst. Elect. Eng.*, volume 138, pages 371–378, August 1991.

[13] Oliver D.S. The sensitivity of tracer concentration to nonuniform permeability and porosity. *Transport in Porous Media*, 30, 1998.

[14] C. Fragouli, N. Al-Dhahir, and W. Turin. Finite-alphabet constant-amplitude training sequence for multiple-antenna broadband transmissions. In *Proceedings of IEEE International Conference of Communication*, volume 1, pages 6–10, New York, NY, USA, May 2002.

[15] P.H. Gentil. The use of multilinear regression models in patterned waterfloods: Physical meaning of the regression coefficients. Master's thesis, The University of Texas at Austin, Austin, Texas, USA, 2005.

[16] S.W. Golomb and G. Gong. *Signal Design for Good Correlation.* Cambridge, U.K.: Cambridge Univ. Press, 2005.

[17] G.C. Goodwin. Experiment design. In *6th IFAC Symposium on System Identification*, Washington D.C., USA, 1982.

[18] G.C. Goodwin and R.L. Payne. *Dynamic System Identification: Experiment Design and Data Analysis*, volume 136 of Mathematics in Science and Engineering. Academic Press, 1977.

[19] A. Grant. Joint decoding and channel estimation for linear MIMO channels. In *IEEE Wireless Communications Networking Conference*, Chicago, Illinois, USA, September 2000.

[20] F.J. Guevara. *Improved Methodologies for Stochastically Forecasting Oil Recovery Processes.* PhD thesis, The University of Texas at Austin, Austin, Texas, USA, 1997.

[21] B. Hassibi and B.M. Hochwald. How much training is needed in multiple-antenna wireless links? *IEEE Transactions on Information Theory*, 49:951–963, 2003.

[22] K.J. Heffer, R.J. Fox, C.A. McGill, and N.C. Koutsabeloulis. Novel techniques show links between reservoir flow directionality, earth stress, fault structure and geomechanical changes in mature waterfloods. In *SPE Annual Technical Conference and Exhibition*, Dallas, Texas, USA, October 1995.

[23] P.S.C. Heuberger, PMJ Van den Hof, and B. Wahlberg. *Modelling and identification with rational orthogonal basis functions.* Springer-Verlag New York Inc, 2005.

[24] R.N. Horne. *Modern Well Test Analysis: A Computer-Aided Approach*. Petroway, Inc., Palo Alto, CA, 2nd edition, 1995.

[25] O. Izgec and C.S. Kabir. Establishing injector/producer connectivity before breakthrough during fluid injection. In *SPE Western Regional Meeting*, Son Jose, California, USA, March 2009.

[26] P.R. JBallin, A.G. Journel, and Aziz. K. Prediction of uncertainty in reservoir performance forecast. *Journal of Canadian Petroleum Technology*, 31:52–62, 1992.

[27] C.R. Johnson, R.A. Greenkron, and E.G. Woods. Pulse-testing: A new method for describing reservoir flow properties between wells. *Journal of Petroleum Technology*, pages 1599–1604, 1966.

[28] T. Kailath. *Linear systems*. Prentice-Hall Englewood Cliffs, NJ, 1980.

[29] M.M. Kamal. Interference and pulse testing - a review. *Journal of Petroleum Technology*, pages 2257–2270, 1983.

[30] D. Kaviani, J.L. Jensen, L.W. Lake, and M. Fahes. Estimation of interwell connectivity in the case of fluctuating bottomhole pressures. In *Abu Dhabi International Petroleum Exhibition and Conference*, Abu Dhabi, UAE, November 2008.

[31] E.G. Larsson and P. Stoica. *Space-Time Block Coding for Wireless Communications*. Cambridge, U.K.: Cambridge Univ. Press, 2003.

[32] K.H. Lee, N. Jafroodi, A. Ortega, and I. Ershaghi. A distributed capacitance model for performance evaluation and prediction in waterfloods from injection and production rates fluctuations. *Plan to submitt to Journal of Petroleum Science and Engineering*, 2010.

[33] K.H. Lee, A. Ortega, N. Jafroodi, and I. Ershaghi. A multivariate autoregressive model for characterizing producer-producer relationships in waterfloods from injection/production rate fluctuations. In *SPE Western Regional Meeting*, Anaheim, California, USA, May 2010.

[34] K.H. Lee, A. Ortega, A.M. Nejad, and I. Ershaghi. A method for characterization of flow units between injection-production wells using performance data. In *SPE Western Regional and Pacific Section Joint Meeting*, Bakersfield, California, USA, March 2008.

[35] K.H. Lee, A. Ortega, A.M. Nejad, N. Jafroodi, and I. Ershaghi. A novel method for mapping fractures and high permeability channels in waterfloods using injection and production rates. In *SPE Western Regional Meeting*, Son Jose, California, USA, March 2009.

[36] M.J. Levin. Optimal estimation of impulse response in the presence of noise. *IRE Transactions on Circuit Theory*, 7:50–56, 1960.

[37] Y. Li. Optimal training sequences for ofdm systems with multiple transmit antennas. In *IEEE GLOBECOM*, volume 3, pages 1478–1482, 2000.

[38] X. Liang, B. Weber, T.F. Edgar, L.W. Lake, M. Sayarpour, and A.A. Yousef. Optimization of oil production in a reservoir based on capacitance model of production and injection rates. In *SPE Hydrocarbon Economics and Evaluation Symposium*, Dallas, Texas, USA, April 2007.

[39] F. Liu, J.M. Mendel, and A.M. Nejad. Forecasting injector-producer relationships from production and injection rates using an extended kalman filter. In *SPE Annual Technical Conference and Exhibition*, Anaheim, California, USA, September 2007.

[40] N. Liu and D.S. Oliver. Critical evaluation of the ensemble Kalman filter on history-matching of geologic facies. *SPE Reservoir Evaluation and Engineering Journal*, 8:470–477, 2005.

[41] L. Ljung. *System identification: Theory for the User*. Upper Saddle River, NJ: Prentice Hall, 2nd edition, 1999.

[42] Computer Modeling Group Ltd. CMG numerical simulators. "http://www.cmgroup.com/software/completesuite.htm", October 2010.

[43] James A. M. Monte Carlo simulation: Its status and future. *Journal of Petroleum Technology*, 49:361–373, 1997.

[44] T.L. Marzetta. BLAST training: Estimating channel characteristics for high capacity space-time wireless. In *37th Annual Allerton Conference on Communications, Control, and Computing*, Monticello, Illinois, USA, September 1999.

[45] J.L. Massey and T. Mittelholzer. Welchąęs bound and sequence sets for code-division multiple-access systems. *Sequences II: Methods in Communication, Security and Computer Science*, 1991.

[46] R.K. Mehra. Optimal input signals for parameter estimation in dynamic systems - survey and new results. *IEEE Transactions on Automatic Control*, 19:753–768, 1974.

[47] R.K. Mehra. Choice of input signals. In *Trends and Progress in System Identification*, Pergamon Press, Oxford, 1981.

[48] T.S. Ng, G.C. Goodwin, and Payne R.L. On maximal accuracy estimation with output power constraints. *IEEE Transactions on Automatic Control*, 22:133–134, 1977.

[49] T.S. Ng, G.C. Goodwin, and Soderstrom T. Optimal experiment design for linear systems with input-output constraints. *Automatica*, 13:571–577, 1977.

[50] M.N. Panda and A.K. Chopra. An integrated approach to estimate well interactions. In *SPE India Oil and Gas Conference and Exhibition*, New Delhi, India, February 1998.

[51] F. Pukelsheim. *Optimal design of experiments*. Society for Industrial Mathematics, 2006.

[52] G.C. Reinsel. *Elements of multivariate time series analysis*. Springer Verlag, 2003.

[53] M.A. Sabet. *Well Test Analysis*. Gulf Publishing Company, 1991.

[54] M. Sayarpour, E. Zuluaga, C.S. Kabir, and L.W. Lake. The use of capacitance-resistive models for rapid estimation of waterflood performance and optimization. In *SPE Annual Technical Conference and Exhibition*, Anaheim, California, USA, September 2007.

[55] M. Sayarpour, E. Zuluaga, C.S. Kabir, and L.W. Lake. The use of capacitance-resistive models for rapid estimation of waterflood performance and optimization. In *SPE Annual Technical Conference and Exhibition*, Anaheim, California, USA, September 2008.

[56] A. Scaglione and A. Vosoughi. Turbo estimation of channel and symbol in precoded MIMO systems. In *ICASSP*, volume 4, pages 413–416, Montreal, PQ, Canada, May 2004.

[57] M. Stone. Cross-validity choice and assessment of statistical predictors. *Journal of Royal Statistical Society*, 36(B):111–147, 1974.

[58] M. Terrado, S. Yudono, and G. Thakur. Waterflooding surveillance and monitoring: Putting principles into practice. *SPE Reservoir Evaluation and Engineering Journal*, 10:552–562, 2007.

[59] Marco R. Thiele. Streamline simulation. In *6th International Forum on Reservoir Simulation*, Schloss Fuschl, Austria, September 2001.

[60] Marco R. Thiele and Rod. P Batycky. Water injection optimization using a streamline-based workflow. In *SPE Annual Technical Conference and Exhibition*, Denver, Colorado, USA, October 2003.

[61] H.J.A.F. Tulleken. Grey-box modelling and identification using physical knowledge and bayesian techniques. *Automatica*, 29(2):285–308, 1993.

[62] D. Weber, T.F. Edgar, L.W. Lake, L. Lasdon, S. Kawas, and M. Sayarpour. Improvements in capacitance-resistive modeling and optimization of large scale reservoirs. In *SPE Western Regional Meeting*, Son Jose, California, USA, March 2009.

[63] A.A. Yousef. *Investigating Statistical Techniques to Infer Interwell Connectivity from Production and Injection Rate Fluctuations*. PhD thesis, The University of Texas at Austin, Austin, Texas, USA, 2005.

[64] A.A. Yousef, P.H. Gentil, J.L. Jensen, and L.W. Lake. A capacitance model to infer interwell connectivity from production and injection rate fluctuations. *SPE Reservoir Evaluation and Engineering Journal*, 9:630–646, 2006.

[65] A.A. Yousef and L.W. Lake. Analysis and interpretation of interwell connectivity from production and injection rate fluctuations using a capacitance model. In *SPE Symposium on Improved Oil Recovery*, Tulsa, Oklahoma, USA, April 2006.

[66] M. Zarrop. *Design for Dynamic System Identification*. Lecture Notes in Control and Information Sciences. Sci. 21. Springer Verlag, Berlin, 1979.

[67] D. Zhai, J. Mendel, and F. Liu. A new method for continual forecasting of interwell connectivity in waterfloods using an extended kalman filter. In *SPE Western Regional Meeting*, 2009.